論文 / 著書情報
Article / Book Information

題目(和文)	
Title(English)	High Temperature Carbon Dioxide Reduction in Tubular Solid Oxide Electrolysis Cells for a Carbon Recycling Ironmaking System
著者(和文)	DipuArnoldus Lambertus
Author(English)	Arnolduslambertus Dipu
出典(和文)	学位:博士(工学), 学位授与機関:東京工業大学, 報告番号:甲第9474号, 授与年月日:2014年3月26日, 学位の種別:課程博士, 審査員:加藤　之貴,小澤　正基,矢野　豊彦,竹下　健二,塚原　剛彦
Citation(English)	Degree:Doctor (Engineering), Conferring organization: Tokyo Institute of Technology, Report number:甲第9474号, Conferred date:2014/3/26, Degree Type:Course doctor, Examiner:,,,,
学位種別(和文)	博士論文
Type(English)	Doctoral Thesis

High Temperature Carbon Dioxide Reduction in Tubular Solid Oxide Electrolysis Cells for a Carbon Recycling Ironmaking System

A Thesis Submitted for the Degree of Doctor of Engineering

Arnoldus Lambertus Dipu

Supervised by Assoc. Prof. Yukitaka Kato

Tokyo Institute of Technology

2014

High Temperature Carbon Dioxide Reduction in Tubular Solid Oxide Electrolysis Cells for a Carbon Recycling Ironmaking System

A Thesis Submitted for the Degree of Doctor of Engineering

Arnoldus Lambertus Dipu

Supervised by Assoc. Prof. Yukitaka Kato

Department of Nuclear Engineering

The Graduate School of Science and Engineering

Tokyo Institute of Technology

Submitted February 2014

Abstract

The feasibility study of high temperature carbon dioxide (CO_2) reduction using tubular yttria stabilized zirconia (YSZ)-based electrolyte was conducted for carbon monoxide (CO) regeneration in active carbon recycling energy system (ACRES) driven by high temperature gas reactor. In this new energy system, carbon in the form of CO is reused cyclically, consuming non-CO_2-emitting primary energy sources, thus reducing emissions of CO_2 to the atmosphere. One promising aspect of CO regeneration using ACRES is that CO_2 reduction using solid oxide electrolysis cells (SOECs) occurs at high temperatures. This research aims to study the feasibility of high temperature electrolysis of CO_2 using tubular SOECs.

Three CO_2 electrolysis processes were demonstrated using different electrode materials on the YSZ-based electrolyte. Cell-1, with a structure of Pt-$La_{0.8}Sr_{0.2}MnO_3$ (LSM)|YSZ|Pt-LSM for the cathode|electrolyte|anode, had higher current density levels than those of Cell-2, with a LSM|YSZ|LSM structure, and Cell-3, with a Pt|YSZ|LSM structure due to special structure of Pt-LSM. Some improvements to SOEC test reactor were also carried out to increase current efficiency of Ni-LSM|YSZ|LSM-YSZ cell and Ni-YSZ|YSZ|LSM-YSZ cell. It was found that current densities achieved in the experiment with Ni-YSZ|YSZ|LSM-YSZ cell at 800 °C were higher in comparison with those of Ni-LSM|YSZ|LSM-YSZ cell due to special structure of Ni-YSZ and LSM-YSZ prepared by ball milling. CO and O_2 production rates of 0.78 and 0.38 μmol/(min cm^2) respectively were achieved at an operating temperature of 900 °C and a current density of 2.97 mA/cm^2.

Evaluation of ACRES Energy balances for ironmaking showed that the required surface area of the SOECs was estimated to be 65.6 km^2/BF unit for a conventional blast furnace. It is expected that the combined system may contribute to carbon supply security and a low-carbon society.

Table of Contents

List of Figures

List of Tables

Nomenclature

Notation

E_S : Total energy input at recovery and separation process
E_R : Energy for regeneration process
E_U : Energy output of the usage process
ΔH : Enthalpy changes
ΔS : Entropy changes
T : Absolute temperature
ΔG : Gibb's free energy
V_i : Electromotive force for electrolysis [V]
ΔG_i : Electrical energy for electrolysis
n : Mole number of migrated electrons associated with electrolysis reaction
F : Faraday's constant [96500 (C/mol)]
$\dot{m}_i$: Gas mass flow in and out of the test reactor [mL/min]
V_{Tn} : Thermoneutral voltage [V]
$\Delta H^{\circ}_{800℃}$: Enthalpy change for the electrolysis reaction at 0.1 MPa and 800 °C

Abbreviation

ACRES : Active carbon recycling energy system
SOEC : Solid oxide electrolysis cell
SOFC : Solid oxide fuel cell
HTGR : High temperature gas reactor
YSZ : Yttria stabilized zirconia
Cermet : Composite of metal and ceramic
LSM : Strontium-doped lanthanum manganite, $La_{0.8}Sr_{0.2}MnO_3$
OCV : Open circuit voltage
GC-1 : Gas chromatograph number 1
GC-2 : Gas chromatograph number 2
TCD : Thermal conductivity detector
PPQ : Porapak Q, column name in gas chromatograph
MS 13X : Molecular sieve 13X, column name in gas chromatograph
SEM : Scanning electron microscope
XRD : X-ray diffraction
BF : Blast furnace

Chapter 1

Introduction to Active Carbon Recycling Energy System

1.1 Introduction

Energy security is critical to the industrial and economic development of a society. Rapid changes and instability in the market prices of primary energy sources will lead to the economic confusion in any age. Up to now, most of primary energy is derived from carbon, thus, making carbon security essential for a sustainable society. However, the excessive use of carbon as the primary energy in fossil fuels for the sustainable of society has brought to the significant increase of concentration level of carbon dioxide (CO_2) in atmosphere. The excessive amount of CO_2 has disturbed the delicate balance by trapping to much energy, which causes the average temperature of the earth to rise and the climate at some localities to change. These undesirable consequences are referred to as global warming or global climate change [1].

In a 1995 report, the world's leading climate scientists concluded that the earth has already warmed about 0.5 °C. A rise of this magnitude is feared to cause severe changes in weather pattern with storms and heavy rains and flooding at some parts and drought in others, major flood due to the melting of ice at the poles, loss of wetlands and coastal areas due to rising sea levels, variation in water supply, changes in the ecosystem, increases in the epidemic diseases

due to the warmer temperature and adverse side effects on human health and socioeconomic conditions in some areas [1].

Recognizing the threat posed by rising concentrations of CO_2 in the atmosphere, 150 nations from around the world signed the united nations framework convention on climate change (UNFCCC) in 1992, to cut CO_2 emissions on a voluntary basis to 1990 levels by 2000. In 1997, the parties to the UNFCCC met in Kyoto and negotiated a protocol that established legally binding limits or reductions in CO_2 for industrialized countries [2,3]. Japan, as one of the industrialized countries undertook the obligation adhering to the Kyoto protocol, which came into effect in 2005, and therefore need to drastically reduce CO_2 emission.

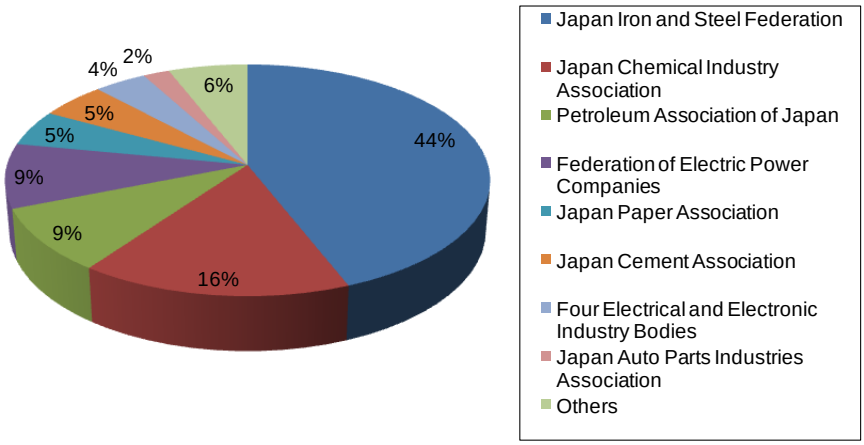

Fig. 1.1 Energy conversion-industrial sector CO_2 emission share in Japan [4].

Emissions in the industrial sector in Japan which covering the energy conversion and industrial sectors are shown in Fig. 1.1. The

steel industry accounts for as much as 44% of the industrial sector's total CO_2 emissions following by paper (16%) and auto parts industries (9%). Apparently, the steel industry's CO_2 emission reduction is significant for Japan's emission-cutting measures [4].

Any limit imposed on CO_2 emissions will directly restrict the use of carbon resources, which will, in turn, severely affect the manufacturing and service industries. The simultaneous establishment of carbon security and lower CO_2 emissions is thus an important subject for the development of modern society. This doctoral thesis discusses and demonstrates the feasibility of carbon material in the form of carbon monoxide (CO) regeneration via CO_2 electrolysis for the application in new energy system called active carbon recycling energy system (ACRES).

1.2 Active Carbon Recycling Energy System

A new carbon recycling energy system has been proposed and developed in order to reduce the emission of CO_2 into atmosphere from industrial processes.

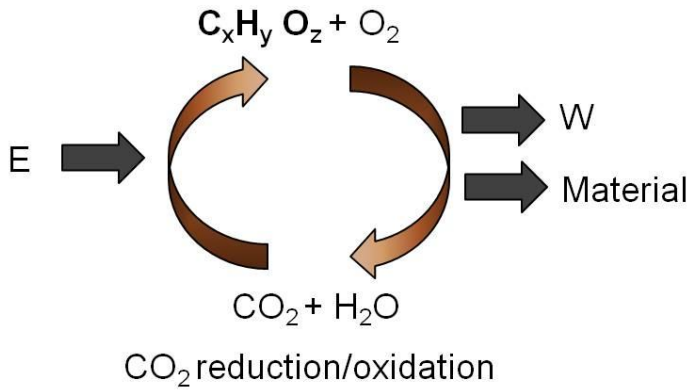

Fig. 1.2 Carbon recycling energy system.

Here in this new energy system i.e. ACRES, carbon is reused cyclically and therefore can reduce the emission of CO_2 to atmosphere [5-8]. The proposed concept of ACRES is shown in Fig. 1.2.

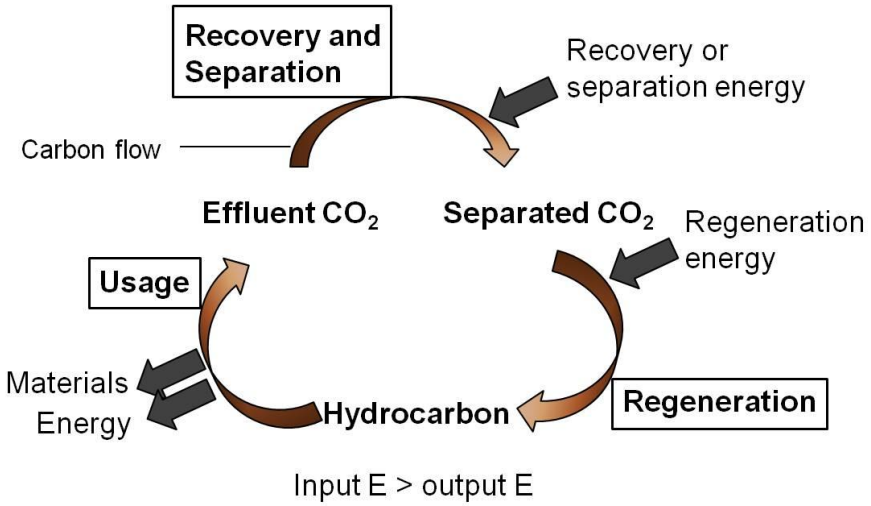

Fig. 1.3 Principle of ACRES with three elemental processes.

CO_2 with/without water (H_2O) is ground state of carbon. CO_2 is converted into hydrocarbons or alcohol by an energy input using some catalytic technologies. The produced hydrocarbons are useful for conventional manufacturing industry as thermal energy sources and raw materials. These hydrocarbons provide thermal and electrical energies during the oxidation into CO_2. The hydrocarbons can be used as raw materials for making industrial materials. These hydrocarbons are easy to be stored and can be transferred under low compression pressure with a small explosion risk in comparison with hydrogen (H_2). The hydrocarbons have a considerable potential for use in common manufacturing industries. A natural carbon recycle energy system already exists in plant kingdom and is an ideal recycling system.

However the potential amount of bio-mass recycled by this system is not sufficient to meet the demands of a modern society. Therefore, an artificial active recycling system for carbon, i.e. ACRES is proposed.

The structure of ACRES consists of three elemental processes; hydrocarbon usage, CO_2 recovery and separation, and hydrocarbon regeneration (Fig. 1.3). In the usage process hydrocarbon can be used as both a heat source and a material. CO_2 generated from hydrocarbon consumption is recovered by physical and chemical sorption. Recovered CO_2 in a sorption material is separated thermally from the material by a heat input. This process produces highly concentrated CO_2. Recovered CO_2 is regenerated into hydrocarbons in the regeneration process. The regeneration process is endothermic and requires an energy input. In ACRES the total energy input at recovery and separation (E_S) and regeneration (E_R) should be larger than the energy output of the usage process (E_U). When regenerated hydrocarbon has higher value than primary energy for an energy demand side, ACRES system becomes useful energy system.

$$E_S + E_R > E_U \tag{1.1}$$

1.3 ACRES Based on CO

CO has been considered as popular energy material with higher energy density that is higher exergy than H_2 and methane (CH_4) (Fig. 1.4). CO is also highly compatible with conventional chemical, steel and high temperature manufacturing processes. Therefore, efficient regeneration of CO is a key technology for ACRES based on CO. There

are two different regeneration methods of CO proposed by Kato among others; CO_2 hydrogenation and CO_2 electrolysis [5].

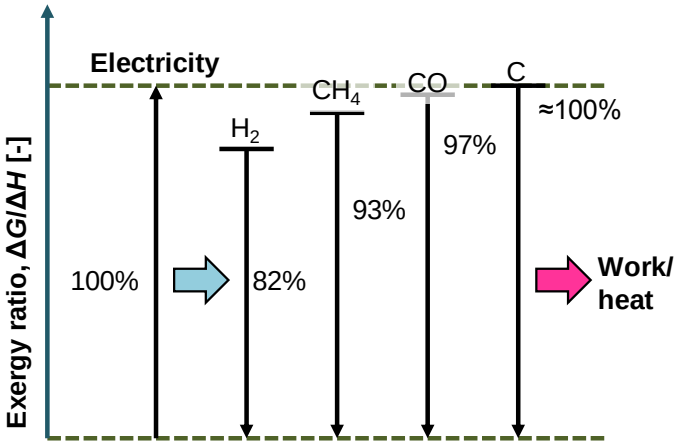

Fig. 1.4 Exergy ratio $(\Delta G/\Delta H)$ for carbon materials and hydrogen at higher heating value (HHV)[5].

The chemical reaction equilibrium for the $H_2/CO_2/CO/H_2O$ in the H_2 production by steam electrolysis and reduction of CO_2 with the hydrogen has been evaluated in the previous work [5,8]. The system is given in Fig. 1.5. It is assumed that the reaction proceeded under an equivalent ratio and a total pressure of 100 kPa. CO_2/CO is reversible around 700 °C. This implies that the CO regeneration by CO_2 hydrogenation requires a heat input of more than 700 °C. Waste heat at a high temperature of around 700 °C generated from the high temperature processes can be utilized in the reaction. Energy saving of the high temperature processes is achievable by which the waste heat generated from the processes is utilized for the regeneration process in the ACRES.

CO_2 electrolysis is another one promising method of CO regeneration. Solid-oxide electrolysis cell (SOEC) in which a reverse operation of a solid oxide fuel cell (SOFC) proceeds has a possibility and has long term durability for the electrolysis [9-17]. SOEC has been discussed for the production of a syngas, which is a mixture of H_2 and CO generated from H_2O and CO_2 [12,14,16]. It also has potential to produce propellants and life-support consumables for space missions [18-21]. Recent developments and performance improvement have brought SOEC close to the practical implementation.

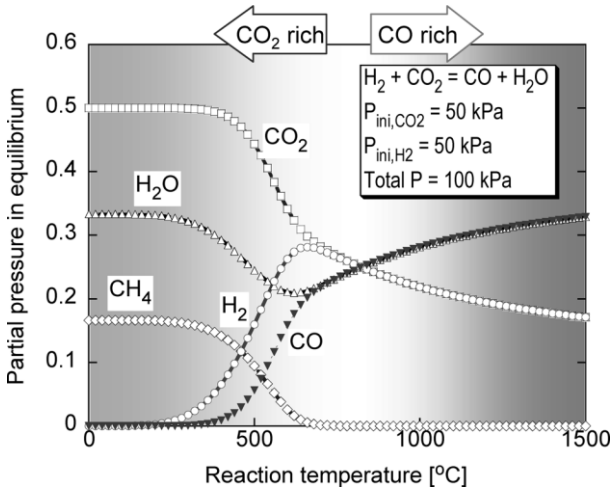

Fig. 1.5 Chemical reaction equilibrium for $H_2/CO_2/CO/H_2O$ reaction system under 100 kPa [5,8].

1.4 ACRES with High Temperature Gas Reactor

1.4.1 High Temperature Gas Reactor

The value of ACRES is that the system uses carbon cyclically and does not emit CO_2 into atmosphere. The use of non-carbon primary energy sources is an essential requirement for a practical realization of

ACRES. An ACRES based on CO is the most effective recycling system. A high temperature gas reactor (HTGR) type nuclear reactor is the most suitable energy source for ACRES due to its advantages in terms of energy production, safety and fuel cycle system.

1.4.1.1 Energy Production

HTGR with reactor coolant temperature of 950 °C is high enough to approach 50% generation efficiency by regenerative Brayton cycle gas turbine. The promise of the HTGR goes beyond power generation. The process heat supplied by the HTGR satisfies the temperature requirements for broad industrial applications from district heating to the direct reduction iron-steel making [22].

1.4.1.2 Passive Safety System

Using graphite and ceramics for core construction makes HTGR capable of withstanding extreme temperature in accident. Moreover, the large quantity of these materials used and the low power density of the core design are intended to limit reactor temperature excursion in any accident. Even in this limit, should an abnormal rise in temperature take place, the strong negative temperature coefficient of reactivity of the core would shut the reactor down. Decay heat is removed from the core by thermal conduction only. The coolant Helium (He) contributes a handful of inherent properties to enhance nuclear passive safety, being strong in cooling, always single phase, practically subsonic, neutronically transparent, noncorrosive (inert) to any material that comes into contact with it. Some of those that direct reactivity excursion, small spontaneous heat release, and prevention of

core-graphite oxidation. Together, these inherent and passive and passive and safety design features provide proof of a core melt and of significant radioactivity release in case of an accident [22].

1.4.1.3 Fuel Cycle

HTGR uses low enriched (<20%) uranium fuel cycle and remains appropriate in the near future. Thorium fuel cycle may be interesting regionally or in the longer term since world thorium reserve is several times more abundant than uranium. Although not fissile, Th-232 is fertile and breeds fissile U-233 by absorbing neutrons produced and almost all HTGRs constructed in the world already employed this type of fuel [22]. There have been several studies on fuel cycle in HTGR that can effectively destroy weapons-grade plutonium and transmute minor actinides while engaging in energy production [22]. The HTGR particle fuel has demonstrated deep-burn trans-uranium (TRU) fuel cycle. Waste management strategy includes recycle and direct repository disposal of spent fuel. Mechanical separation of spent fuel compact from bulk graphite block to the removal of ceramic coating layers by high temperature oxidation or by carbochlorination to access spent kernels of the particles have also been studied [22]. In case of direct disposal of spent fuel, separation and reduction of waste streams could be made prior to disposal. Separated graphite blocks may be treated and reused. Separated fission products and actinides can be confines in the stable matrices such as glasses based on existing industrial practices. The HTGR fuel is proliferation resistant since the fuel structure design adds difficulty to illicit operation of

accessing the isotopes in spent fuel kernels and since the high burn up in commercial systems will leave little and poor isotopes in spent fuel. The low contents of nuclear substance in spent fuel would impede diversion of large nuclear material quantities that pose a weapon's risk [22].

1.4.2 Concept of ACRES-HTGR for Ironmaking Process

The combined system (ACRES-HTGR) obviously has the potential of improving the efficiency of the nuclear power plants, which are operated most efficiently at constant power output. Furthermore, high temperature waste heat from the HTGR (up to 950 °C) can be utilized in the industrial application i.e. high temperature electrolysis of CO_2.

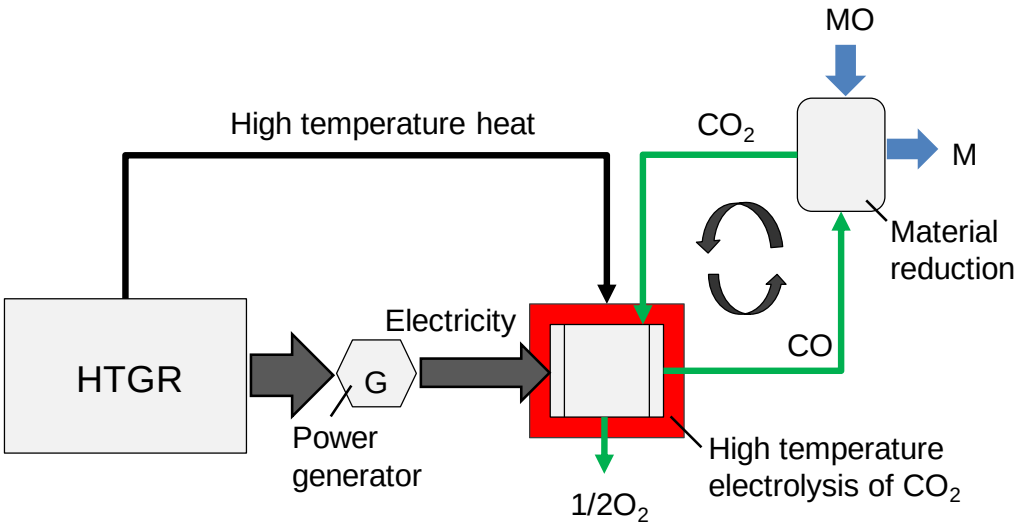

Fig. 1.6 ACRES with high temperature electrolysis of CO_2 driven by HTGR. (MO: metal oxides or raw industrial materials, M: metal or reduced materials).

High temperature electrolysis of CO_2 using both heat and electricity output from HTGR is expected to have high efficiency than high temperature electrolysis of steam because Gibb's free energy for CO_2 reduction, that is electricity consumption for per unit CO_2 electrolysis is decreased at higher temperature [5].

The application of ACRES based on CO regenerated by high temperature CO_2 electrolysis driven by HTGR is proposed in Fig. 1.6. CO is used for the reduction of metal oxides or raw industrial materials (MO) into metals or reduced materials (M), and CO_2 is generated from the reduction process. The generated CO_2 is regenerated into CO during the high temperature electrolysis of CO_2 using electricity and high temperature (up to 950 °C) heat. The electrolysis at 850 °C has electrolysis efficiency (η_{el-CO}) of 65.5%. The ratio at 25 °C under atmospheric pressure is 90.9%. Higher temperature electrolysis can theoretically reduce 28 % of the electricity consumption [5].

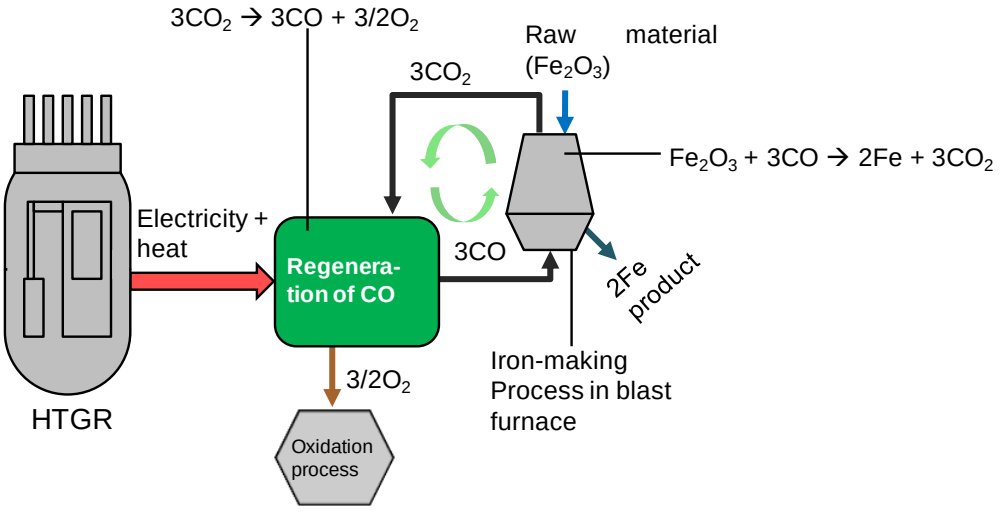

Fig. 1.7 Concept of ACRES for ironmaking process.

Application of ACRES to iron making process is proposed in Fig. 1.7. The application is based on the process given in Fig. 1.6. The system is driven by electricity and thermal energy generated from HTGR. Regenerated CO is used for the reduction of iron monoxide (Fe_2O_3) into pure iron (Fe). CO_2 generated from the reduction is regenerated into CO again by the CO_2 electrolysis process. Oxygen (O_2) as the by-products of CO can be useful material for other oxidation processes.

In conventional ironmaking process Fe_2O_3 as a raw material is reduce by H_2. This reaction is an exothermic reaction and requires external heat input.

$$\mathrm{Fe_2O_3 + 3H_2 \rightarrow 2Fe + 3H_2O}, \qquad \Delta H = +104.9\ \mathrm{kJ/mol} \tag{1.2}$$

In contrast, Fe_2O_3 reduction by CO is an exothermic reaction and proceeds spontaneously with self heating.

$$\mathrm{Fe_2O_3 + 3CO \rightarrow 2Fe + 3CO_2}, \qquad \Delta H = -18.4\ \mathrm{kJ/mol} \tag{1.3}$$

CO reduction is advantageous for the ironmaking process in comparison with hydrogen reduction. The reaction is usual in conventional ironmaking. Direct reduction processes for Fe_2O_3, in which CO and H_2 gasses are used directly for the reduction, have been discussed [1]. ACRES based on CO has a high affinity to such conventional processes. The ironmaking process with ACRES is fundamentally a zero CO_2 emission process. This process could be a possible way to reduce CO_2 emission from steel industrial sector.

1.5 Research Scope

1.5.1 Research Proposal

ACRES is an energy transformation system with energy consumption. In conventional chemical, steel, and other high temperature manufacturing industries, CO has a higher affinity to processes than electricity and heat of primary energies. ACRES has the potential applicability in these industries as shown in Fig. 1.5 and still requires efficient technologies for CO_2 recovery through high temperature electrolysis process.

1.5.2 Research Objectives

This thesis work was carried out based on the ACRES concept for CO regeneration via high temperature electrolysis of CO_2. One promising method for CO regeneration in ACRES is CO_2 electrolysis using SOEC. This work aims to study the feasibility of CO_2 electrolysis using tubular yttria stabilized zirconia (YSZ)-based electrolyte. Various electrode materials were tested for cathode and anode of SOEC to perform CO_2 electrolysis under high temperature operating conditions. Given the results of the SOEC experiments, the performance of a combined system with an ACRES-CO_2 reduction system using heat and power generated by an HTGR within an ironmaking system using the most effective SOEC electrode material is evaluated.

References

[1] Y.A. Cengel, M.A. Boles, Thermodynamics: An Engineering Approach, McGraw-Hill, Singapore, 2007.

[2] S.P. Richard, A Techno-Economic Analysis of Decentralized Electrolytic Hydrogen Production for Fuel Cell Vehicles, Ph.D. Thesis at University of Victoria, Victoria, Canada, 2004.
[3] F. Bonciu, L. Poenaru, Kyoto Protocol-A Milestone on the Road to a Low Carbon Economy, *Romanian Economic and Business Rev.*, **3**(2), 7-18, 2008.
[4] A. Kojima, Steel Industry's Global Warming Measures and Sectoral Approaches, *NISTEP Rev. report*, **33**, 55-68, 2009.
[5] Y. Kato, Carbon Recycling for Reduction of Carbon Dioxide Emission from Iron-making Process, *ISIJ Int.*, **50**(1), 181-185, 2010.
[6] A.L. Dipu, J. Ryu, Y. Kato, Carbon Dioxide Ekectrolysis for a Carbon Recycling Iron-making System, *ISIJ Int.*, **52**(8), 1427-1432, 2012.
[7] Y. Kato, T. Obara, I. Yamanaka, S. Mori, A.L. Dipu, J. Ryu, Y. Ujisawa, M. Suzuki, Performance Analysis of Active Carbon Recycling Energy System, Prog. *Nucl. Energy*, **53**, 1017-1021, 2011.
[8] Y. Kato, Hydrogen Utilization for carbon recycling Iron making System, *ISIJ Int.*, **52**(8), 1433-1438, 2012.
[9] S.D. Ebbesen, M. Mogensen, Electrolysis of carbon Dioxide in Solid Oxide Electrolysis Cells, *J. Power Sources*, **193**, 349-358, 2009.
[10] J. Schefold, A. Brisse, M. Zahid, Electronic Conduction of Yttria-stabilized Zirconia Electrolyte Cells Operated in High Temperature Water Electrolysis, *J. Electrochem. Soc.*, **156**(8), B897-B904, 2009.
[11] G. Schiller, A. Ansar, M. Lang, O. Patz, High Temperature Water Electrolysis Using Metal Supported Solid Oxide Electrolyser Cells (SOEC), *J. Appl. Electrochem.*, **39**, 293-301, 2008.
[12] X.Sun, M. Chen, Y-L. Liu, P. Hjalmarsson, S.D. Ebbesen, Durability of Solid Oxide Electrolysis Cells for Syngas Production, *J. Electrochem. Soc.*, **160**(9), F1074-F1080, 2013.
[13] A. Hauch, S.H. Jensen, S. Ramousse, M. Mogensen, Performance and Durability of Solid Oxide Electrolysis Cells, *J. Electrochem. Soc.*, **153**(9) A1741-A1747, 2006.
[14] C. Graves, S.D. Ebbesen, M. Mogensen, Co-electrolysis of CO_2 and H_2O in Solid Oxide Cells: Performance and Durability, *J. Solid State Ionics*, **192**, 398-403, 2011.
[15] S.D. Ebbesen, M. Mogensen, Exceptional Durability of Solid Oxide Cells, *Electrochem. and Solid State Lett.*, **13**(9), B106-B108, 2010.
[16] S.D. Ebbesen, J. Hogh, K.A. Nielsen, J.U. Nielsen, M. Mogensen, Durable SOEC Stacks for production of Hydrogen and Synthesis Gas by High Temperature Electrolysis, *J. Hydrogen Energy*, **36**, 7363-7373, 2011.
[17] X. Zhang, J.E. O'Brien, R.C. O'Brien, G.K. Housley, Durability Evaluation of reversible Solid Oxide Cells, *J. Power Sources*, **242**, 566-574, 2013.

[18] K.R. Sridhar, B.T. Vaniman, Oxygen Production on Mars Using Solid Oxide Electrolysis, *J. Solid State Ionics*, 93, 321-328, 1997.
[19] G. Tao, K.R. Sridhar, C.L. Chan, Study of Carbon Dioxide Electrolysis at Electrode/Electrolyte Interface: Part I. Pt/YSZ Interface, *J. Solid State Ionics*, **175**, 615-619, 2004.
[20] G. Tao, K.R. Sridhar, C.L. Chan, Study of Carbon Dioxide Electrolysis at Electrode/Electrolyte Interface: Part II. Pt-YSZ cermet/YSZ Interface, *J. Solid State Ionics*, **175**, 621-624, 2004.
[21] J.Y. Park, E.D. Wachsman, Lower Temperature Electrolytic Reduction of CO_2 to O_2 and CO with High-Conductivity Solid Oxide Bilayer Electrolytes, *J. Electrochem. Soc.*, **152**(8), A1654, 2005.
[22] X.L. Yan, R. Hino, K. Ohashi, High-Temperature Gas Reactor, in: X.L. Yan, R. Hino (Eds.), Nuclear Hydrogen Production Handbook, 212-289, CRC Press, USA, 2011.

Chapter 2

Carbon Dioxide Electrolysis in SOEC

2.1 Introduction

ACRES with CO regeneration has the potential applicability in ironmaking system. However, it still requires efficient technologies for CO_2 recovery such as high temperature electrolysis of CO_2 using SOEC. At present, SOEC is still under development and gain much interest. The higher operating temperatures in SOEC lead to the electrode kinetic improvement, reduction in electrolyte resistance and reduction in electrical consumption [1]. In practical application, SOEC performs in combination with reverse SOFC in which energy is produced during the process. This chapter discusses the principle of CO_2 electrolysis and reviews of some technical reports on CO_2 electrolysis in SOECs. The originality of the study is emphasized by comparing this work with similar works conducted by other researchers.

2.2 Solid Oxide Electrolysis Cell

SOEC is a solid oxide cell with its electrolyte generally made of YSZ which has good ionic conductivity to support high temperature electrolysis [2,3]. SOEC has been widely used for high temperature electrolysis of steam to produce H_2 which also in the same way can be used for CO_2 electrolysis to produce CO. Geometrically, there are two types of SOECs namely planar, which have the advantages of compactness and tubular; which have the advantage of excellent sealing characteristics [4]. Planar cells are easy to be assembled in

stacks and also current collection is easily applied over the electrodes surface area. However it is required sealing of the cell layers to prevent the cathode and anode products from bypassing the electrolyte. Tubular cells have the advantage in good excellent sealing between layers. The example of planar and tubular cell is given in Fig. 2.1.

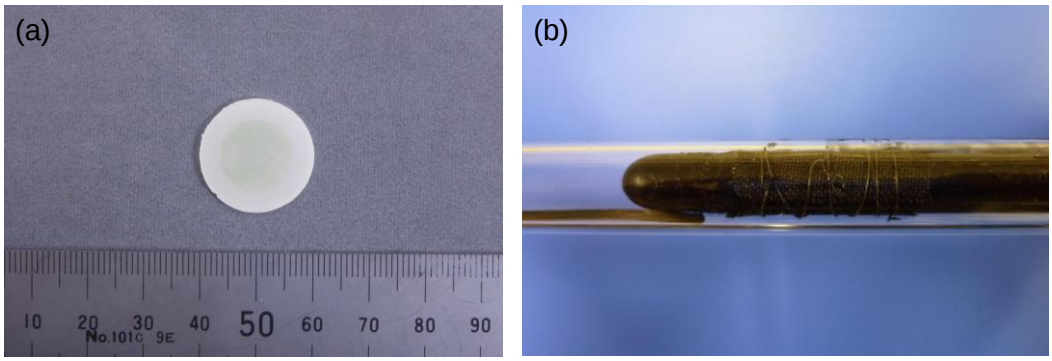

Fig. 2.1 Type of SOEC structure: (a) Planar SOEC (disk diameter of 20 mm) and (b) tubular SOEC (tube diameter of 8.0 mm) manufactured in Kato Lab., Tokyo Tech.

2.3 Component of SOEC

2.3.1 Cathode

Cathode for SOEC should have many properties including high catalytic activity for CO_2 electrolysis which is necessary for the kinetics of the reaction. Besides, the cathode is required to have ionic conductivity which allows the transportation of oxygen ions to the anode-electrolyte interface. Cathode material has to be electrical conductivity in order to convey the electrons produced at cathode to the outside circuit and compatible with electrolyte [5,6]. Platinum (Pt)

is considered as cathode material due to its high temperature stability and catalytic properties. However it must be ruled out due to its high cost. Nickel (Ni) metal is high in catalytic activity and low in cost, but it has evidently thermal mismatch to stabilized Zirconia-based electrolyte. Besides, at high temperature, the metal aggregates by grain growth, finally obstructing the porosity of the cathode and eliminating the active sites for cell operation [5,7]. The use of porous composite of metal and ceramic (cermet) is preferable alternative to single phase metallic material. A cermet which has the Ni catalytic activity and proper thermal match with the stabilized Zirconia-based electrolyte. Perovskite related material is another alternative for cathode material. It has been reported that Perovskite related material worked well as anode in the SOFC mode or as cathode in SOEC [8,9].

2.3.2 Anode

Like the cathode, the anode must possess electronic conductivity, catalytic activity for anodic reaction, and compatibility with electrolyte material. Noble metals such as Pt could be used as the anode material but is not practical in cost-effective commercial cells due to its high cost. Some metal oxides have the required properties for SOEC anode but are much less expensive. Strontium-doped lanthanum manganite (LSM), which shows a good performance in SOFC as a cathode when YSZ is used as an electrolyte, is a commonly favorable material for SOEC anodes [5].

2.3.3 Electrolyte

The electrolyte for SOEC must be stable in both reducing and oxidizing environments, and must have sufficiently high ionic with low electronic conductivity at the cell operating temperature. In addition, the material must be able to be form into a thin, strong film with no gas leaks. Until now, stabilized zirconia, especially YSZ, possessing the fluorite structure has been the most favored electrolyte for SOFCs and SOECs. More recently, a number of other materials, including perovskites and hexagonal structured oxides have also been found to possess good ionic conductivity [10].

2.4 Principle Operation of SOEC

The fundamental working mechanisms for CO_2 electrolysis in SOEC is illustrated in Fig. 2.2. During operation, a sufficient electric potential is applied to the SOEC. CO_2 is fed to the cathode side and diffused through a layer of cathode material to the cathode-electrolyte interface where it is decomposed into CO and oxygen ions (O^{2-}) by the input of electrons (e^-). The CO molecules generated in the cathode side are collected, while the O^{2-} permeate through the dense electrolyte to the anode side. At the anode–electrolyte interface, the O^{2-} are oxidized to form O_2 and e^-. The electrons are transported to the cathode through the external circuit to complete the cycle. The reactions involved in CO_2 electrolysis by an SOEC can be expressed as follows:

Cathode : $CO_2(g) + 2e^- \rightarrow CO(g) + O^{2-}$ (2.1)

Anode : $O^{2-} \rightarrow 1/2O_2(g) + 2e^-$ (2.2)

Total reaction : $CO_2(g) \rightarrow CO(g) + 1/2O_2(g)$ (2.3)

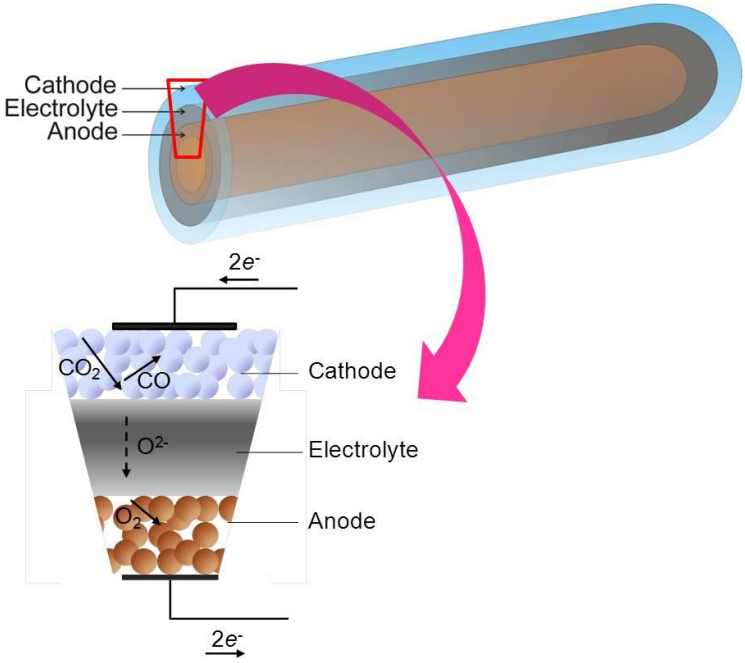

Fig. 2.2 Working mechanism of CO_2 electrolysis in a cross section of SOEC.

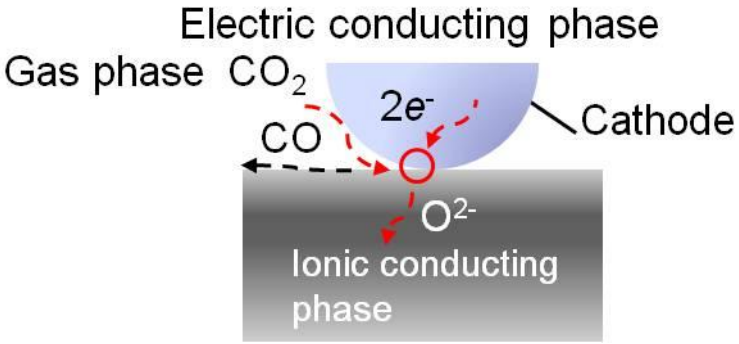

Fig. 2.3 Structure of triple phase boundary.

As illustrated in Fig. 2.3, it is generally believed that CO_2 electrolysis reaction occurs at or very near the triple phase boundary where electronic-conducting phase, ionic-conducting phase, and gas-

phases meet [11]. Based on this idea, electrolysis reaction can be more increased by extending the triple phase boundary area using alternative electrode materials that have both electronic and ionic conducting properties.

2.5 Thermodynamics of CO_2 Electrolysis

The operational temperature of SOCs is in the range of 700-1000°C. As shown in Fig. 2.4, at elevated temperatures a significant part of the heat required for the electrolysis process can be obtained as heat. This provides an opportunity to utilize the inevitably produced joule heat, which is produced due to the passage of electrical current through the cell. This reduces the overall electricity consumption and the kinetics of a SOEC gets increasingly better with increasing temperature due to resistance of SOEC decreases.

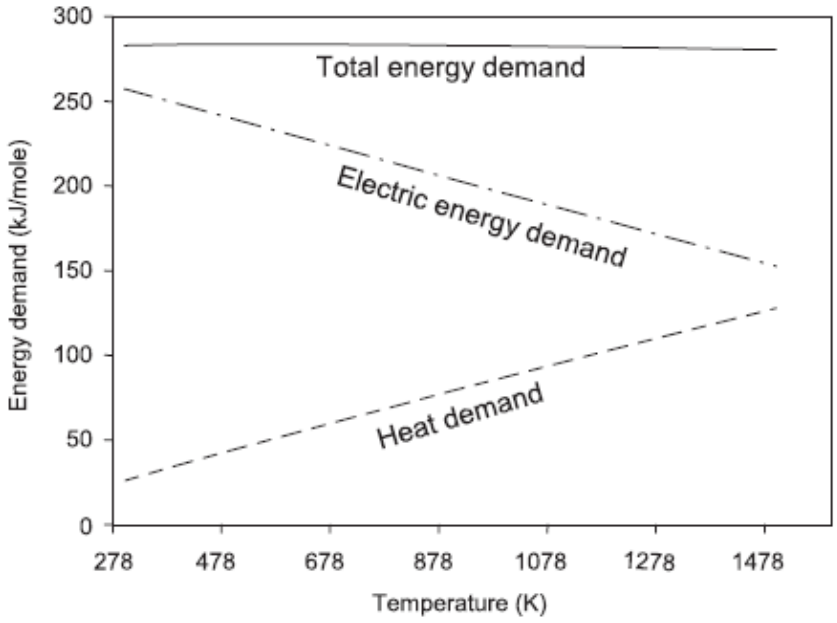

Fig. 2.4 Thermodynamics of CO_2 electrolysis. CO_2 electrolysis becomes increasingly endothermic with temperature [12].

The energy change of the process in Eqs. 2.1. to 2.3. is given by

$$\Delta H = \Delta G + T\Delta S \tag{2.4}$$

Where T is the absolute temperature; ΔH is the enthalpy change; ΔS is the change in entropy; and ΔG is the Gibb's Free Energy, the maximum work for formation of CO_2, or specifically the minimum work required to split CO_2. The term of $T\Delta S$ can be viewed as the amount of thermal energy required to split CO_2 with the minimum of electrical energy, ΔG.

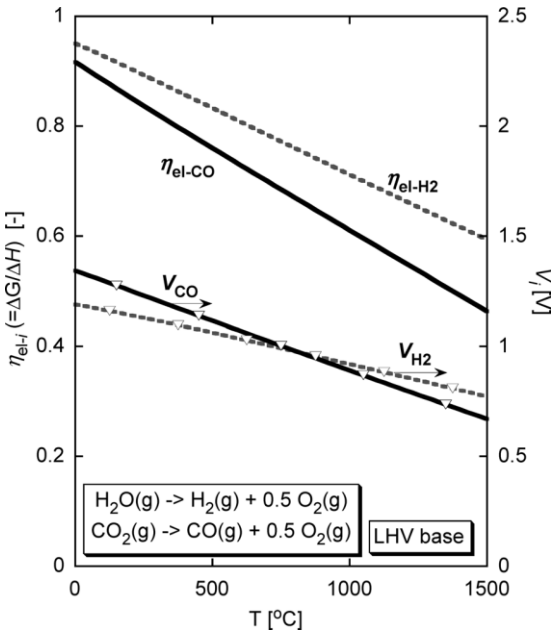

Fig. 2.5 Temperature dependency of electricity consumption ratio for electrolysis and electromotive force for electrolyses of CO_2 and H_2O (LHV base) [13].

The relation between temperature dependencies of electricity consumption ratio for electrolysis and electromotive force, $V_{\mathrm{i}}\,[\mathrm{V}]$ for electrolyses of CO_2 and H_2O in lower heating value (LHV) had been conducted by Kato (eq. 2.5) [13] and the result is depicted in Fig. 2.5.

$$V_{\mathrm{i}} = \frac{-\Delta G_{\mathrm{i}}}{n_{\mathrm{i}} F} \; F = 9.65 \times 10^{4} \; \mathrm{C/mol} \qquad (2.5)$$

With ΔG_{i} $[\mathrm{kJ/mol}]$ corresponds to the electrical energy for electrolysis, n_{i} is the mole number of migrated electrons in a reaction. This figure implies that during electrolysis, the electrical energy consumption of CO_2 electrolysis becomes lower at a higher temperature like H_2O. Electromotive forces of CO (V_{CO}) becomes smaller than that of H_2 $\left(V_{\mathrm{H_2}}\right)$ at a temperature higher than 820 °C. So far, this implies that higher temperature CO_2 electrolysis has a smaller demand for electricity than the H_2O or steam electrolysis.

2.6 Open Circuit Voltage and Cell Polarisation

The open circuit voltage (OCV) also called The Nernst potential is the reversible cell voltage that would exist at a given temperature and partial pressure. Open circuit voltage is produced by the difference in oxygen partial pressure from one side of the cell to the other. The open circuit voltage depends on the temperature, the gas concentration ratio inside the cathode side and the oxygen partial pressure at the anode [14].

The open circuit voltage is a reversible phenomenon that occurs with no external potential load. In an operating cell with an applied potential the system becomes irreversible. This voltage loss is a function of current density and is known as polarisation or overpotential. It can be broken down into a numbers of terms with three dominant polarizations; ohmic polarization or ohmic loss, concentration polarisation and activation polarisation. The concentration and activation polarisations each have a separate

contribution from the cathode and anode portion of the cell [15]. The plot illustrates the different types of polarisations in the operating electrolysis cell is shown in Fig. 2.6.

2.6.1 Ohmic Loss

All matters (except superconductors) give resistance to the motion of electrical charge. The loss due to electrical resistances of the electrodes, electrolyte, wires and interconnections is called ohmic loss. The ohmic loss is dependent on the electrolysis cell materials and geometry. In the most SOEC, the main contribution to ohmic loss is from the electrolyte since its ionic resistivity is much greater than electronic resistivity of the cathode and the anode. The ohmic polarisation is proportional to the current density and has a linear response.

2.6.2 Concentration Polarisation

In SOEC, the reacting species are gaseous and must be transported through the porous electrode materials. The physical resistance to the transport of the gases through the electrodes at a given current density is reflected in the cell performance as an electrical voltage loss. This loss is the concentration polarisation. The concentration polarisation is mainly caused by a low gas concentration at the cathode. The concentration polarisation is a function of the diffusivities of the gas species, the electrode microstructure, the partial pressures of the gases and the current density and has a non linear response [15].

2.6.3 Activation Polarisation

Electrode reactions involve charge transfer as fundamental step, wherein a neutral step species is converted into an ion, or an ion is converted into a neutral species. The external energy required to overcome the maximum activation energy barrier in order to maintain the electrode reaction is called activation polarisation. The electrode reaction can have several possible reaction schemes such as:

(1) surface adsorption of gaseous species

(2) dissociation of adsorbed molecules to adsorbed atoms

(3) surface diffusion to three-phase boundaries

(4) formation of ions by electron transfer and incorporation of ions into electrolyte.

The rate of the electrode reaction is proportional to the current density. The activation polarization is a function of material properties and microstructure, temperature, atmosphere, and current density [14,15].

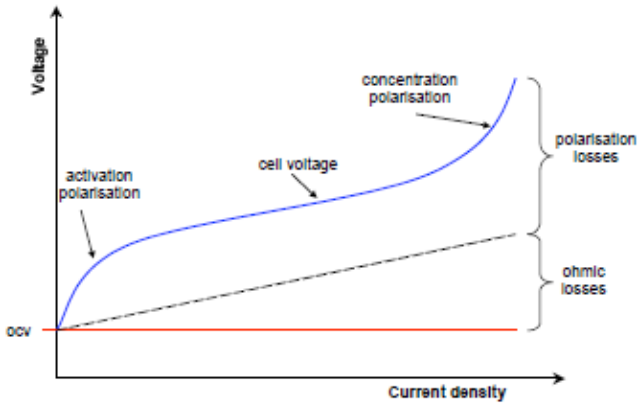

Fig. 2.6 Irreversible losses as a function of current density. A plot illustrates the different types of polarisations in the operating SOEC [15].

2.7 Reviews of CO_2 Electrolysis in SOECs

Up to now, there are only limited studies have been reported for CO_2 electrolysis where mainly Pd, Pt and Ni are used. There have been several studies on the use of CO_2 electrolysis to produce propellant and life-support consumables for space missions using SOECs at high temperatures. For production of O_2, CO was treated as an undesired product and converted back into CO_2 and to be recycled again. Planar cell with Pt electrodes was used by Sridhar and Vaniman to study the performance characteristics of a SOEC for O_2 production from CO_2 electrolysis. Cell exhibited no noticeable degradation in performance for up to 2000 h with operating temperature of 750-1000 °C [16]. Since the thermodynamic stability of CO_2 prevents conversion to other molecules and CO_2 electrolysis involves complicated processes a thorough study of CO_2 electrolysis kinetics was done by Tao et al. to fully understand the electrochemical reaction mechanisms [17,18]. The results demonstrated that the current density was improved by using Pt-YSZ cermet electrodes. Both the ohmic resistance and activation overpotential at the anode decreased significantly for the Pt-YSZ cermet electrodes. It was suggested that the contact resistance and the electrode delamination were greatly reduced. List of electrode materials used in the experiment by Sridhar and Vaniman and Tao et al. is given in Table 2.1. Results from the experiments are summarized in Table 2.2. Fig. 2.7 shows the illustration of a solid oxide electrolysis cell assembly used in the experiment by Tao et. al.

Table 2.1 List of electrode materials used in the experiment by Sridhar and Vaniman and Tao et al. [16-18].

Component	Material
Cathode	Pt [18,19], Pt-YSZ [20],
Anode	Pt [18,19], Pt-YSZ [20]
Electrolyte	YSZ (8% Y_2O_3) [18-20]

Table 2.2 Major results obtained in the experiments by Sridhar, Vaniman and Tao et al. [16-18].

Cell Structure Cathode|Electrolyte|Anode	Temperature [°C]	Voltage [V]	Current [mA]
Pt|YSZ|Pt [18]	750	1.80	51
Pt|YSZ|Pt [19]	750	1.95	33
Pt-YSZ|YSZ|Pt-YSZ [20]	750	1.95	90

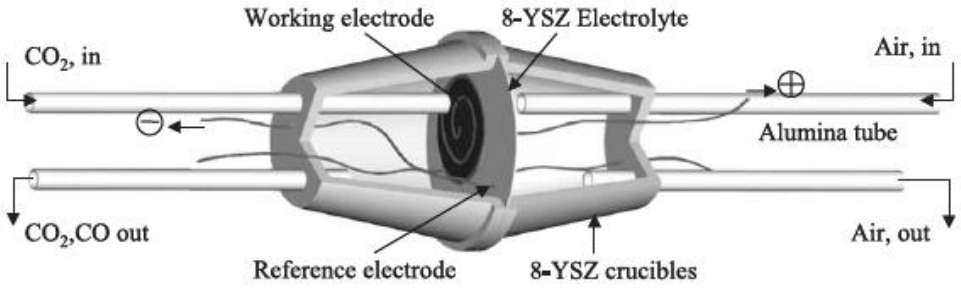

Fig. 2.7 Illustration of a solid oxide electrolysis cell assembly used in the experiment by Tao et. al. [19].

Using SOECs for recycling or reuse of CO_2 from energy systems or CO_2 captured from air also an attractive alternative idea to storage of

CO_2 and would provide CO_2 neutral hydrocarbon fuels. A study to examine the feasibility of CO_2 electrolysis in Ni-based SOECs was conducted by Ebessen and Mogensen [19]. This study showed that long term CO_2 electrolysis was possible in SOEC with nickel electrodes. The passivation rate of the SOEC obtained was in between 0.22 and 0.44 mV/h when operated in mixtures of CO_2/CO = 70/30 or CO_2/CO = 98/02 for industrial grade at 850 °C and current densities between – 0.25 and -0.50 A/cm^2. The passivation rate was independent of the current density and irreversible when operated at conditions that would oxidize carbon. In addition, this study showed that the passivation was not caused by coke formation and partly reversible when introducing H_2. It was predicted that the passivation might be a consequence of impurities in the gas stream, most likely sulphur, adsorbing on some specific nickel sites in the cathode of the SOEC. Reactivation of the cell could be achieved by introducing H_2 which reacted with adsorbed sulphur to form the volatile compound H_2S which in turn was removed by gas stream. Fig. 2.8 shows the assembly of cell and gas distributor plates in a cross flow pattern used in the experiment by Ebbesen and Mogensen.

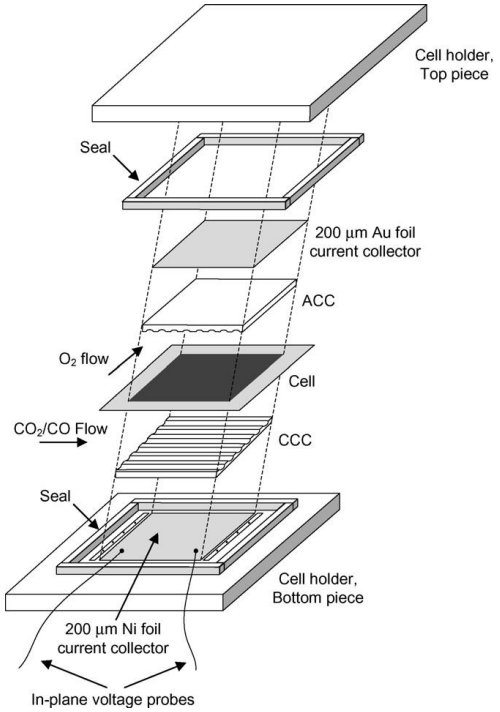

Fig. 2.8 The assembly of cell and gas distributor plates in a cross flow pattern used in the experiment by Ebbesen and Mogensen [19,20].

The use of Ni, raise concerns of Ni oxidation under high CO_2 concentration which is harmful for long term operation. As suggested by Yue and Irvine, Ceria has good catalytic properties toward CO_2 reduction and has also been considered to have good resistance to coking, hence may be a promising cathode materials component for CO_2 electrolysis [21].

Ni/YSZ cermet, $(La_{0.75}Sr_{0.25})_{0.97}Cr_{0.5}Mn_{0.5}O_{3-\delta}$ (LSCM)/YSZ composite and LSCM/ $Gd_{0.1}Ce_{0.9}O_{2-\delta}$ (GDC) composite were employed for high temperature electrolysis of CO_2. Differences were observed between the impedance spectra of these three cathodes, implying different rate limiting processes on these cathodes. Ni-YSZ cathode exhibited lower polarization resistance (Rp) with increasing CO

concentration and higher Rp when CO content reached up to 50%, probably due to carbon deposition on Ni surface, which limits its application in CO_2 electrolysis.

The Rp of the LSCM/YSZ cathode at OCV was twice as that of Ni/YSZ, indicating insufficient activity toward CO_2 reduction. Compared with the LSCM/YSZ cathode, the LSCM/GDC cathode displayed lower performance at OCV while higher performance under load probably due to the reduction of GDC which enhanced the cathode activity. In addition, the LSCM/GDC cathode showed stable performance in the 200 h test for CO_2 reduction, suggesting a promising alternative cathode material for CO_2 electrolysis by SOEC.

Another alternative cathode and electrolyte material for SOEC was Ni-Fe cathode and $La_{0.9}Sr_{0.1}Ga_{0.8}Mg_{0.2}O_3$ (LSGM) electrolyte. By comparing pure Ni and other Ni-based metallic cathodes, Wang et al. found that a Ni–Fe cathode showed a superior performance for CO_2 electrolysis. This observation was attributed to Fe suppressing Ni particle growth, thus retaining smaller metal particles. The formation rate of CO was slightly lower than the consumption rate of CO_2, suggesting coke formation during the initial period. However, stable CO_2 electrolysis could be performed for at least 12 h, and Fe addition was effective for increasing long-term stability of electrolysis [22].

2.8 Research Originality

As described in the section 2.7, some CO_2 electrolysis processes were carried out with O_2 as the main product with CO production to be considered as an undesired side product and need to be converted

back into CO_2 [16-18]. Another investigations were carried out which mainly focused on the feasibility of CO_2 electrolysis using state of the art SOEC technology for fuel production [19,21,22]. This thesis work was carried out based on the ACRES concept for CO regeneration. One promising method for CO regeneration in ACRES is CO_2 electrolysis using SOEC. Table 2.3 provides comparison between this thesis work similar works by other researchers in the field of CO_2 electrolysis.

Table 2.3 Comparison between this work and similar works by other researchers.

Researcher	Cell type	Cell structure	Aim of study
Sridhar and Vaniman	Planar	Pt|YSZ|Pt	Performance characterization of CO_2 electrolysis for O_2 production used in space mission.
Tao et al.	Planar	Pt|YSZ|Pt	Study on the mechanisms of CO_2 electrolysis by SOEC to produce O_2 from CO_2 for the application of human exploration to Mars.
Tao et al.	Planar	Pt-YSZ|YSZ|Pt-YSZ	Improvement of SOECs performance by mixing Pt with YSZ. This study also aims to reduce the anode activation overpotential and the anode ohmic resistance.
Ebbesen and Mogensen	Planar	Ni-YSZ|YSZ|LSM-YSZ	Study on the mechanism of SOECs degradation during CO_2 electrolysis.
Yue and Irvine	Planar	Ni-YSZ|YSZ|LSM-ScSZ, LSCM-YSZ|YSZ|LSM-ScSZ, LSCM-GDC|YSZ|LSM-ScSZ	Study on alternative cathode materials for CO_2 electrolysis and their CO_2 reduction kinetics.
Wang et al.	Planar	Ni|LSGM|BLC Ni-Fe|LSGM|BLC NiCu|LSGM|BLC NiCo|LSGM|BLC NiPt|LSGM|BLC NiRu|LSGM|BLC	Study on performance of Ni-Fe bimetallic cathode for intermediate temperature electrolysis of CO_2.
A.L. Dipu (this thesis work)	Tubular	LSM|YSZ|LSM Pt|LSM|YSZ Pt-LSM|YSZ|Pt-LSM, Ni-LSM|YSZ|LSM-YSZ Ni-YSZ|LSM|YSZ	Study on CO_2 electrolysis in SOECs for CO regeneration in ACRES.

ScSZ = Scandium stabilized zirconia, LSCM = $(La_{0.75}Sr_{0.25})_{0.97}Cr_{0.5}Mn_{0.5}O_{3-\delta}$, GDC = $Gd_{0.1}Ce_{0.9}O_{2-\delta}$, LSGM = $La_{0.9}Sr_{0.1}Ga_{0.8}Mg_{0.2}O_3$, BLC = $Ba_{0.6}La_{0.4}CoO_3$

References

[1] P.K. Lohsoontorn, D.J.L. Brett, N. Laosiripojana, Y.M. Kim, J.M. Bae, Performance of Solid Oxide Electrolysis Cells Based on Composite $La_{0.8}Sr_{0.2}MnO_{3-\delta}$–Yttria Stabilized Zirconia and $Ba_{0.5}Sr_{0.5}Co_{0.8}Fe_{0.2}O_{3-\delta}$ Oxygen Electrodes, *J. Hydrogen Energy*, **35**, 3958-3966, 2010.

[2] Meng Ni, Modeling of a Solid Oxide Electrolysis Cell for Carbon Dioxide Electrolysis, *Chem. Eng. Journal*, **164**, 246-254, 2010.

[3] J. Udagawa, P. Aguiar and N.P. Brandon, Hydrogen Production through Steam Electrolysis: Model-Based Steady-State Performance of a Cathode-Supported Intermediate Temperature Solid Oxide Electrolysis Cell, *J. Power Sources*, **166**, 127–136, 2007.

[4] E. Resch, Numerical and Experimental Characterization of Convective Transport in Solid Oxide Fuel Cells, MSc Thesis at Queen's University, Kingston, Canada, 2008.

[5] X. Yang, Cathode Development for Solid Oxide Electrolysis Cells for High Temperature Hydrogen production, PhD Thesis at University of St. Andrews, UK, 2010. Available online at: http://hdl.handle.net/10023/979

[6] H. Yokokawa, T. Horita, Cathodes, in: S.C. Singhal, K. Kendall (Eds.), High temperature Solid Oxide Fuel Cell-Fundamentals, Design and Application, 119-147, Elsevier, Netherland, 2009.

[7] A. McEvoy, Anodes, in: S.C. Singhal, K. Kendall (Eds.), High temperature Solid Oxide Fuel Cell-Fundamentals, Design and Application, 148-171, Elsevier, Netherland, 2009.

[8] S. Tao, J.T.S. Irvine, A Redox-stable Efficient Anode for Solid-Oxide Fuel Cells, *Nature Materials*, **2**, 320-322, 2003.

[9] S.P. Jiang, X.J. Chen, S.H. Chan, J.T. Kwok, K.A. Khor, *J. Solid State Ionics*, **177**, 149-157, 2006.

[10] T. Ishihara, N.M. Sammes, O. Yamamoto, Cathodes, in: S.C. Singhal, K. Kendall (Eds.), High temperature Solid Oxide Fuel Cell-Fundamentals, Design and Application, 83-117, Elsevier, Netherland, 2009.

[11] R.D. Green, Carbon Dioxide Reduction on Gadolinia-doped Ceria Cathodes, PhD Thesis at Case Western Reserve University, 2010.

[12] S.H. Jensen, P.H. Larsen, M. Mogensen, Hydrogen and Synthetic Fuel Production from Renewable Energy Sources, *J. Hydrogen Energy*, **32**, 3253-3257, 2007.

[13] Y. Kato, Carbon Recycling for Reduction of Carbon Dioxide Emission from Iron-making Process, *ISIJ Int.*, **50**(1), 181-185, 2010.

[14] J. Larminie, A. Dicks, Fuel Cell Systems Explained, John Wiley & Sons, England, 2003.

[15] K.L. Eccleston, Solid Oxide Steam Electrolysis for High Temperature Hydrogen Production, PhD Thesis at University of St. Andrews, UK, 2007. Available online at: http://hdl.handle.net/10023/322

[16] K.R. Sridhar, B.T. Vaniman, Oxygen Production on Mars using Solid Oxide Electrolysis, *J. Solid State Ionics*, **93**, 321-328, 1997.
[17] G. Tao, K.R. Sridhar, C.L. Chan, Study of Carbon Dioxide Electrolysis at Electrode/Electrolyte Interface: Part I. Pt/YSZ Interface, *J. Solid State Ionics*, **175**, 615-619, 2004.
[18] G. Tao, K.R. Sridhar, C.L. Chan, Study of Carbon Dioxide Electrolysis at Electrode/Electrolyte Interface: Part II. Pt-YSZ cermet/YSZ Interface, *J. Solid State Ionics*, **175**, 621-624, 2004.
[19] S.D. Ebbesen, M. Mogensen, Electrolysis of Carbon Dioxide in Solid oxide Electrolysis Cells, *J. Power Sources*, **193**, 349-358, 2009.
[20] M. Mogensen, P.V. Hendriksen, in: S.C. Singhal, K. Kendall (Eds.), High temperature Solid Oxide Fuel Cell-Fundamentals, Design and Application, 261-289, Elsevier, Netherland, 2009.
[21] X. Yue, J.T.S. Irvine, Alternative Cathode Material for CO_2 Reduction by High Temperature Solid Oxide Electrolysis Cells, *J. Electrochem. Soc.,* **159**(8)*,* F442-F448, 2012.
[22] S. Wang, A. Inoshi, J-E, Hong, Y-W Ju, H. Hagiwara, S. ida, T. Ishihara, Ni–Fe Bimetallic Cathodes for Intermediate Temperature CO_2 Electrolyzers Using a $La_{0.9}Sr_{0.1}Ga_{0.8}Mg_{0.2}O_3$ Electrolyte, *J. Mater. Chem. A*, **1**, 12455-12461, 2013.

Chapter 3

Basic Studies on Carbon Dioxide Electrolysis in YSZ-based Electrolyte

3.1 Introduction

One promising method for CO regeneration in ACRES is CO_2 electrolysis using SOEC. To that end, experimental studies had been carried out to study the feasibility of CO_2 electrolysis in SOECs and to investigate the effect of some electrolysis characteristic indicators to the performance of SOECs. This chapter presents basic studies on CO_2 electrolysis in YSZ-based electrolyte using several cathode and anode materials namely $La_{0.8}Sr_{0.2}MnO_3$ (LSM), Pt and combination of Pt-LSM in cermet form. Cells' electrolytic characteristics were evaluated in relation with current density, temperature, CO and O_2 production rates.

3.2 Experimental

An experimental apparatus was constructed to support the study on CO_2 electrolysis in tubular SOECs (Fig. 3.1). This test apparatus enabled the use of the following gasses to the cathode side: CO_2, CO, H_2 and Ar while O_2 and N_2 to the anode side. The test apparatus was placed in the experiment room equipped with H_2 detector and CO detector. CO effluent gas from gas chromatographs columns after analysis was channeled out via a tube to atmosphere.

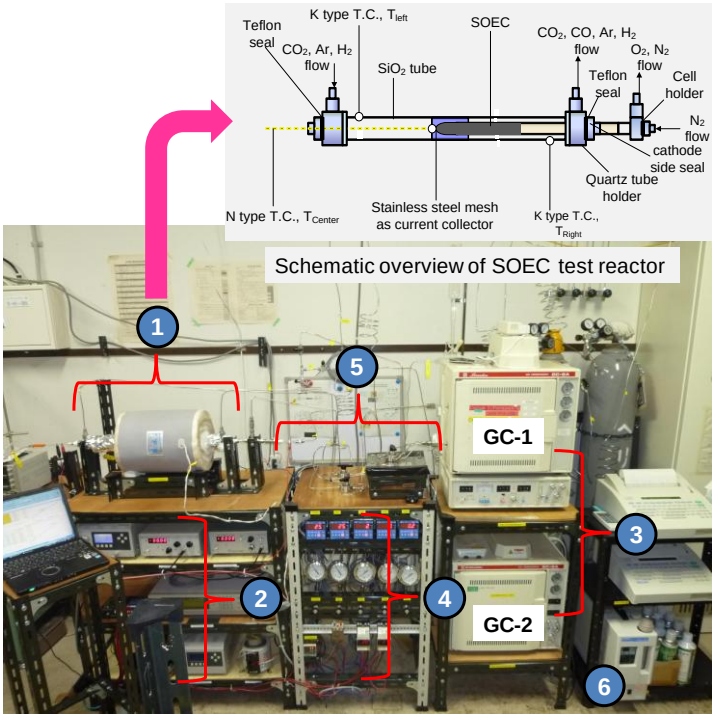

(1) SOEC test reactor

(2) Data logger and electrochemical equipment

(3) Regulator and controller system

(4) Gas chromatographs (GC-1 and GC-2)

(5) GC valve system

(6) Hydrogen generator

Fig. 3.1 Experimental SOEC apparatus for CO_2 electrolysis.

3.2.1 SOEC Test Reactor Setting Up

The illustration of test reactor where the CO_2 electrolysis reaction occurs is shown in Fig. 3.2 and its photograph is given in Fig. 3.1. In this work, stainless steel mesh (SUS 304, 100 mesh) was used as current collector and placed well on the surface of cathode and anode with size of 5.0 cm^2 and 3.0 cm^2 respectively. This current collector assured an equi-potential at each electrode. Electric current was supplied to the cell using a Galvanostat (HAL 3001, Hokuto Denko).

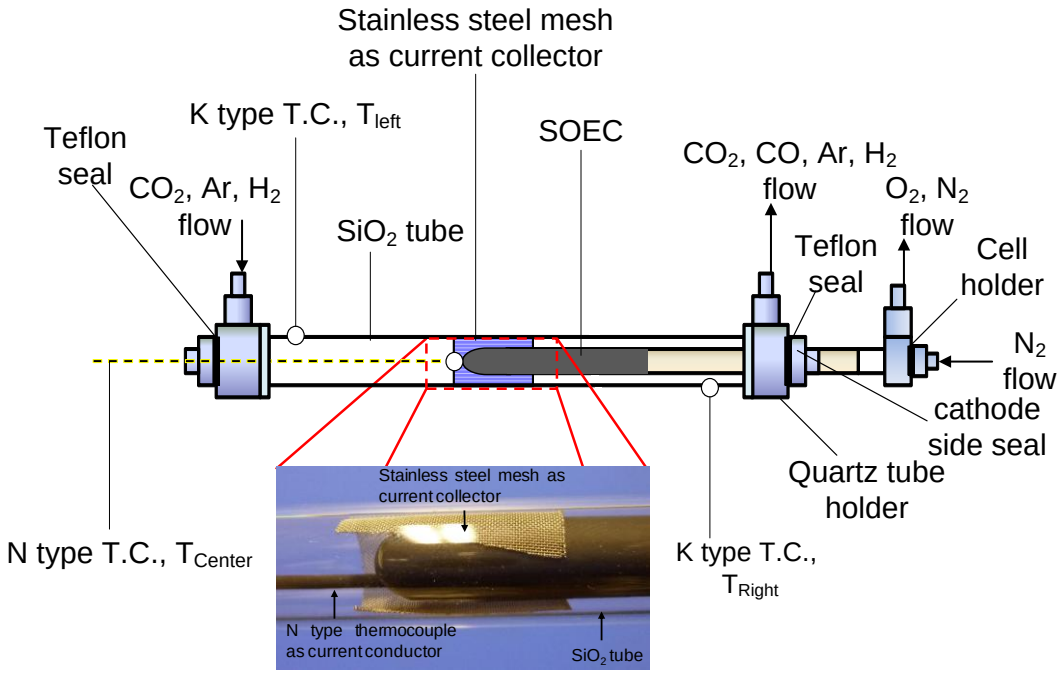

Fig. 3.2 SOEC test reactor: gas tubes inlet and outlet, thermocouples and current collector.

SiO_2 tube and cell were attached well in the tube holder and cell holder respectively. Holders are made of stainless steel (Swagelok). Two K type thermocouples (diameter of 1.0 mm, Yamari Ltd.) were placed on the right and the left side of the SiO_2 tube with aimed to monitor the temperature changed nearby teflon sealing and keeping below its melting point (Fig. 3.2). N type thermocouple (diameter of 1.6 mm, Yamari Ltd.) was inserted on top of the cell to measure the temperature near the active area of the cell and also functioned as a current conductor. It was set to attach the steel mesh (current collector) which was placed carefully surrounded the cathode and anode surface after placing cell inside the SiO_2 tube (Fig. 3.2). Besides, this N type thermocouple was used to measure the temperature of

feed gas (the mixture of CO_2 and Ar) nearby the triple phase boundary. Feed gas was fed to the cell via a tube in the left top of the SiO_2 tube holder. Products of cathode side (mixture of Ar, CO and CO_2) were carried away by carrier gas (Ar) to the gas chromatograph number 1 (GC-1) via a gas outlet tube located on the top right of the SiO_2 tube holder. N_2 was fed to the anode side via the small tube located inside the cell (anode side). O_2 as the byproduct of electrolysis was carried away to the gas chromatograph number 2 (GC-2) to be analyzed.

3.2.2 Data Communication and Data Logging System

Gas mass flow rates were controlled by digital mass flow controllers (Kofloc 3660) and connected via flow meters (Kofloc CR 300) as shown in Fig. 3.1-4. All gas pressure was kept constant at 0.1 MPa using pressure regulators. An electric heater (Tokyo Technological Labo) was used as heater for heating. The heater temperature was controlled by a temperature controller unit (SR 91, Shimaden). Several thermocouples (Yamari Ltd.) were used to log temperatures such as T_{center}, T_{right}-T_{left} (described in the Fig. 3.2.) and they were connected via Ni-Cr/Mg wire (N type) and Ni-Cr/Mn (K type) wires respectively to a screw terminal. Ni-Cr/Mg wire was connected to Galvanostat and functioned as current conductor. DC current load to the cell was controlled by the Galvanostat. Data, such as temperatures (T_{center}, T_{right}, T_{left}.), cell voltage and current were logged and stored on a midi data logger system (GL 200A, Graphtec) every one second. The data stored in data logger was in the Microsoft Excel

format which could be directly transferred to the personal computer via external USB mass storage device for further analysis (Fig. 3.1-4).

3.2.3 Current Density vs. Cell Voltage Curve

Current density vs. cell voltage was performed by recording currents at various temperatures under gas constant flow rate of 25 mL/min in the cathode and anode side (Table 3.3). Current density was obtained by dividing the measured current with geometric surface area of the cell (25.1 cm^2). Voltage limit of 2.0 V was applied in this study.

3.2.4 Gas Chromatograph with Thermal Conductivity Detector

Two gas chromatographs (GC-8A, Shimadzu) equipped with thermal conductivity detector (TCD) were used for gas chromatography analysis. Tube connections were made to connect cathode side and anode side from the SOEC test reactor to GC-1 and GC-2 for gas species analysis (Fig. 3.1-3). These connections equipped with three 5-way valves (Fig. 3.1-5). Two columns were used for gas species separator namely Porapak Q (PPQ) and Molecular Sieve 13X (MS 13X) both with He as carrier gas. Separation of CO_2 from (Ar-CO mixture) was occurred in the 2.0 m long of PPQ column in GC-1 while the MS 13X column of 4.0 m long could identify gas of Ar, CO, N_2 and O_2. Figures 3.3a to 3.3f show gas species separation technique applied to GC-1 and GC-2.

In Fig. 3.3a 5-way valve (valve-A1 condition) was in the closed loop condition and no gas sample was being analyzed in GC-1. Fig.

3.3b shows 5-way valve was turned into an opened loop condition (valve-A2 condition). Amount of gas sample was being analyzed in GC-1. CO_2 was then separated well inside the PPQ column from the mixture of Ar and CO. By the time CO and Ar reached MS 13X column, they were separated and contained well for several minutes inside the column to let CO_2 to be analyzed by TCD. This condition was obtained by turning 5-way valve into valve-B2 condition (Fig. 3.3c). After CO_2 had been analyzed by TCD, 5-way valve was turned back into valve-B1 condition to allow Ar and CO to be analyzed by TCD (Fig. 3.3d). In the case of anode side, N_2 and O_2 gas were separated well inside the MS 13X column in GC-2 after 5-way valve was turned into valve-C2 condition (Fig 3.3f).

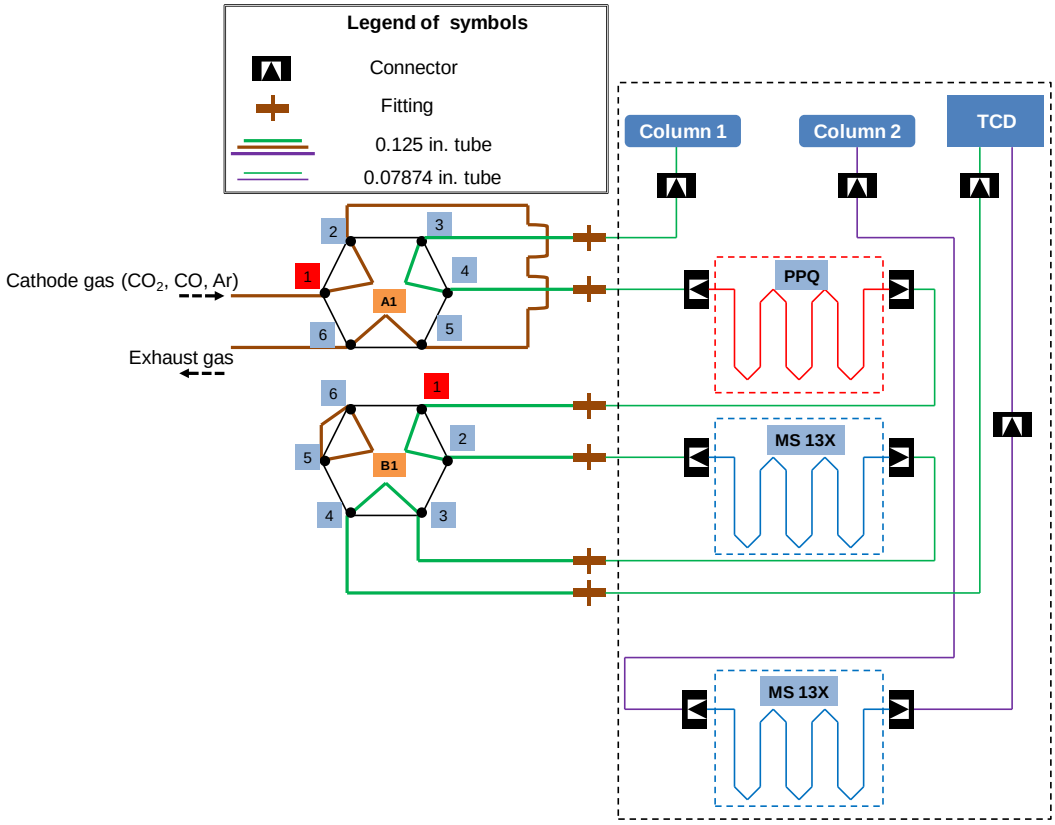

Fig. 3.3a 5-way valve is in the closed loop condition (valve-A1 condition). Arrow indicates the flow direction of gas stream.

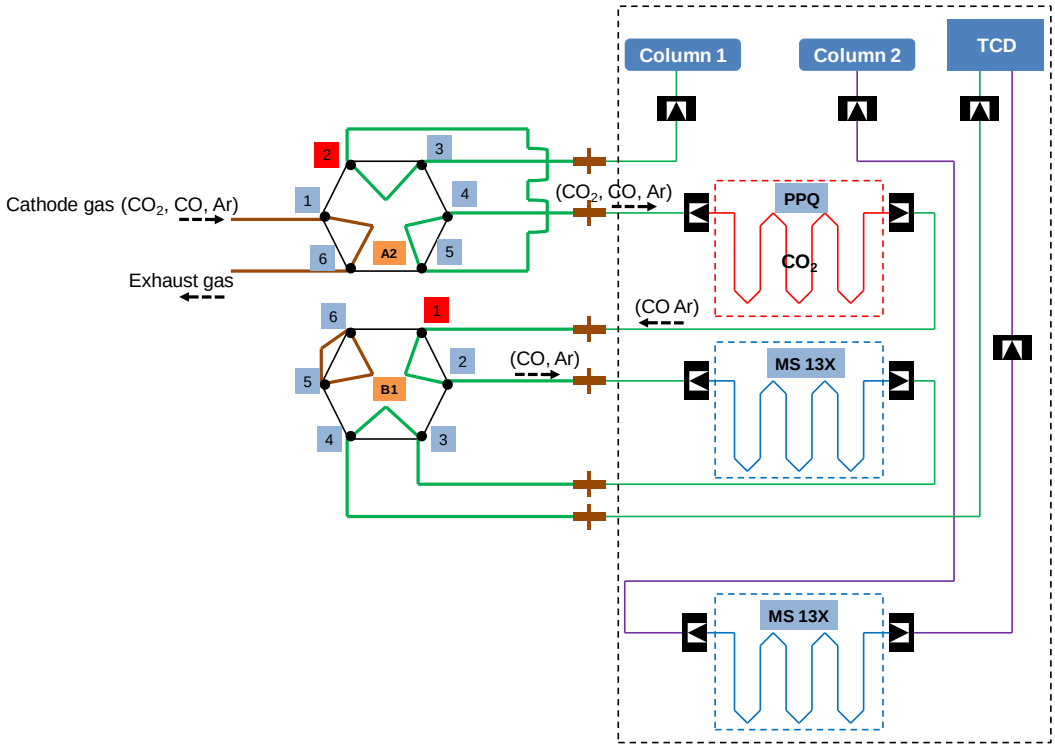

Fig. 3.3b 5-way valve is in the opened loop condition (valve-A2 condition). CO_2 was separated from the mixture gas (Ar, CO) in GC-1. Arrow indicates the flow direction of gas stream.

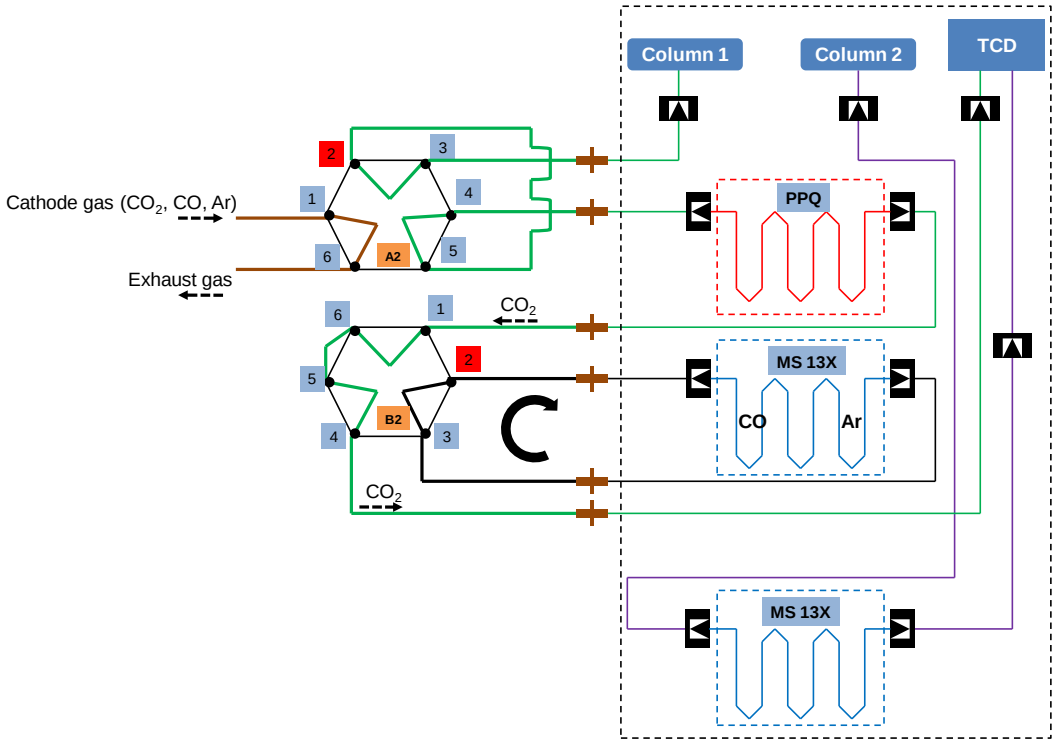

Fig. 3.3c 5-way valve is in the valve-B2 condition. CO and Ar were separated inside the MS 13X column and CO_2 was analyzed by TCD in GC-1. Arrow indicates the flow direction of gas stream.

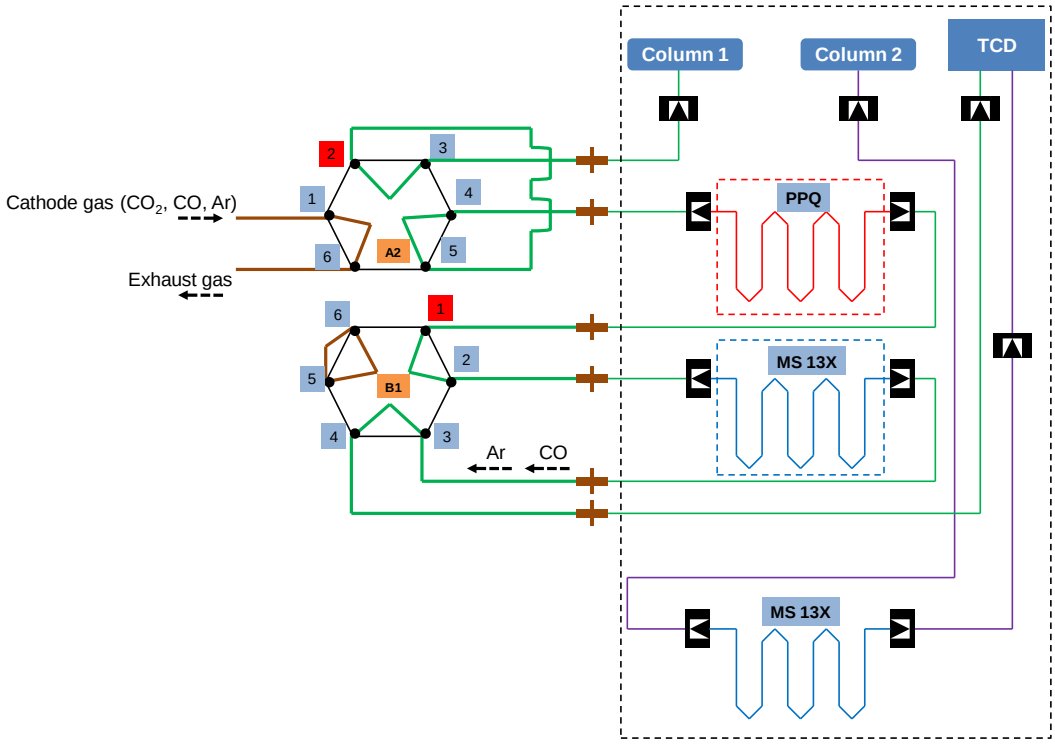

Fig. 3.3d Ar and CO were identified by TCD in GC-1. Arrow indicates the flow direction of gas stream.

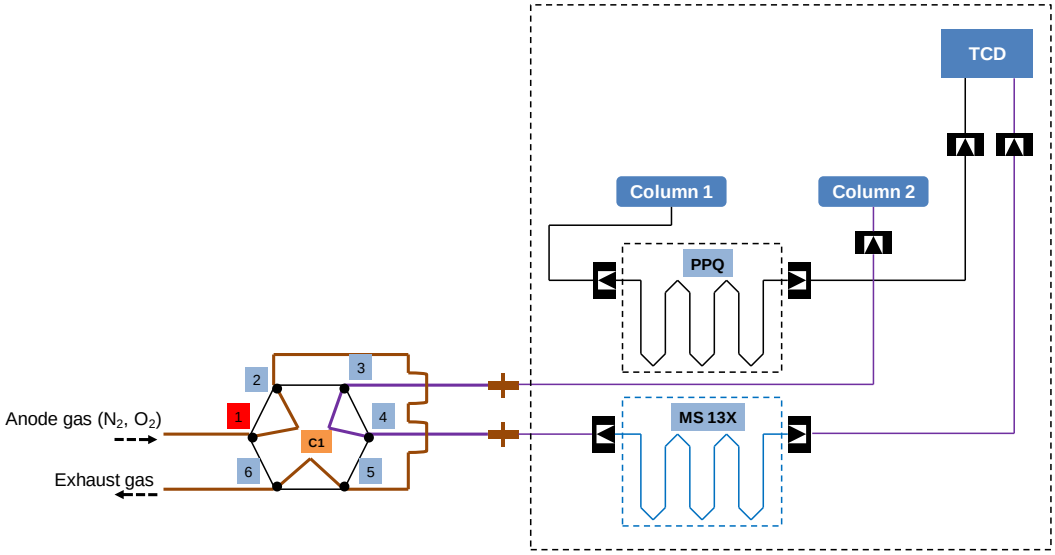

Fig. 3.3e Closed loop condition at GC-2. No gas was being analyzed. Arrow indicates the flow direction of gas stream.

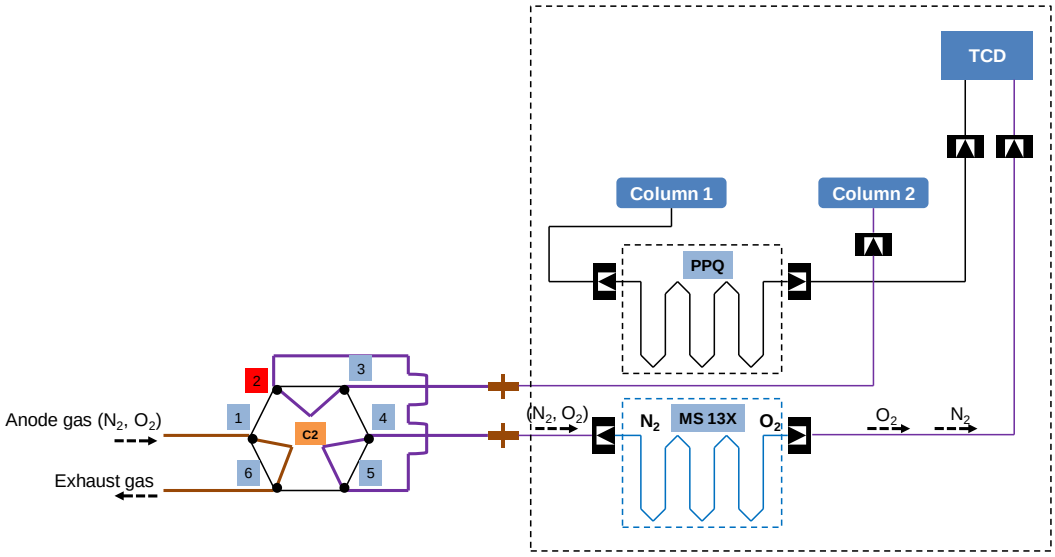

Fig. 3.3f Opened loop condition at GC-2 (valve-C2 condition). N_2 and O_2 were separated inside the MS 13X column. Arrow indicates the flow direction of gas stream.

In this study, the total volume of analyzed gas was 1.14 mL. The percentage of each gas contained in the mixture was analyzed by using mass balance equation.

$$\dot{m}_{\text{in}} = \dot{m}_{\text{out}} \tag{3.1}$$

$$\left[\dot{m}_{\text{CO}_2} + \dot{m}_{\text{Ar}}\right] = \left[\dot{m}_{\text{CO}_2} + \dot{m}_{\text{CO}} + \dot{m}_{\text{Ar}} + \dot{m}_{\text{O}_2} + \text{ carbon layer}\right] \tag{3.2}$$

With $\dot{m}_{\text{i}}\ [\text{mL/min}]$ is gas flow in and out of the test reactor.

3.2.5 YSZ-based Electrolyte

Up to now, stabilized zirconia, especially YSZ has been the most favored electrolyte for SOFCs and SOECs. Pure zirconia (ZrO_2) has a monoclinic structure up to a temperature of about 1446 K, and transforms to the tetragonal modification [1]. This high temperature transformation can be partially or completely stabilized by doping with some metal oxide such as yttria (Y_2O_3), calcia (CaO), or magnesia

(MgO). Yttria is the most commonly used dopant for stabilizing the cubic phase of zirconia. A fully cubic stabilized zirconia is obtained with a Y_2O_3-content of > 7mol% [2]. Cubic stabilized zirconia has improved mechanical and thermal properties such as high strength, toughness, and thermal-shock resistance. Yttria stabilized by zirconia is popular as electrolyte material caused by its constituent provides good ionic conductivity during electrolysis process [3]. Doping with yttrium, which has a lower valence (+3) compared to zirconium (+4), produces oxygen vacancies in the crystal lattice. This allows oxygen ion conductivity during electrolysis process. The conductivity of YSZ electrolyte depends on the operating temperature as indicated in Fig. 3.4 [4].

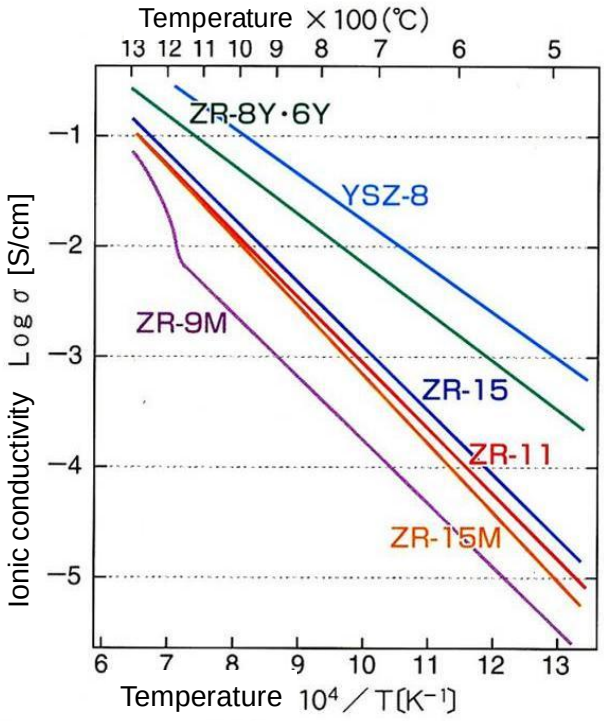

Fig. 3.4 Temperature vs. ionic conductivity of YSZ electrolyte [4].

Table 3.1 YSZ Electrolyte specifications.

Length [mm]	300
Inner Diameter [mm]	8.0
Outer Diameter [mm]	5.0
Density [g/cm^3]	5.4
Coefficient of Thermal Expansion [20 ~ 1,000] x 10^{-6}/K	10.2

The commercially tubular YSZ electrolyte, ZR-8Y (Nikkato Corp.) was used in this study (Fig. 3.5). Tubular electrolyte was chosen due to its advantage that its geometry resulted in an inherent seal between layers and prevent cathode side product and anode side product crossover the electrolyte. The specification of YSZ electrolyte cell used in this study is listed in Table 3.1. Fig. 3.6 shows the scanning electron microscope (SEM) micrograph of dense YSZ electrolyte which allows only O^{2-} ions to permeate.

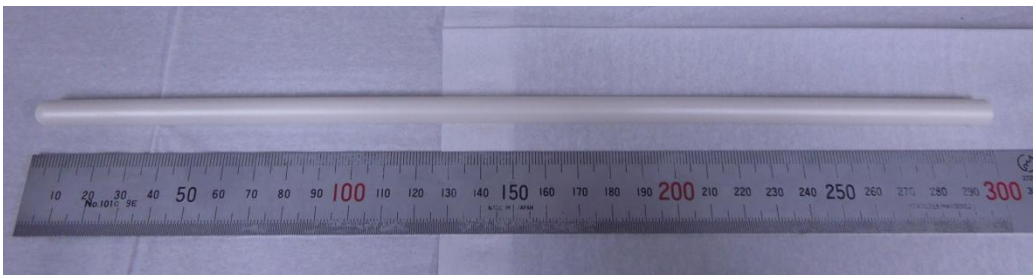

Fig. 3.5 Tubular YSZ electrolyte.

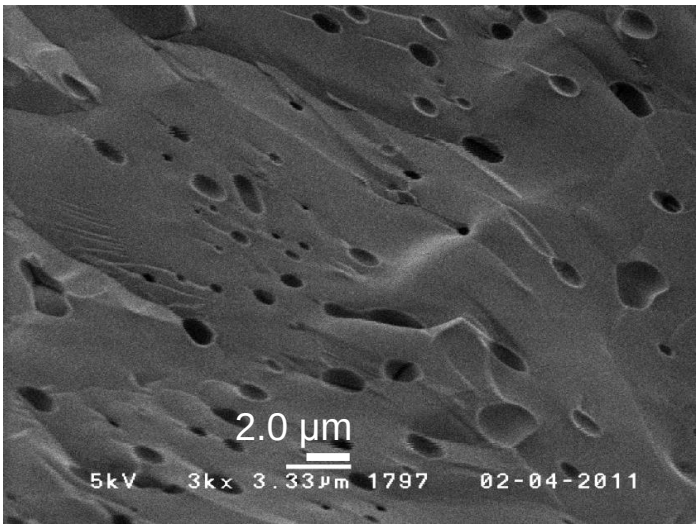

Fig. 3.6 SEM micrograph of dense YSZ electrolyte.

3.2.6 LSM|YSZ|LSM Cell preparation

LSM is widely used as the cathode material for SOECs or SOFCs and displays good thermal and chemical stability [3]. During electrolysis process, LSM provides electron conductivity for electrode. SEM micrograph of LSM powder with 1.0 µm long in particle diameter is shown in Fig. 3.7. In this work, LSM paste was prepared by mixing together of 10 g LSM powder (Powlex), 1.0 mL binder (Toagosei Ltd.), 2.0 mL dispersant (Toagosei Ltd.) and 5.0 mL distilled water at room temperature in the 50 mL beaker. Binder and dispersant were added to the mixture to improve the adhesion to the electrolyte substrate and to adjust viscosity. The mixture components dispersed thoroughly for about 2 h using ultrasonic dispersing machine. The obtained paste was coated onto the surface of YSZ electrolyte as anode by dip-coating method. Afterward, cell was dried for 12 h under room temperature. Cathode was coated using dip-coating method. Cell was dried for 12 h

under room temperature. The coated cell was sintered at 1150 °C for 4 h. During sintering process, 25 mL/min Ar gas and 25 mL/min N_2 gas was fed to the cathode side and anode side respectively in order to prevent cell from oxidizing.

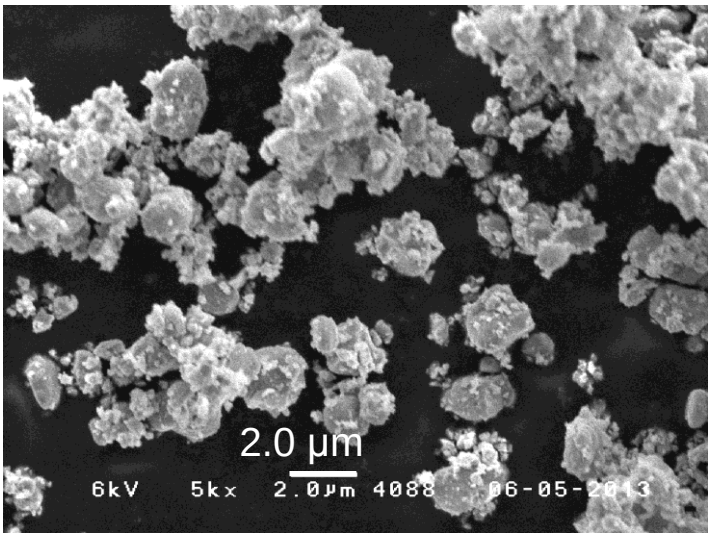

Fig. 3.7 SEM micrograph of LSM powder.

3.2.7 Pt|YSZ|LSM Cell Preparation

The porous electrodes facilitate the formation of triple phase boundary in cathode. Noble metals, such as Pt, work well as cathode and anode material since it is porous enough to allow the gas to diffuse easily, but not so porous as to become poor for electronic conductivity.

The commercially available Pt paste, TR-7907 (Tanaka Kikinzoku Kogyo) was used for cathode. High purity Pt paste of 0.5 g was dissolved with 0.5 mL of ethanol and 1.0 mL binder in the 50 mL beaker. The obtained Pt paste was coated onto the surface of YSZ

electrolyte as cathode by dip-coating method. LSM paste for anode was prepared using the same method as for the LSM paste preparation in section 3.2.6. Cell was then sintered at 800 °C to erase the inorganic material which involved in Pt paste. After sintering, it was measured that 0.14 g of Pt paste was successfully attached onto YSZ electrolyte surface as cathode.

3.2.8 Pt-LSM|YSZ|Pt-LSM Cell Preparation

Pt-LSM paste was prepared by mixing thoroughly LSM powder and Pt paste (mass ratio 20:1), 1.0 mL binder, 2.0 mL dispersant and 7.0 mL distilled water in the 50 mL beaker. The resulting Pt-LSM cermet paste was coated onto the surfaces of YSZ electrolyte as cathode and anode side using dip-coating method and sintered at 800 °C.

3.2.9 Cells Characterizations

Digital microscope (VHX-100, Keyence) was used for cells' microstructure investigation. Scanning electron microscope apparatus (SM-200, Topcon) was used for cells' microscopic material observation. A cell piece (~1 cm long) of each tested cell was prepared for SEM observation. The cell pieces were embedded in the carbon tape and analyzed using SEM.

3.2.10 Experiment Procedures

After cells preparations, each cell was tested under same operation conditions. Tested cells were named as Cell-1, Cell-2 and Cell-3. Cell-1 had a Pt-LSM |YSZ|Pt-LSM structure for the cathode|electrolyte|anode. The structures of Cells 2 and 3 were LSM|YSZ|LSM and Pt|YSZ|LSM, respectively.

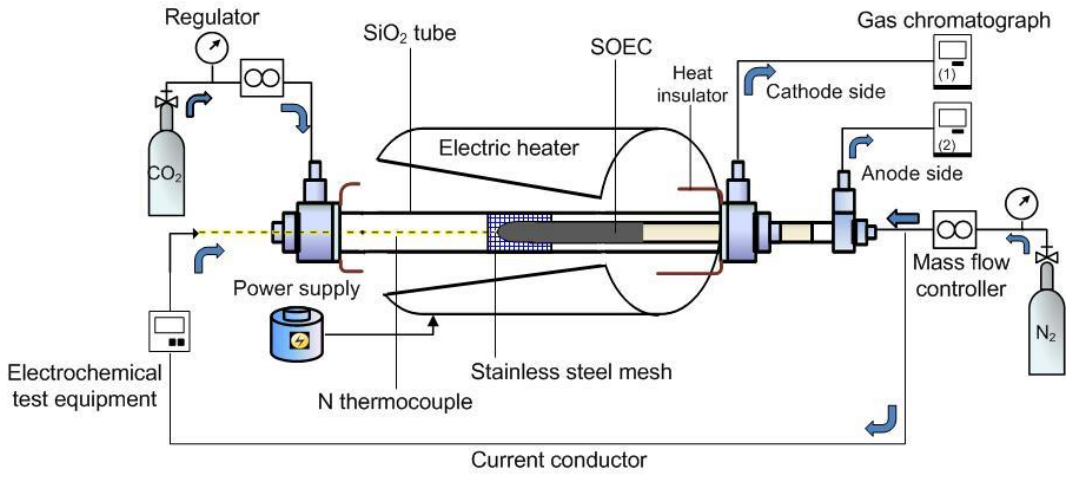

Fig. 3.8 Simplification of schematic overview of experimental SOEC apparatus for CO_2 electrolysis.

Tables 3.2 to 3.4 show the information of tested cells used in this work and the operating conditions during CO_2 electrolysis measurements. After cell was placed inside the test reactor, the test reactor was then covered with electric heater and equipped with well insulated glass fiber insulator (Fig. 3.8). The SOEC test apparatus was operated by heating up the test reactor to 900 °C and applying 25 mL/min of Ar to the cathode side and 25 mL/min of N_2 to the anode side. When cell voltage and the SOEC test apparatus reached steady condition, the temperature was lowered to 800 °C. The reduction of cathode as pretreatment under inert atmosphere was obtained by passing 25 mL/min of pure H_2 for 5 h. After the pretreatment, operating temperature was increased again to 900 °C and 25 mL/min of CO_2 was applied to the cathode side along with 25 mL/min of Ar. Meanwhile, 25 mL/min of N_2 was fed to the anode side. During

electrolysis process, current was observed and recorded to data logger. CO and O_2 production rates were determined by measuring the actual produced CO and produced O_2 using gas chromatograph analysis. The same procedures were also applied to experiment at operating temperature of 800 °C. It was assumed that SOEC test apparatus was in the steady condition during measurements period.

Table 3.2 Electrodes specifications.

Cell name	Cathode	Electrolyte	Anode
Cell-1	Pt-LSM		Pt-LSM
Cell-2	LSM	YSZ	LSM
Cell-3	Pt		LSM

Table 3.3 Experiment conditions.

Parameter	Value
Operating Temperature [°C]	800 and 900
Voltage [V]	0.0-2.0
Gas mass flow rate at cathode side [mL/min]	25
Gas mass flow rate at anode side [mL/min]	25
Gas pressure at cathode side [MPa]	0.1
Gas pressure at anode side [MPa]	0.1

Table 3.4 Gas chromatograph operating conditions.

Parameter	GC-1	GC-2
TCD temperature [°C]	90	100
Columns temperature [°C]	70	50
Current [mA]	80	50
He mass flow rate [mL/min]	40	40

3.3 Results and Discussion

3.3.1 Current Densities for Different Electrode Materials

The relationships between the current density and the cell voltage during electrolysis at 900 °C for Cell-1, Cell-2, and Cell-3 are shown in Fig. 3.9. Current densities at the same applied cell voltage were strongly affected by the choice of electrode materials.

Cell-1 showed a higher current density of 0.52 mA/cm^2 compared to the current densities of Cell-2 and Cell-3. This may be attributed to the lower area specific resistance [3], in the Cell-1 electrodes as compared with Cell-2 and Cell-3. Furthermore, for Cell-2 and Cell-3, cathodic and anodic overpotentials might have caused high levels of resistance in the LSM cathode and anode [5,6].

The Pt-LSM used for both the cathode and anode in Cell-1 exhibited the highest current density. The current density performance in Cell-1 was caused by the special structure of the Pt-LSM cathode and anode. Since Pt has a low overpotential and LSM has good ionic conductivity and mechanical/chemical compatibility with the YSZ electrolyte, the mixture of Pt and LSM in the cermet form resulted

in an improved current density for Cell-1 [7]. The similar coefficients of thermal expansion for the Pt-LSM cathode and anode and the YSZ electrolyte helped to reduce contact resistance, which in turn reduced the cathode resistance and resulted in higher current density levels. SEM micrographs showed that the Pt-LSM cathode and anode were intact and adhered well to the YSZ electrolyte (Fig. 3.10). No gap was found between cathode-YSZ electrolyte interface and between anode-YSZ electrolyte interface. Therefore, no delamination between electrodes and YSZ electrolyte at 800 °C or 900 °C. It was suggested that during electrolysis, the Pt and LSM particles in the cermet form remained in good condition.

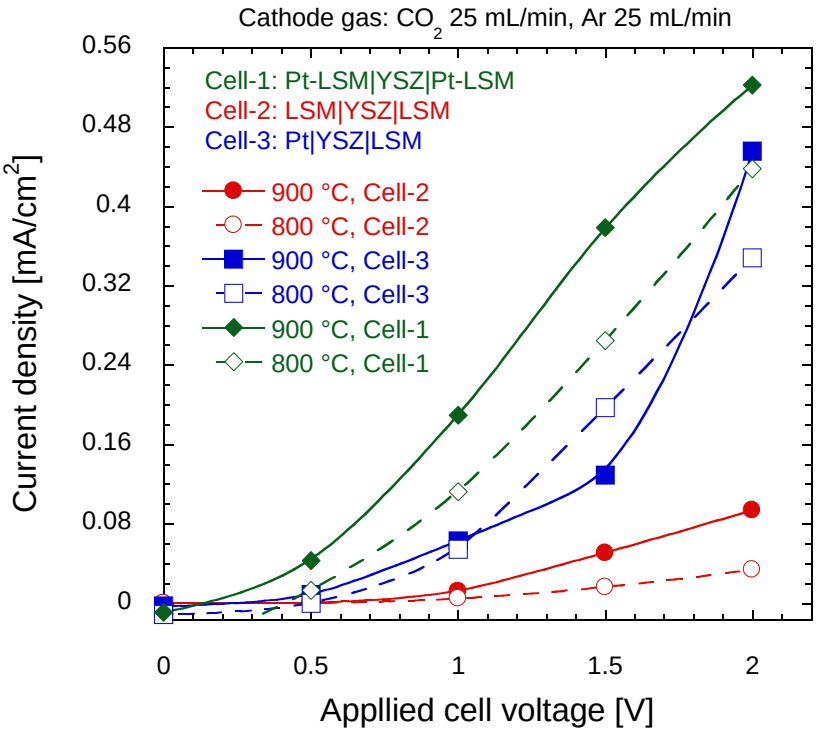

Fig. 3.9 Current density as a function of applied cell voltage for Cell-1, Cell-2 and Cell-3 at 800 °C and 900 °C.

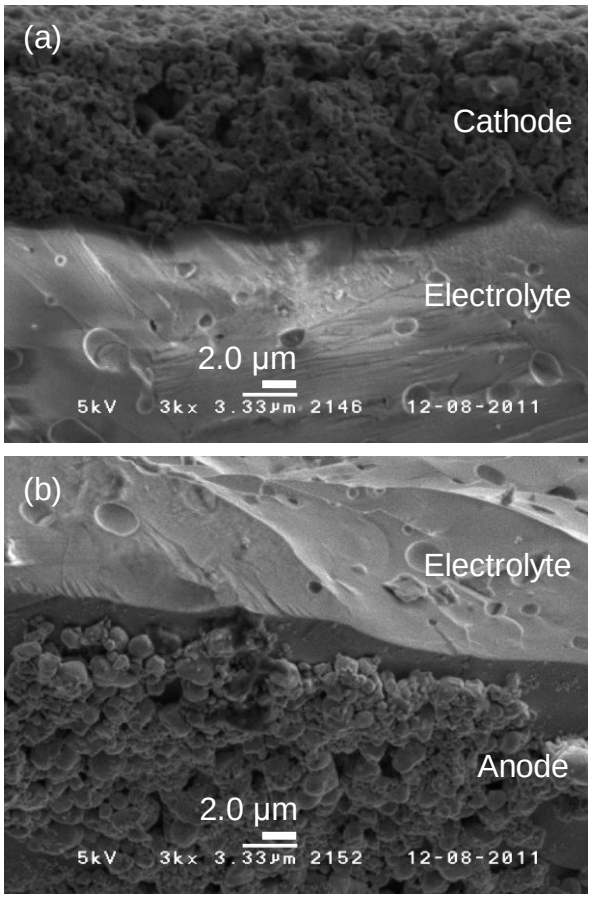

Fig. 3.10 SEM micrograph of a cross section of Cell-1. (a) Interface between Pt-LSM cathode and YSZ electrolyte and (b) interface between YSZ electrolyte and Pt-LSM anode.

Observations of SEM micrographs of the cross sections of Cell-2 after electrolysis (Fig. 3.11) showed that small gaps had formed between the interfaces of both the cathode and anode and the YSZ electrolyte. This indicated that delamination of the LSM and the YSZ electrolyte had occurred during electrolysis. The delamination of the LSM cathode and anode resulted in higher ohmic resistance in Cell-2 and eventually resulted in low current densities. Pt cathode in Cell-3, has exhibited generally higher current densities in other SOEC

electrolysis applications [8], thus it showed higher current density. The SEM micrograph of the Cell-3 cross section in Fig. 3.12 showed that there was no gap along the interface between the LSM anode and the electrolyte and therefore such delamination might not have occurred. Further, it was observed that Pt was intact and adhered well to the surface of the YSZ electrolyte. Overall, the Cell-1 SOEC with Pt-LSM cathode and anode had better performance and higher current density than in the case of Cell-2 and Cell-3.

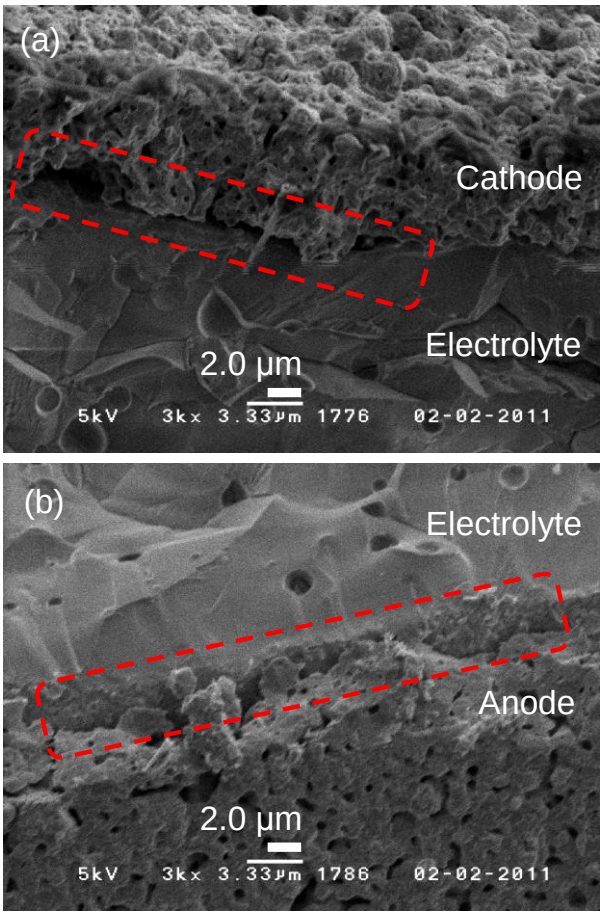

Fig. 3.11 SEM micrograph of a cross section of Cell-2. (a) Interface between LSM cathode and YSZ electrolyte and (b) interface between YSZ electrolyte and LSM anode.

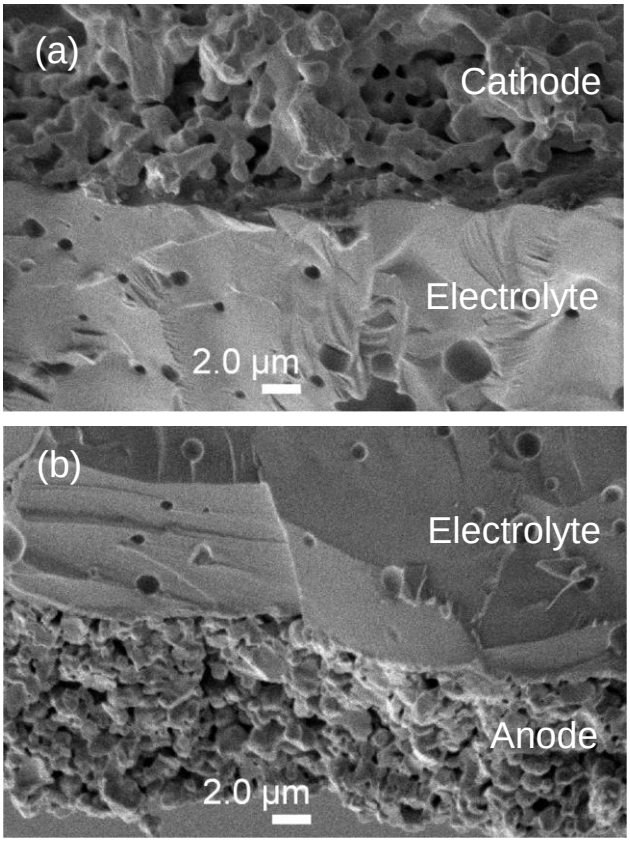

Fig. 3.12 SEM micrograph of a cross section of Cell-3. (a) Interface between Pt cathode and YSZ electrolyte and (b) interface between YSZ electrolyte and LSM anode.

3.3.2 Effect of Operating Temperature on CO and O_2 Production Rates

Cell-1 exhibited the highest current density levels as it performed electrolysis. Therefore, it was chosen as the subject for further analysis of CO_2 electrolysis. Fig. 3.13 shows the CO and O_2 production rates for Cell-1 as a function of current density at 800 and 900 °C. CO and O_2 production rates at 900 °C seemed to be proportional to the applied cell voltage. There have been relatively few reports on cermet that contained a noble metal such as Pt or perovskite oxide ($LaMnO_3$ or

$SrMnO_3$). This was presumably due to the high cost of the noble metals [9]. However, as reported by Ni et al. [10], the Pt cathode exhibited a lower overpotential resulting in a higher current density. The mixture of Pt and LSM in cermet form for the cathode and anode in Cell-1 worked well under a high operating temperature. Both the ionic conduction and chemical kinetics of the CO_2 decomposition reaction increased with increasing temperature. The highest CO and O_2 production rates that occurred during this work was 0.50 and 0.15 μmol/(min cm^2) respectively and which was achieved at an operating temperature of 900 °C and an applied cell voltage of 2.0 V.

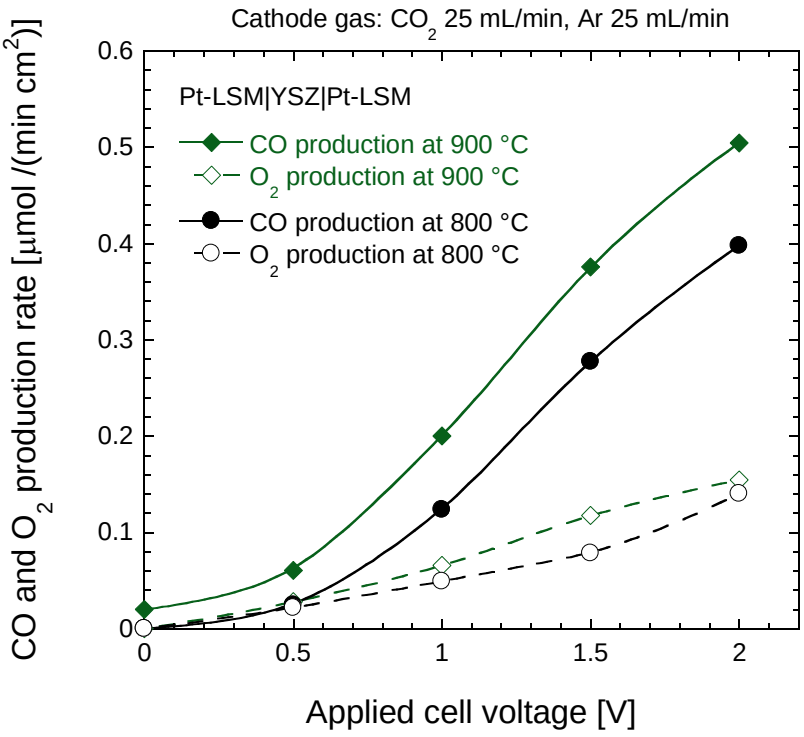

Fig. 3.13 CO and O_2 production rates of Cell-1 as a function of applied cell voltage at 800°C and 900°C.

In addition, LSM in the anode has been reported to have poor ionic conductivity. Thereafter, it was assumed that a relatively small amount of O^{2-} permeated the anode and formed O_2 molecules. In order to improve the reaction rate in the anode, the addition of YSZ into the LSM mixture would be required. The mixture of LSM and YSZ would improve the adhesion between the anode and YSZ electrolyte. This improved adhesion would effectively increase the electrochemically active area of the LSM-YSZ-gas triple phase boundary [11]. The study was addressed in Chapter 4.

3.3.3 Relationship between Applied Cell Voltage and Production ratio of O_2/CO

The relationship between applied cell voltage and the production ratio of O_2/CO is shown in Fig. 3.14. It was seen that the production ratio of O_2/CO was close to the stoichiometric ratio of 0.5. At lower current density levels, the O_2/CO production ratio was slightly higher. After passing the initial stage of CO_2 electrolysis, the current density increased with increasing cell voltage and then the production ratio of O_2/CO became stable and remained lower than the stochiometric ratio of 0.5. This result also indicated that the reactions in Eq. 2.1 to 2.3 in Chapter 2 were proceeded mainly on the cell.

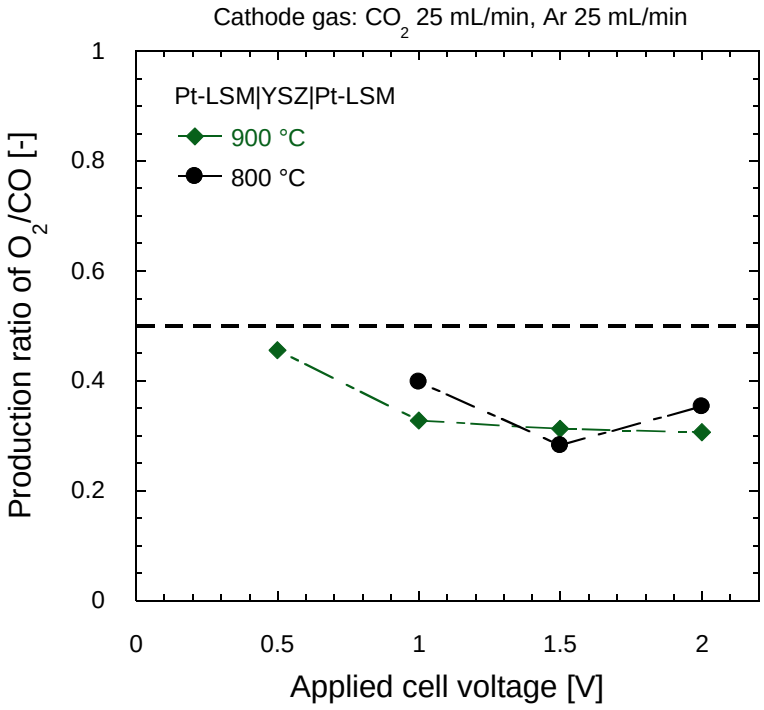

Fig. 3.14 Relationship between applied cell voltage and production ratio of O_2/CO.

3.3.4 Relationship between Applied Cell Voltage and the Mole Ratio of Produced CO and Amount of Charged Passed

According to the reaction in Eq. 2.1, during the decomposition process, 2.0 mol electrons are needed to decompose 1.0 mol CO_2 into 1.0 mol CO and O^{2-}. This means that the ratio between the CO produced and electrons flowing in will ideally be 0.5. The relation between applied cell voltage and the mole ratio of Cell-1 is shown in Fig. 3.15. At lower applied cell voltage levels and corresponding lower current densities, the ratios were somewhat higher, close to 0.5, than ratios at higher current densities. At higher voltage levels and higher current densities, the ratios decreased.

At lower applied voltages, electrons were consumed primarily for CO production. On the other hand, at higher voltage levels, electrons could be consumed in unknown reactions, and thus, the ratio was reduced. Carbonation would be one of the candidates for the unknown reaction

$$CO + 2e^- \rightarrow C + O^{2-} \qquad (3.3)$$

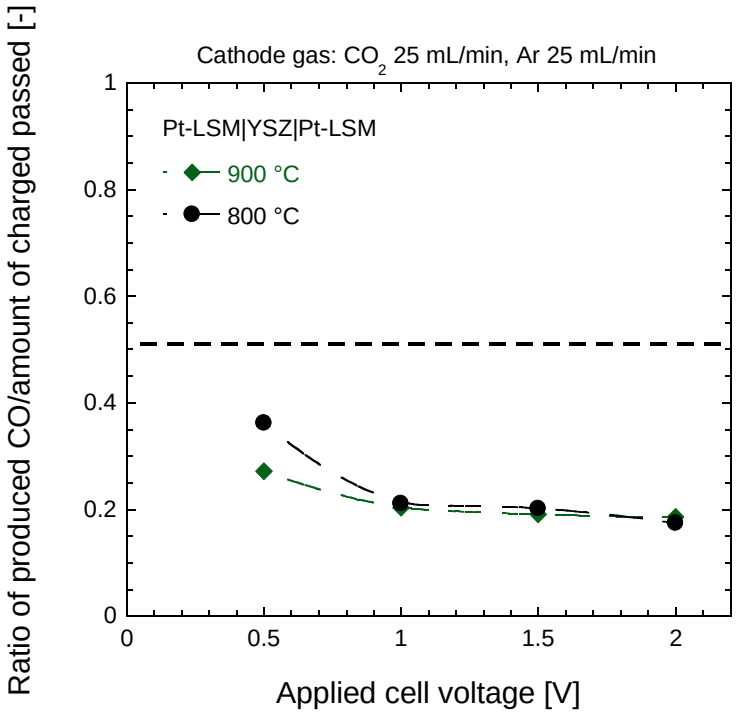

Fig. 3.15 Relationship between applied cell voltage and the mole ratio of produced CO and amount of charged passed in cell-1.

3.4 Conclusions

Basic studies on CO_2 electrolysis in YSZ-based electrolyte had been conducted to study the feasibility of CO_2 electrolysis in SOECs. Three CO_2 electrolysis processes were demonstrated using different

electrode materials on the YSZ-based electrolyte. Cell-1, with a structure of Pt-LSM |YSZ|Pt-LSM for the cathode|electrolyte|anode, had higher current density levels than those of Cell-2, with a LSM|YSZ|LSM structure, and Cell-3, with a Pt|YSZ|LSM structure. It was observed that CO and O_2 production rates were higher at 900 °C than at 800 °C. A CO and O_2 production rates of 0.50 and 0.15 μmol/(min cm^2) respectively were measured at an operating temperature of 900 °C with a cell voltage of 2.0 V. On the other hand, low O_2 production rate was thought to be caused by the anodic reaction became the rate-determining step for O_2 production during the electrolysis process.

At lower applied cell voltages, it was found that electrons were consumed primarily for CO production. On the other hand, at higher voltage levels, electrons could be consumed for carbonation process. CO_2 electrolysis using SOECs for CO regeneration in ACRES was feasible.

References

[1] A. Eichler, Tetragonal Y-doped zirconia: Structure and ion conductivity, *Phys. Rev. B*, **64**, 174103, 2001.

[2] C. Pascual, J.R. Jurado, P. Duran, Electrical Behaviour of Doped-Yttria Stabilized Zirconia Ceramic Materials, *J. mater. Science*, **18**, 1315-1322, 1983.

[3] P.K. Lohsoontorn, D.J.L. Brett, N. Laosiripojana, Y.M. Kim, J.M. Bae, Performance of Solid Oxide Electrolysis Cells Based on Composite $La_{0.8}Sr_{0.2}MnO_{3-\delta}$–Yttria Stabilized Zirconia and $Ba_{0.5}Sr_{0.5}Co_{0.8}Fe_{0.2}O_{3-\delta}$ Oxygen Electrodes, *J. Hydrogen Energy*, **35**, 3958-3966, 2010.

[4] Nikkato Corp., Catalog No. 600, *Zirconia Solid Electrolyte*, 2008.

[5] Y. Huang, J.M. Vohs, R.J. Gortez, SOFC Cathodes Prepared by Infiltration with Various LSM Precursors, *Electrochem. and Solid-state Lett.*, **9**(5), A237-A240, 2006.

[6] K. Chen and S.P. Jiang, Failure Mechanism of (La,Sr)MnO_3 Oxygen Electrodes of Solid Oxide Electrolysis Cells, *J. Hydrogen Energy*, **36**, 10541-10549,2011.
[7] M. Liang, B. Yu, M. Wen, J. Chen, J. Xu and Y. Zhai, Preparation of LSM–YSZ Composite Powder for Anode of Solid Oxide Electrolysis Cell and Its Activation Mechanism, *J. Power Sources*, **190**, 341-345, 2009.
[8] T. Ishihara, N. Jirathiwathanakul, H. Zong, Intermediate Temperature Solid Oxide Electrolysis Cell Using LaGaO3 based Perovskite Electrolyte, *J. Royal Soc. Of Chemistry*, **3**, 665-672, 2010.
[9] L.S. Wang, S.A Barnett, Ag-perovskite Cermets for Thin Film Solid Oxide Fuel Cell Air-electrode Applications, *J. Solid State Ionics*, **76**, 103-113, 1995.
[10] M. Ni, M.K.H. Leung and D.Y.C. Leung, Technological Development of Hydrogen Production by Solid Oxide Electrolyzer Cell (SOEC), *J. Hydrogen Energy*, **33**, 2337-2354, 2008.
[11] C. Yang, A. Coffin, F. Chen, High Temperature Solid Oxide Electrolysis Cell Employing Porous Structured $(La_{0.75}Sr_{0.25})_{0.95}MnO_3$ with Enhanced Oxygen Electrode Performance, *J. Hydrogen Energy*, **35**, 3221-3226, 2010.

Chapter 4

Improvement of Carbon Dioxide Electrolysis Performance Using Ni-LSM|YSZ|LSM-YSZ Cell and Ni-YSZ|YSZ|LSM-YSZ Cell

4.1 Introduction

CO_2 electrolysis was feasible in YSZ-based electrolyte employing Pt-LSM as cathode and anode. However, the use of noble metal like Pt has been of concern due to its high cost. For practical application of ACRES, less expensive but high chemical reactivity electrode materials are needed. In recent times, Ni-based cermet has been used as an alternative electrode material as the cathode and perovskite structures as the anode [1,2].

This chapter discusses the use of alternative materials for cathode and anode to perform CO_2 electrolysis. Two different materials were used for cathode namely Ni-LSM and Ni-YSZ while LSM-YSZ was used as anode since it has been extensively used as anode for steam electrolysis cells and showed excellent performance. The combination of LSM-YSZ gives long-term stability, good catalyst properties at high temperature and good ionic conductivity [3,4]. Cells' electrolytic characteristics were identified in relation with current density, temperature, CO_2 concentrations in cathode side and CO and O_2 production rates. Cell durability at high temperature and carbon deposition on Ni-based cathode was also discussed.

4.2 CO_2 Electrolysis Performance in Ni-LSM|YSZ|LSM-YSZ Cell

4.2.1 Experimental

4.2.1.1 Experiment Apparatus Modification

In order to improve current efficiency during electrolysis process, Pt mesh (Nilaco Corp.) and Pt wire (Nilaco Corp.) were used as current collector and current conductor respectively. Some modifications to SOEC test reactor were carried out to improve cell performance. Pt mesh (55 mesh, 0.12 mm in diameter and dimension of 50 × 50 mm) which was used as current collector was covered on both surface of cathode and anode with effective surface area of 5.0 cm^2 and 3.0 cm^2 respectively. Pt wire (diameter of 0.20 mm and effective length of 25 cm) as current conductor was used to connect the electrodes (cathode and anode) to the electrochemical equipment as shown in Fig. 4.1 and its schematic overview is depicted in Fig. 4.2. Pt mesh and Pt wire were utilized due to its high current conductivity at higher operating temperature compared to that of stainless steel mesh.

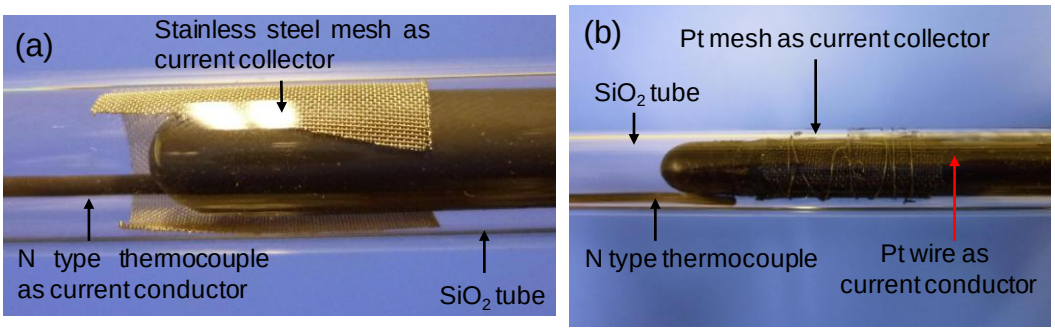

Fig. 4.1 Cathode side structures with N type thermocouples. (a) Stainless steel mesh was used as current collector in the experiment with Pt-LSM|YSZ|Pt-LSM cell, (b) Pt mesh and Pt wire were used as current collector and current conductor in the experiment with Ni-LSM|YSZ|LSM-YSZ cell and Ni-YSZ|YSZ|LSM-YSZ cell.

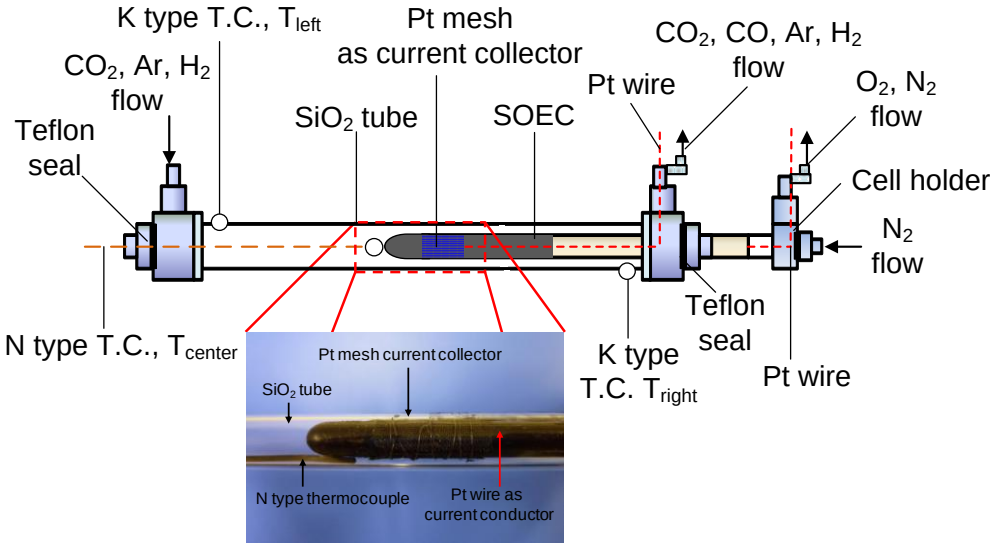

Fig. 4.2 Schematic drawing of SOEC test reactor after some modifications: Pt mesh was attached well on the surface of electrodes as current collector and Pt wire was used as current conductor.

4.2.1.2 Ni-LSM|YSZ|YSZ-LSM Cell Preparation

YSZ electrolyte under commercial name of YSZ-8 (Nikkato Corp.) was again used in this work. It has higher ionic conductivity in comparison with ZR-8Y type used in the experiment with Pt-LSM|YSZ|Pt-LSM cell [5]. Ni-LSM paste was prepared by mixing 15 g of $Ni(NO_3)_2 \cdot 6H_2O$ (Wako Pure Chemicals, Ltd.) and 10 g of LSM, 1.0 mL of binder, 5.0 mL of distilled water, and 2.0 mL of dispersant in the 50 mL beaker. The components were thoroughly mixed, and the resulting paste was coated onto the surface of YSZ electrolyte as cathode by dip-coating with geometric surface area of 25.1 cm^2.

LSM-YSZ paste was prepared by mixing 12.5 g of LSM and 12.5 g of YSZ powder (8YSZ, TZ-8Y, Tosoh Corp.) using mortar and pestles. 1.0 mL of binder, 10 mL of distilled water, and 2.0 mL of dispersant were added to the mixture. The components were thoroughly mixed in the 50 mL beaker and the resulting paste was coated onto the surface of YSZ electrolyte as anode by dip-coating. After coating, the cell was then dried at room temperature for several hours before being sintered at 800 °C under inert conditions for 4 h.

4.2.1.3 Cell Characterizations

The cathode-electrolyte sample diffraction pattern was measured by X-ray diffraction (XRD) (D8 DISCOVER, Bruker AXS) before and after the electrolysis measurement. The sample was taken by crunching the cell into pieces with 3 mm-length of the Ni-LSM|YSZ sample for analysis. SEM micrographs of fractured cells were taken

using SEM apparatus (S 4800, Hitachi). Carbon coating was applied to the sample before the SEM observation.

4.2.1.4 Experiment Procedures

Prior to beginning the electrolysis experiments, H_2 reduction was performed as pretreatment to the NiO-LSM cathode for about 5 h at 800 °C to prevent Ni oxidation and to fix the final form of the Ni-LSM. During the electrolysis process, pure CO_2 at a flow rate of 25 mL/min and Ar at 25 mL/min were supplied to the cathode while N_2 at 25 mL/min flowed into the anode. Experiment conditions and gas chromatographs operating conditions were kept the same as for the experiment with Pt-LSM|YSZ|Pt-LSM cell (Table 3.3 and 3.4 in Chapter 3).

Table 4.1 Cells operating conditions during CO_2 concentration measurements.

CO_2 concentrations [%]	**Gas flow rates [mL/min]**		
	Cathode side	**Anode side**	
	CO_2	**Ar**	**N_2**
20	30	120	25
50	75	75	25
80	120	30	25

In the experiments on the effects of CO_2 concentrations on current density, CO_2, Ar, and N_2 were applied at various gas flow rates

(Table 4.1). The simplified schematic overview of experimental SOEC apparatus for CO_2 electrolysis after the modifications is given in Fig. 4.3.

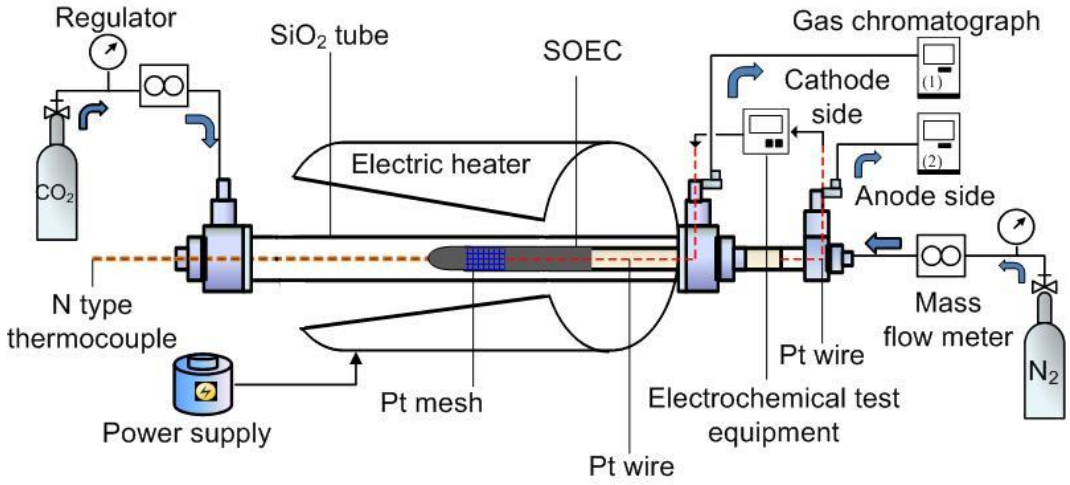

Fig. 4.3 Schematic overview of experimental SOEC apparatus for CO_2 electrolysis after some modifications.

4.2.2 Results and Discussion

4.2.2.1 Effect of Temperature to Cell Performance at Constant CO_2 Flow Rate of 25 mL/min

The relationship between the current density and the applied cell voltage at 800 °C, 850 °C, and 900 °C with constant CO_2, Ar, and N_2 flow rates of 25 mL/min are shown in Fig. 4.4. Current densities at the same levels of applied cell voltage were strongly affected by the operating temperature. Higher operating temperatures reduced the resistance of the cell, which in turn resulted in higher current densities.

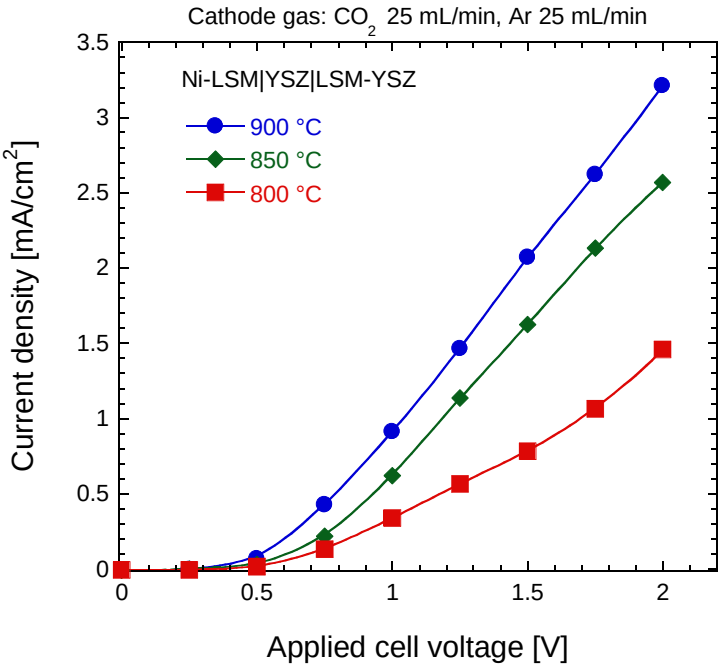

Fig. 4.4 Current density as a function of applied cell voltage at 800 °C, 850 °C, and 900 °C.

Furthermore, the YSZ electrolyte functioned well at higher temperatures. Electrical conductivity specifications for the YSZ electrolyte provided by Nikkato Corp. (Fig. 3.4 in Chapter 3) indicate that at 800 °C, the electrical conductivity of the cell is 0.03 S/cm, while at 850 °C, it is 0.05 S/cm, and at 900 °C, it is 0.06 S/cm. Therefore, at higher operating temperatures, the current density was higher than at lower temperatures due to the dependency of the electrical conductivity of the electrolyte on temperature. The highest current density of 3.21 mA/cm^2 was measured at an operating temperature of 900 °C.

Both negative and positive current densities were observed at temperatures of 800 °C, 850 °C, and 900 °C. As reported previously

by Tao et al. [6], very small negative current densities were observed at low applied cell voltages (0.0–0.25 V), because the current density was largely consumed in overcoming the initial OCV. Most of the applied energy was used to overcome OCV and diffusion of CO_2 to the surface of the cathode. As the applied cell voltage overcame and exceeded OCV, the current density became positive. At that point, a large positive current density was observed that increased exponentially with increasing cell voltage.

It is assumed that the catalytic surface area (A_s) of the cell was larger than that of its geometric surface area (A_g) [7,8]. In the further calculation the ratio of $A_s/A_g = 1.5$ was used. Figure 4.5 shows the CO and O_2 production rates as a function of the current density and temperature at constant CO_2, Ar, and N_2 flow rates of 25 mL/min. The CO production rate at 800 °C, 850 °C, and 900 °C was proportional to the current passing through the cell. Both ionic conduction and the chemical kinetics of CO_2 electrolysis increased with increasing temperature. The mixture of LSM and YSZ appeared to improve adhesion between the anode electrode and the YSZ electrolyte. This improved adhesion effectively increased the electrochemical active area of the LSM-YSZ gas triple phase boundary, resulting in a higher O_2 production rate. The highest CO and O_2 production rates achieved in this study were 0.83 and 0.43 μmol/(min cm^2), respectively, at an operating temperature of 900 °C and a current density of 3.21 mA/cm^2.

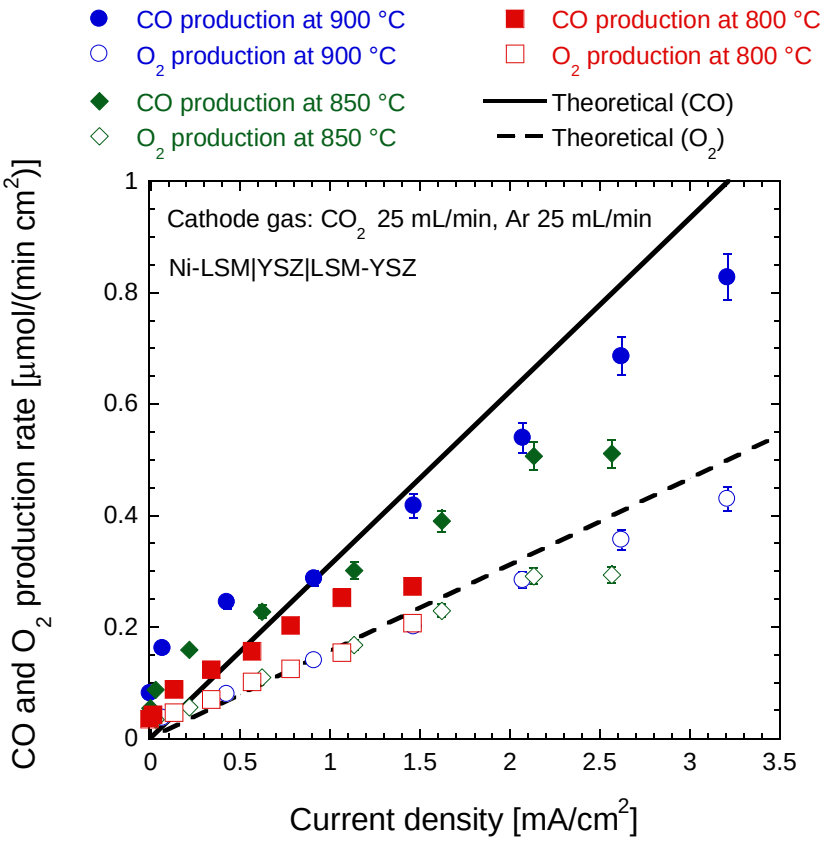

Fig. 4.5 CO and O_2 production rates as a function of current density at 800 °C, 850 °C, and 900 °C.

However, there were small deviations in the experimental CO and O_2 production rates from those theoretically calculated based on Faraday's law of electrolysis. These small deviations were likely due to small instrument errors, particularly at lower current densities; at smaller CO and O_2 production rates, these deviations were slightly larger. Under these conditions, the concentrations were close to the detection limit of the gas chromatograph TCD.

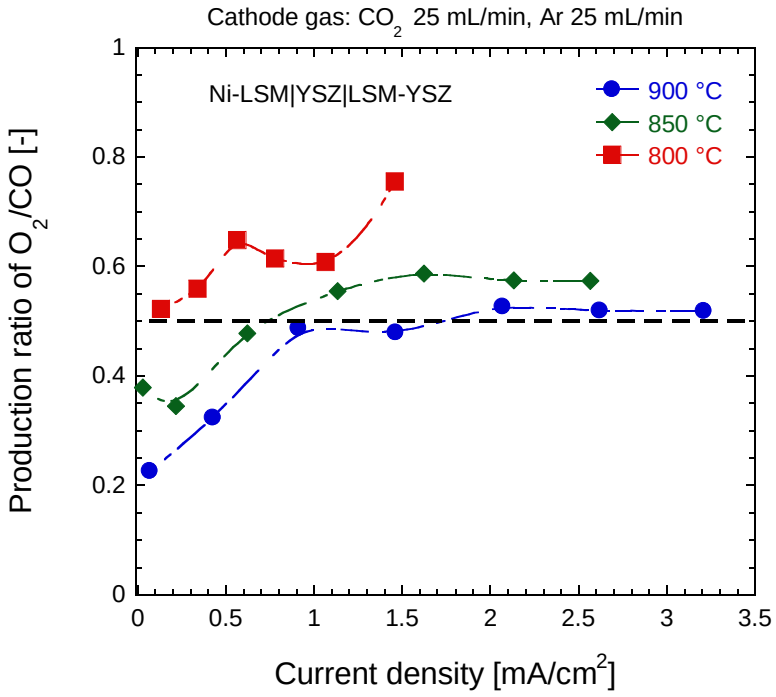

Fig. 4.6 Relationship between the current density and the production ratio of O_2/CO at 800 °C, 850 °C, and 900 °C.

The relationship between the current density and the production ratio of O_2/CO at constant CO_2, Ar, and N_2 flow rates of 25 mL/min is shown in Fig. 4.6. The production ratios of O_2/CO were fairly close to the stoichiometric ratio of 0.5. At 800 °C, the O_2/CO production ratios were slightly higher. Upon increasing the temperature to 850 °C and 900 °C and increasing the current density, the production ratios approached the stoichiometric ratio of 0.5. These results indicated that at higher operating temperatures and higher current densities, the CO_2 electrolysis reaction proceeded mainly on the cell.

4.2.2.2 Effect of CO_2 Concentrations on the Cathode Side at 800 °C and 900 °C

Figure 4.7 shows the current density at 900 °C and 800 °C at CO_2 concentrations of 20%, 50%, and 80% in the cathode side as a function of applied cell voltage. The cell operating conditions during the CO_2 concentrations measurement are shown in Table 4.1. The current density increased with increasing CO_2 concentrations due to the increase in the reactant, i.e., CO_2, at the cathode side. The increase in the current density at 900 °C was not significant for higher CO_2 concentrations of 50% and 80% at lower applied cell voltages (<1.75 V), as previously reported by Wang et al. [9]. It could be suggested that the surface activity become the rate-determining step for the electrolysis reaction at CO_2 concentrations higher than 50%. Increased current density at higher CO_2 concentrations could be explained by a decrease in the activation and concentration overpotential (diffusion resistance). As suggested by Ishihara et al., the gas diffusion rate in the pores decreases with increasing temperature, particularly for hydrophilic molecules with high molecular weight [10]. Considering that the CO_2 molecule has a high molecular weight, the gas diffusion theory based on Knudsen flow may apply. Therefore, the higher CO_2 concentrations were likely effective in decreasing the cathodic overpotential and increasing the current density of the cell.

At lower temperature i.e. 800 °C, current density was hardly affected by the CO_2 concentrations. It was considered that the surface

activity became the rate determining step for the electrolysis reaction with decreasing operating temperature. Therefore the current density might not be strongly affected by the gas partial pressure at lower operating temperature. The highest current density of 3.25 mA/cm^2 was achieved at 900 °C under 80% CO_2 concentration.

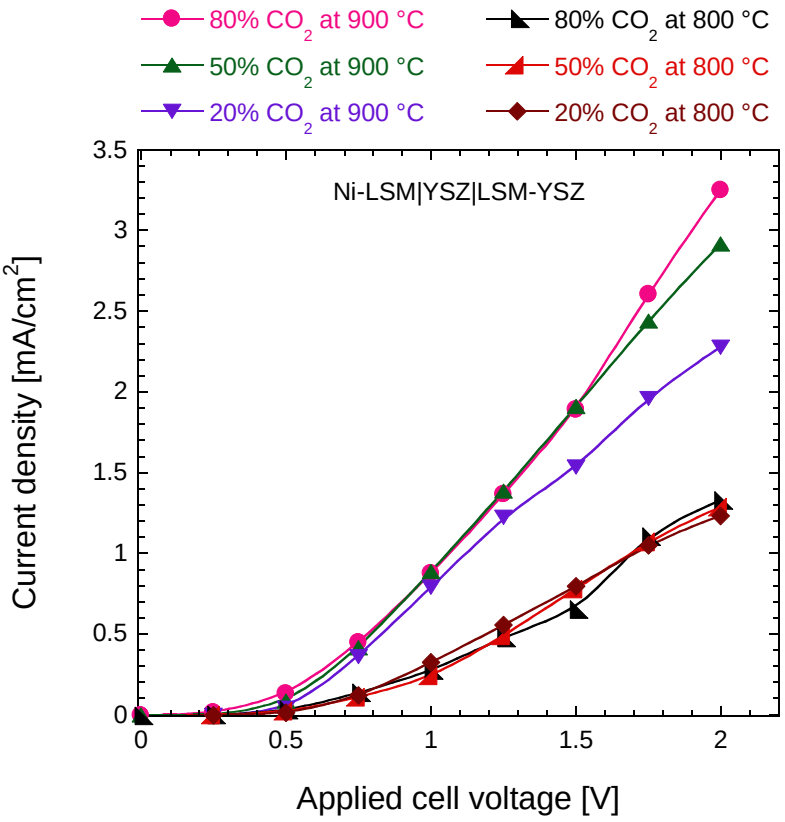

Fig. 4.7 Current density at 800 °C and 900 °C at CO_2 concentrations of 20%, 50%, and 80% in the cathode side as a function of applied cell voltage.

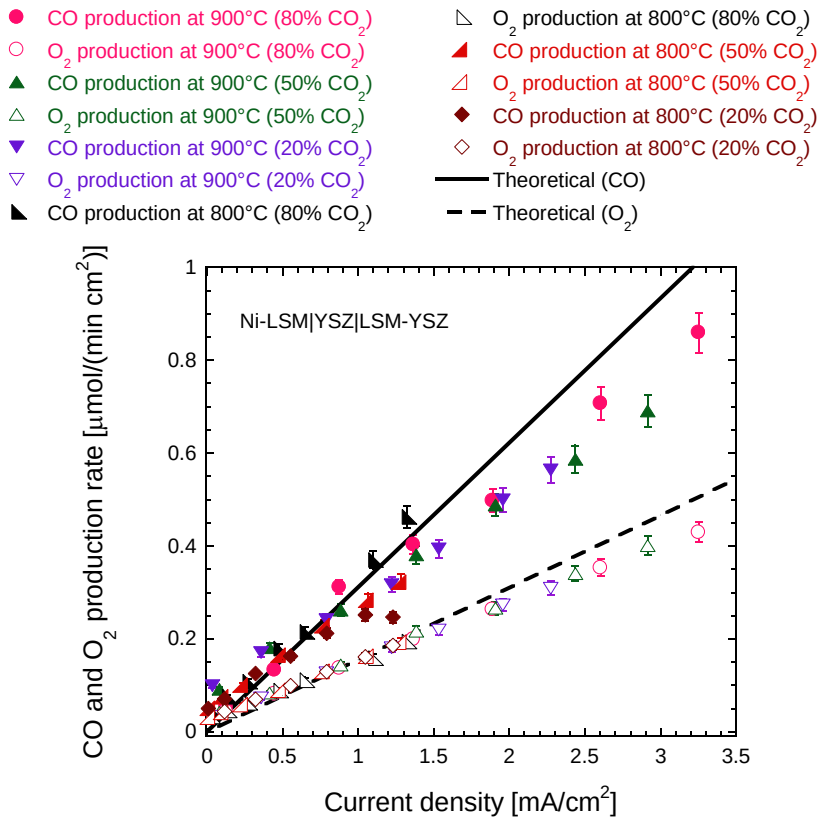

Fig. 4.8 CO and O_2 production rates measured at 800 °C and 900 °C under various CO_2 concentrations.

CO and O_2 production rates as function of current density at various CO_2 concentrations at 800 °C and 900 °C is shown in Fig. 4.8. It was seen that at 900 °C, CO was produced proportionally to current passing through the cell and dependent of CO_2 concentrations. At higher operating temperature i.e. 900 °C, CO production rate was seen dependent on CO_2 concentrations level due to increase of reactant that is CO_2 in the cathode side. By lowering CO_2 concentrations level in the cathode side, CO production decreased. Ishihara et al. reported in their steam electrolysis research that under intermediate temperature (800 °C); H_2 production rate was hardly dependent on steam partial

pressure [10]. Likewise, it was seen in the Fig. 4.8 that under lower cell voltage i.e. 800 °C, CO production rate was hardly dependent on CO_2 concentrations level. The highest CO and O_2 production rates of 0.86 μmol/(min cm^2) and 0.43 μmol/(min cm^2) respectively were achieved at 900 °C under 80% CO_2 concentration.

4.2.2.3 Cell Durability Measurement

As for a high temperature electrolysis cell, the durability is an important research issue. Degradation in the CO_2 electrolysis performance of the tubular cell over 250 h is shown in Fig. 4.9. The cell potential was relatively stable over the measurement period of 250 h. Voltage drop was not observed during the measurement. Thus, cell stability was relatively high under CO_2 electrolysis conditions.

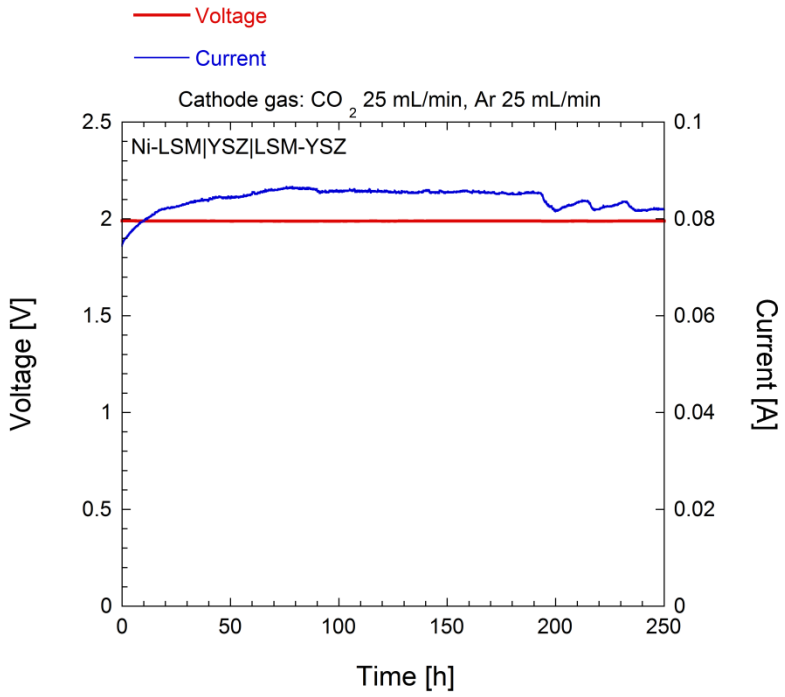

Fig. 4.9 Time history of voltage and current over 250 h measured at 900 °C.

4.2.2.4 Post Test Material Analysis

Ni-LSM|YSZ|LSM-YSZ cell after cell operation over 600 h is shown in Fig. 4.10 and its cross-sectional SEM micrograph is shown in Fig. 4.11. Three distinguishable layers, Ni-LSM (cathode), YSZ (electrolyte), and LSM-YSZ (anode), were intact and well attached to one another. No degradation was found after the CO_2 electrolysis measurement and it was suggested that during high temperature electrolysis, the Ni and LSM particles in the cermet form, remained in good condition. Further observation showed that no delamination of Ni-LSM and the YSZ electrolyte was found nor delamination of LSM-YSZ and the YSZ electrolyte.

Fig. 4.10 Ni-LSM|YSZ|LSM-YSZ cell after tested over 600 h.

Figure 4.12 shows the XRD pattern of cathode after the CO_2 electrolysis measurement. It was clearly seen that XRD peaks for Ni, LSM and YSZ were observed. This suggested that Ni-LSM at cathode side was generally stable during measurement. However, the unknown peak was observed around 2θ of 32 degree. This peak was rather

difficult to identify, and it was predicted that the peak was from a part of LSM-YSZ in the cathode side which was reacted each other and resulted into small phase of perovskite structure of $SrZrO_3$ [11].

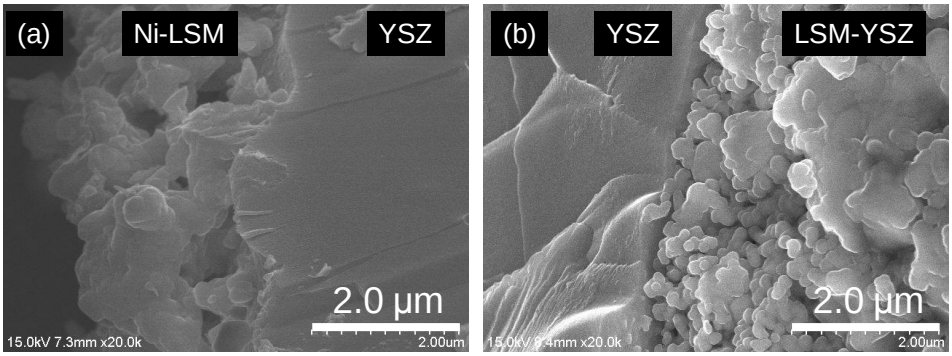

Fig. 4.11 SEM micrograph of a cross-section of the Ni-LSM|YSZ|LSM-YSZ cell taken after cell operations. (a) Ni-LSM|YSZ, (b) YSZ|LSM-YSZ.

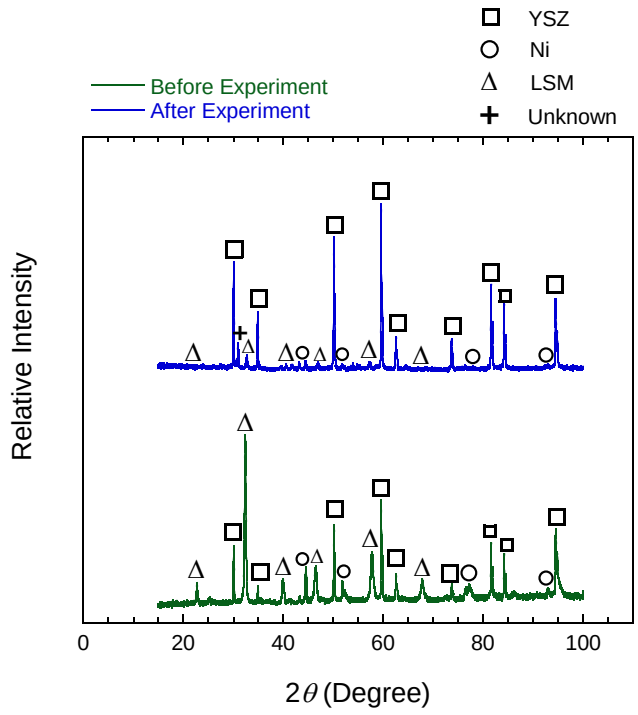

Fig. 4.12 XRD pattern of cathode-electrolyte sample (Ni-LSM|YSZ) before and after the CO_2 electrolysis measurement.

4.3 CO_2 Electrolysis Performance Using Ni-YSZ|YSZ|LSM-YSZ Cell with Ball Milling Preparation

4.3.1 Experimental

4.3.1.1 Ni-YSZ Powder Prepared by Ball Milling

Microstructure improvement of Ni-YSZ composite cathode was attempted using Ni-YSZ composite particles in order to electrochemically enhance the cathode reactivity by extending triple phase boundary area. YSZ powder and NiO powder (Wako Pure Chemicals, Ltd.) are mechanically mixed using a planetary ball mill (Pulverisette 7, Fritszch). Before ball milling, YSZ powder of 8.0 g and NiO powder of 12 g were mixed using mortar and pestles. The mixture powder of 20 g was then put into two zirconia bowls with a grinding bowl size of 45 mL. Each grinding bowl contained 10 g of mixture NiO-YSZ powder and 12 zirconia balls of 10 mm in diameter. The powder was ball milled for 40 minutes with rotation speed of 400 Rpm.

Mixing of NiO powder and YSZ powder by ball mill produced composite material of Ni-YSZ (Fig. 4.13). The mixing process is begun by adhesion of the guest particles to the host or core particle surface. This process will increase their contact area by means of deformation caused by compression, impact and shear forces; formation of chemical bridges; reduction of the surface energy. Fusion of the deposited guest particles with each other to form a dense shell around the core; further reduction of the surface energy [12,13].

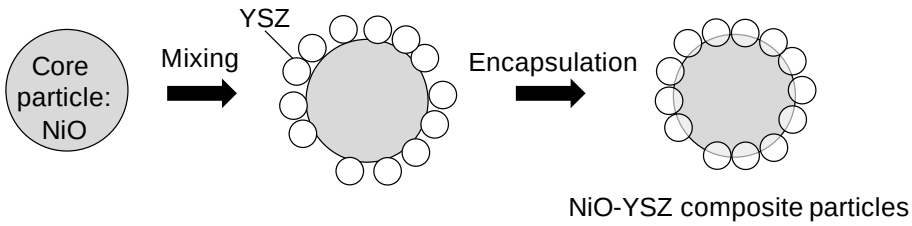

Fig. 4.13 Surface modification model of NiO-YSZ particles [13].

4.3.1.2 LSM-YSZ Powder Prepared by Ball Milling

LSM and YSZ powder were also mechanically prepared by mixing 10 g of LSM powder with 10 g of YSZ powder using a planetary ball mill. Powder mixing by ball milling produced composite material of LSM-YSZ as shown in Fig. 4.14 [14].

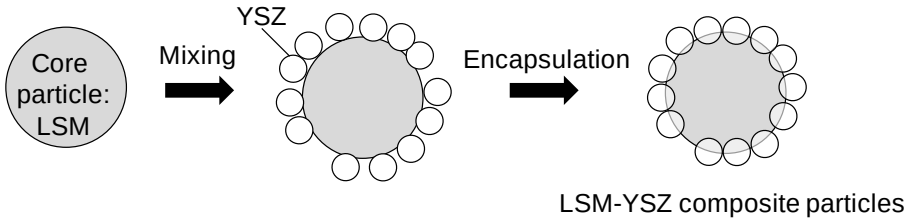

Fig. 4.14 Surface modification model of LSM-YSZ particles [14].

4.3.1.3 Ni-YSZ|YSZ|LSM-YSZ Cell Preparation

After ball milling, the obtained LSM-YSZ composite powder was mixed thoroughly with 2.0 mL of binder, 1.0 mL of dispersant and 10 mL of distilled water in the 50 mL beaker. The obtained paste then dispersed using ultrasonic dispersing machine. Paste then stirred up using magnetic stirrer for 1 h. The resulting paste then coated with dip-coating onto the inner side of YSZ electrolyte as anode.

In the case of cathode, paste preparation was begun by mixing the obtained NiO-LSM composite powder with 2.0 mL of binder, 1.0 mL of dispersant and 10 mL of distilled water in the 50 mL beaker. Paste then stirred up using magnetic stirrer for 1h. The resulting paste then coated onto outer side of YSZ electrolyte with dip-coating. The geometric surface area of cathode was 25.1 cm^2. After coating, the cell was dried for 24 h in open air. Cell was sintered at 1100 °C under inert condition for 4 h.

4.3.1.4 Powder and Cell Characterizations

Powder characterizations were performed by using XRD (Ultima IV, Rigaku) and SEM (SM-200, Topcon). Cell characterizations were performed by using XRD (D8 DISCOVER, Bruker AXS) and SEM (S-4800, Hitachi). At first, cell was crunched into pieces. Part of crunched cell with the length of 2.0 mm was used for XRD pattern analysis and SEM observation. Pt-Pd coating was applied to the sample prior to the SEM observation.

4.3.1.5 Experiment Procedures

Prior to beginning the electrolysis experiments, H_2 reduction was performed as pretreatment to the NiO-YSZ cathode for about 2 h at 900 °C to prevent Ni oxidation and to fix the final form of the Ni-YSZ. During the electrolysis process, pure CO_2 at a flow rate of 25 mL/min and Ar at 25 mL/min were supplied to the cathode while N_2 at 25 mL/min flowed into the anode. Experiment conditions and gas chromatographs operating conditions were kept the same as for the experiment with Pt-LSM|YSZ|Pt-LSM cell and Ni-LSM|YSZ|LSM-YSZ cell

(Table 3.3 and 3.4 in Chapter 3). In the experiments on the effects of CO_2 concentration on current density, CO_2, Ar, and N_2 were applied at various gas flow rates (Table 4.1).

4.3.2 Results and Discussion

4.3.2.1 Ni-YSZ and LSM-YSZ Powder Characterizations

Fig. 4.15 shows the NiO-YSZ powder prepared by hand mixing using mortar and pestles and mechanical mixing with planetary ball mill. It was seen that NiO-YSZ powder prepared by ball milling had dark green color compared to that of NiO-YSZ powder prepared by hand mixing. The dark green color assigned by the homogeneous mixing between NiO powder and YSZ powder.

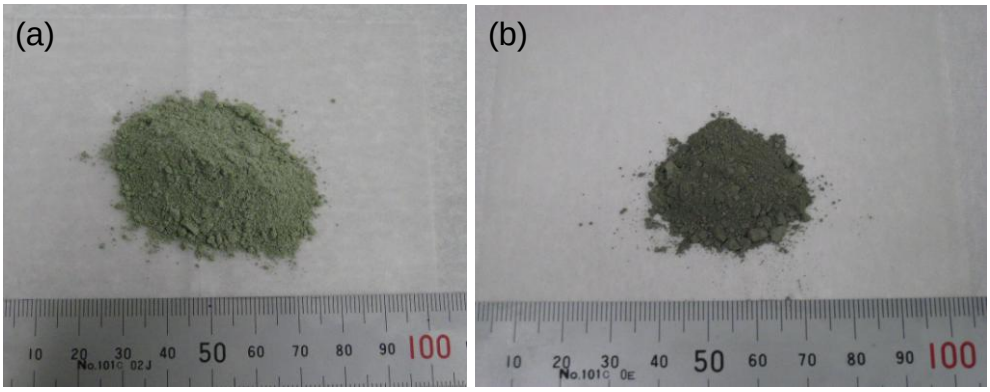

Fig. 4.15 NiO-YSZ powder prepared by (a) hand mixing and prepared by (b) ball milling.

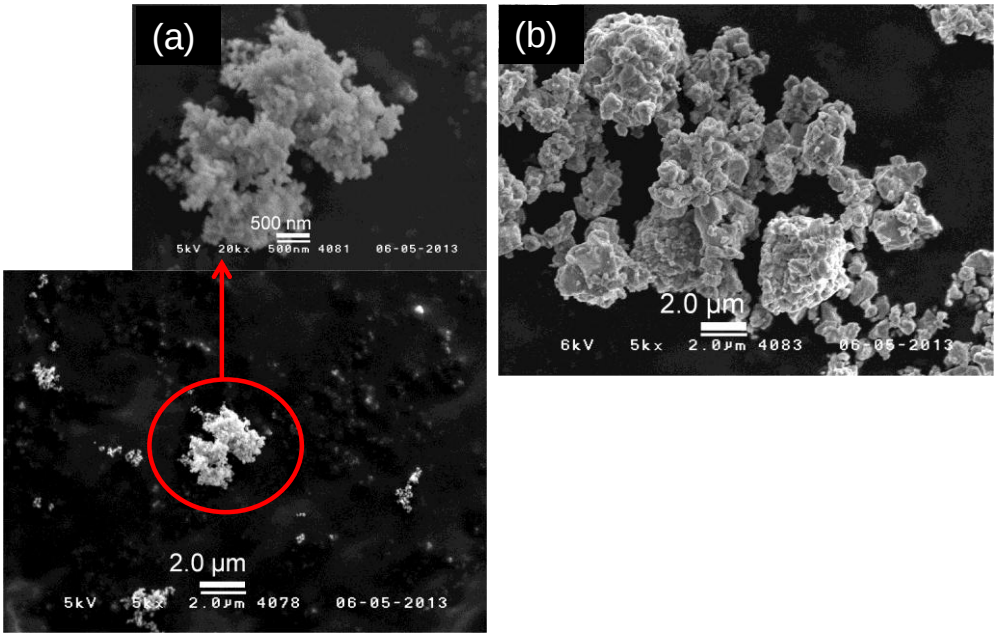

Fig. 4.16 SEM micrograph of (a) pure YSZ powder and (b) pure NiO powder.

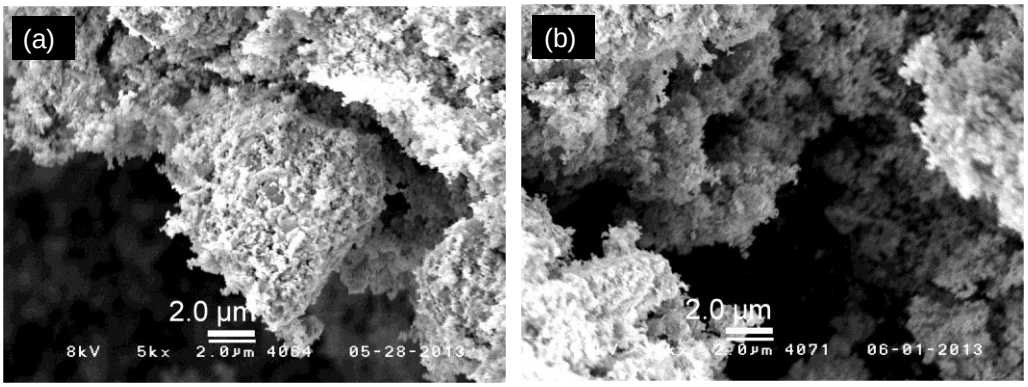

Fig. 4.17 SEM micrograph of NiO-YSZ powder prepared by (a) hand mixing and prepared by (b) ball milling.

SEM micrograph of mixture NiO-YSZ powder is presented in Fig. 4.17 and SEM micrograph of pure YSZ powder and NiO powder is shown in Fig. 4.16. It was observed that NiO-YSZ powder prepared by ball milling more homogeneously mixed in comparison with NiO-YSZ

powder prepared by hand mixing. NiO particles were covered by YSZ fine particles. This homogeneous mixing of YSZ and NiO powder was expected to enhance the length of triple phase boundary and hence could enhance the electrochemical reaction on cathode side.

In order to make sure that there was no phase changing during the ball milling process, XRD pattern analysis for NiO-YSZ powder prepared by hand mixing and ball milling was conducted and the result is presented in Fig. 4.18. It was clearly seen that only NiO and YSZ phases were identified. Any zirconate phases were not observed.

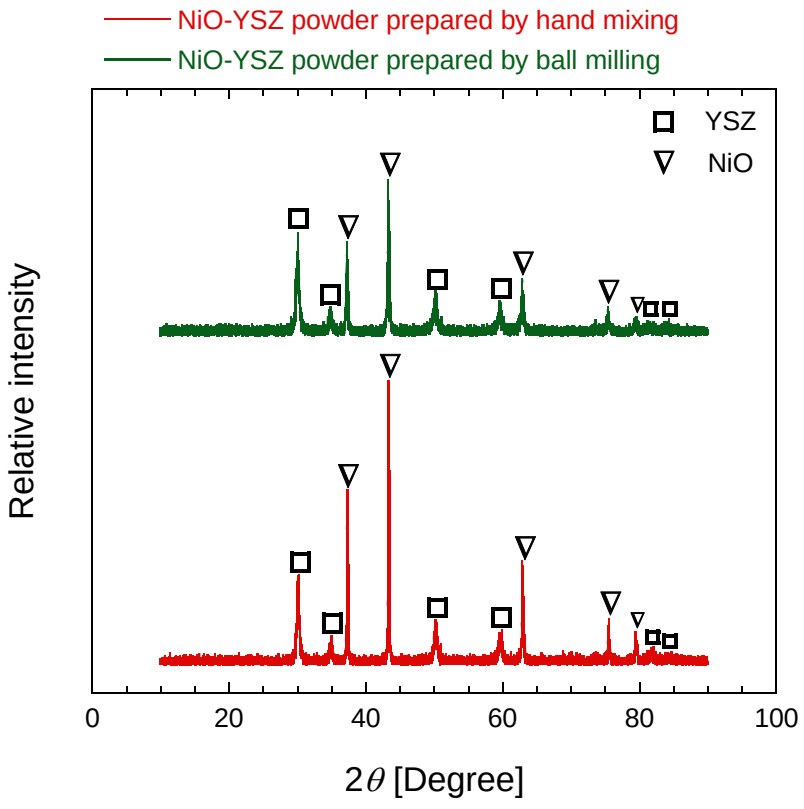

Fig. 4.18 XRD pattern of NiO powder and YSZ powder.

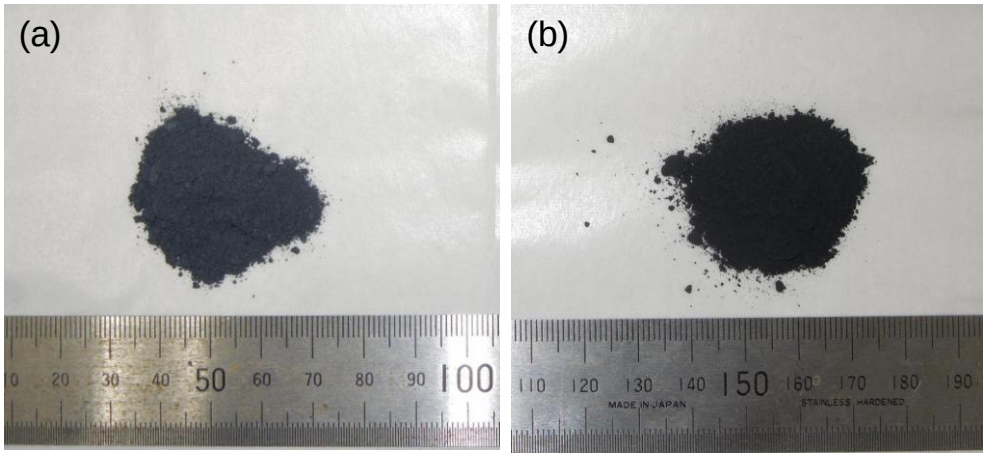

Fig. 4.19 LSM-YSZ powder prepared by (a) hand mixing and prepared by (b) ball milling.

LSM-YSZ powder prepared by hand mixing and ball milling was shown in Fig. 4.19. SEM micrograph of pure LSM and YSZ powder is presented in Fig. 4.20. It was seen that LSM-YSZ powder prepared by ball milling had more uniformly distributed porous structure than that of LSM-YSZ powder prepared by hand mixing (Fig. 4.21). During ball milling process, YSZ grains were dispersed almost homogeneously into the LSM particles. This uniform LSM-YSZ structure was expected substantially increased LSM-YSZ gas triple phase boundary sites as well as to enlarge anode electrochemical active area. XRD pattern analysis of mixed LSM-YSZ powder using planetary ball mill in Fig. 4.22 showed no existence of other secondary phase.

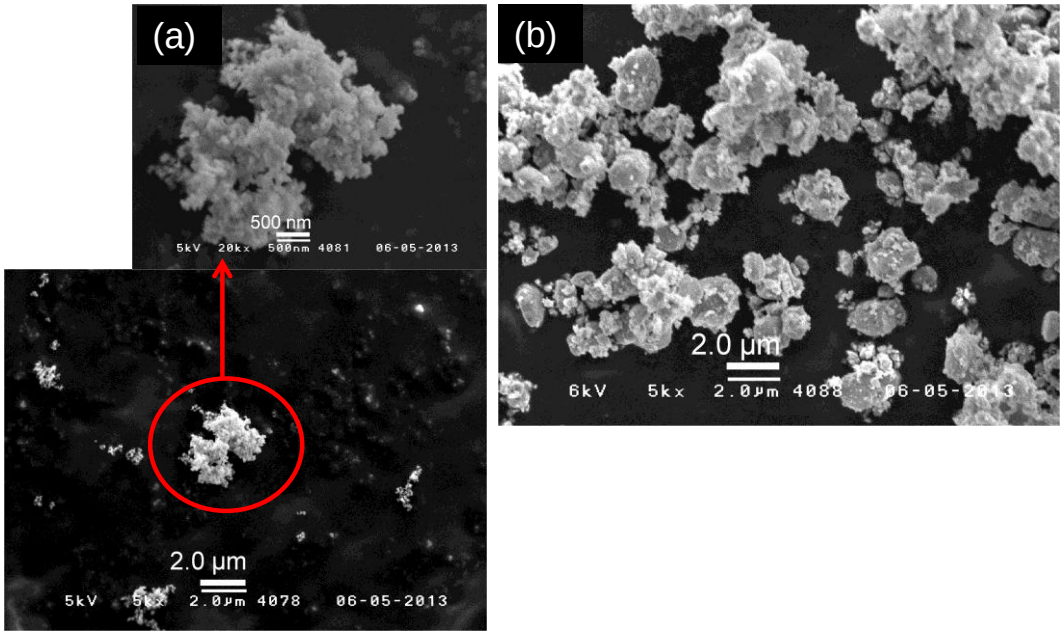

Fig. 4.20 SEM micrograph of (a) pure YSZ powder and (b) pure LSM powder.

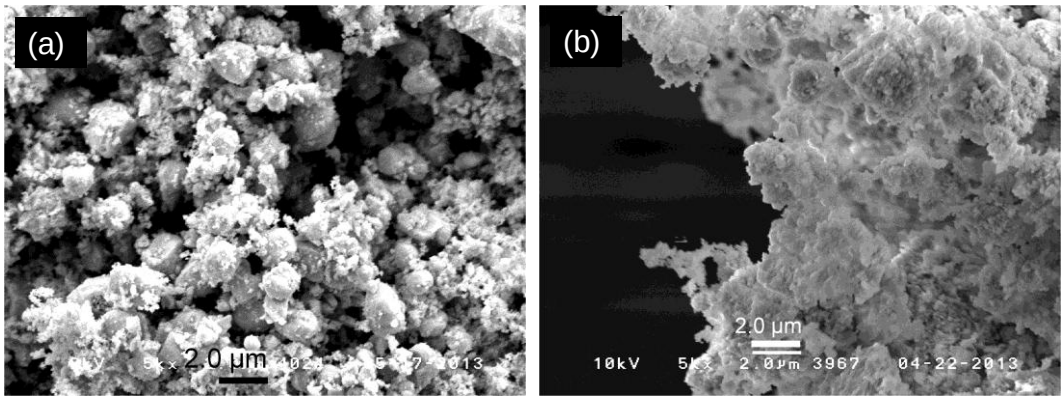

Fig. 4.21 SEM micrograph of LSM-YSZ powder prepared by (a) hand mixing and prepared by (b) ball milling.

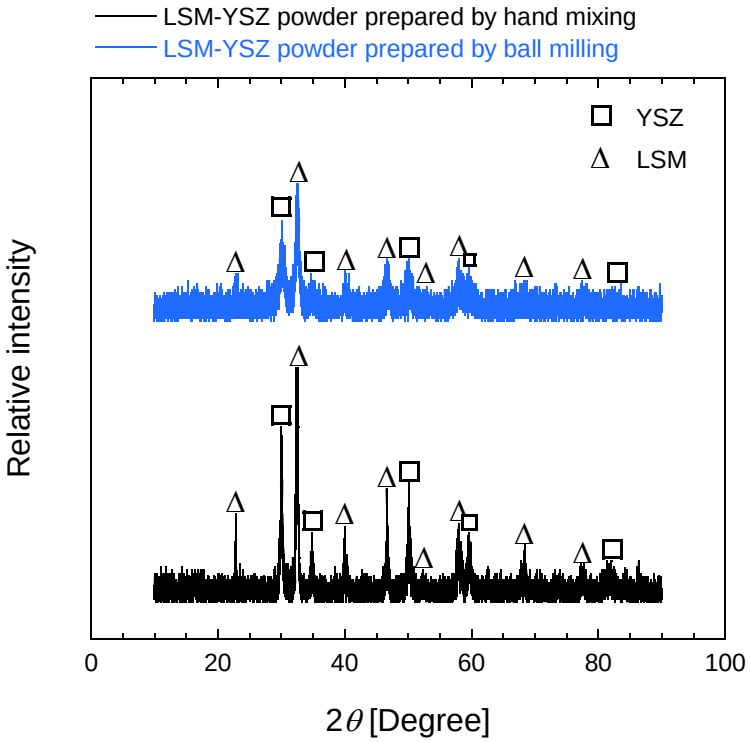

Fig. 4.22 XRD pattern of LSM and YSZ powder.

4.3.2.2 Effect of Temperature to Cell Performance at Constant CO_2 Flow Rate of 25 mL/min

The relationship between the current density and the applied cell voltage at 800 °C, 850 °C, and 900 °C of Ni-YSZ|YSZ|LSM-YSZ cell is shown in Fig. 4.23. As comparison, the current densities achieved in the experiment at 800 °C, 850 °C, and 900 °C using Ni-LSM|YSZ|LSM-YSZ cell were also provided in the figure (experiments with Ni-LSM|YSZ|LSM-YSZ cell and Ni-YSZ|YSZ|LSM-YSZ cell were conducted under the same experiment conditions). As for Ni-YSZ|YSZ|LSM-YSZ cell, current densities at the same levels of applied cell voltage were strongly affected by the operating temperature due to reduce in cell

resistance. The highest current density of 2.97 mA/cm^2 was measured at an operating temperature of 900 °C.

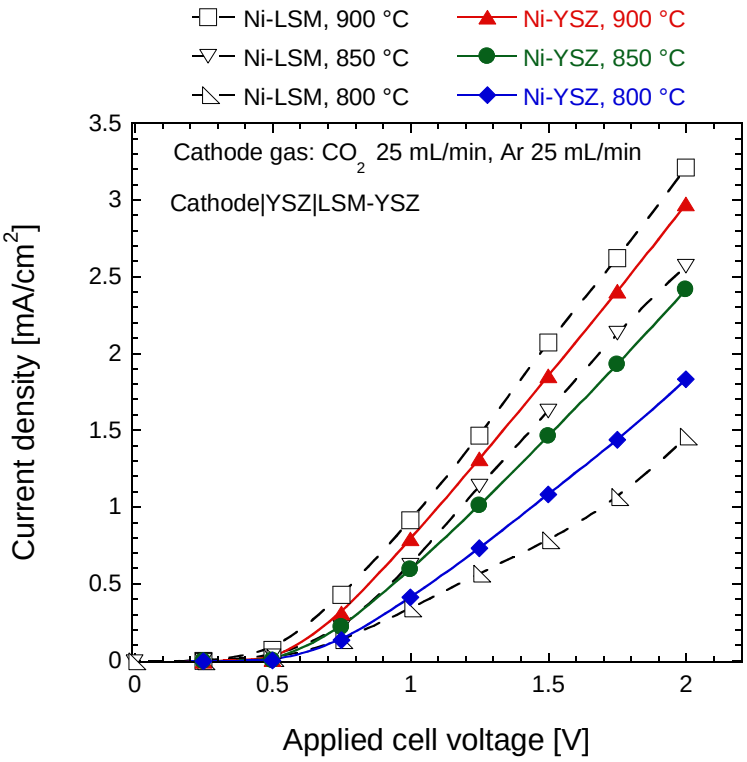

Fig. 4.23 Current density as a function of applied cell voltage at 800 °C, 850 °C, and 900 °C with different cathode materials.

Current densities achieved in the experiment with Ni-YSZ|YSZ|LSM-YSZ cell at 800 °C were higher in comparison with current densities achieved in the experiment with Ni-LSM|YSZ|LSM-YSZ cell. However, when temperature increased to 850 °C and 900 °C, current densities of Ni-LSM|YSZ|LSM-YSZ cell were slightly higher than those of Ni-YSZ|YSZ|LSM-YSZ cell. It was predicted that at higher temperature, LSM worked well as cathode but did not work well at lower temperature (800 °C). LSM has high chemical stability at higher

temperature. The combination between Ni and LSM contributed to increase chemical reactivity of Ni-LSM cathode at higher temperature [15]. Therefore at higher temperature, current densities achieved from Ni-LSM|YSZ|LSM-YSZ cell were slightly higher in comparison to those of Ni-YSZ|YSZ|LSM-YSZ cell.

CO and O_2 production rates at 800 °C, 850 °C, and 900 °C as function of current density obtained in the experiment using Ni-YSZ|YSZ|LSM-YSZ cell and Ni-LSM|YSZ|LSM-YSZ cell is shown in Fig. 4.24. In the case of Ni-YSZ|YSZ|LSM-YSZ cell, it was observed that ionic conduction and the chemical kinetics of CO_2 electrolysis increased with increasing temperature. The highest CO and O_2 production rates achieved were 0.78 and 0.38 μmol/(min cm^2), respectively, at an operating temperature of 900 °C and a current density of 2.97 mA/cm^2.

In addition, CO and O_2 production rates at 800 and 850 °C obtained in the experiment using Ni-YSZ|YSZ|LSM-YSZ cell were higher than CO and O_2 production rates achieved using Ni-LSM|YSZ|LSM-YSZ cell. The special structures of Ni-YSZ cathode and LSM-YSZ anode prepared by ball milling as shown in Fig. 4.25 had contributed to increase triple phase boundary length in cathode and anode side. It resulted into the excellent performance of Ni-YSZ|YSZ|LSM-YSZ cell in comparison with Ni-LSM|YSZ|LSM-YSZ cell.

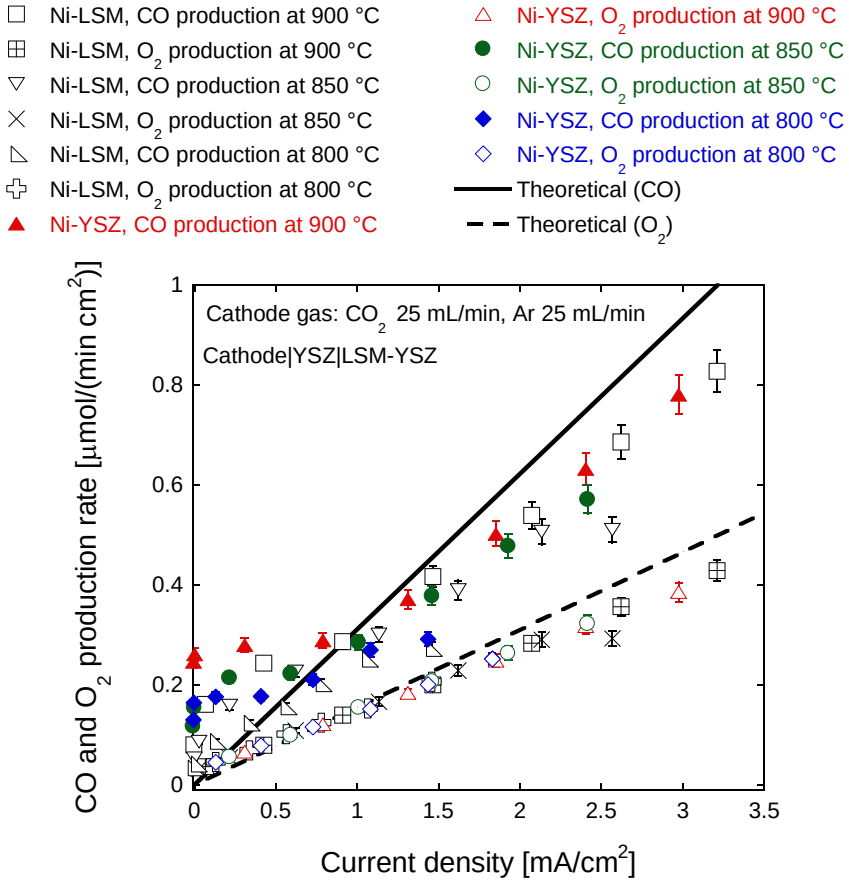

Fig. 4.24 CO and O_2 production rates as a function of current density at 800 °C, 850 °C, and 900 °C with different cathode materials.

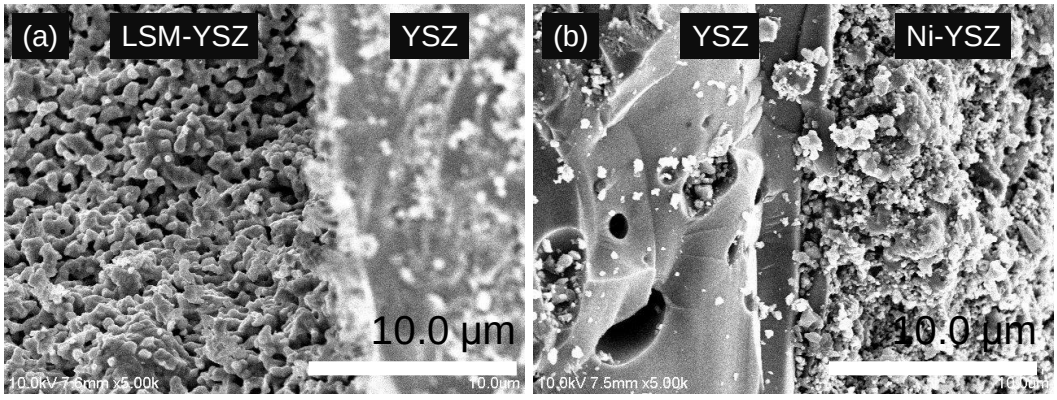

Fig. 4.25 SEM micrograph of a cross-section of the Ni-YSZ|YSZ|LSM-YSZ reference cell similar to tested cell taken before cell operation. (a) LSM-YSZ|YSZ (b) YSZ|Ni-YSZ.

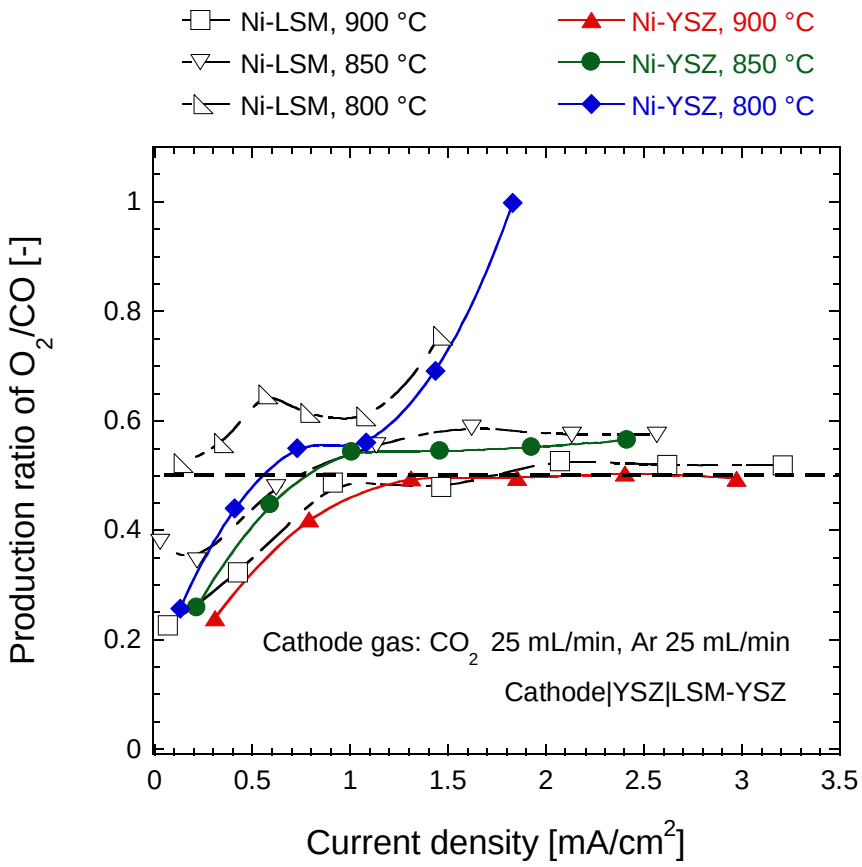

Fig. 4.26 Relationship between the current density and the production ratio of O_2/CO at 800 °C, 850 °C, and 900 °C with different cathode materials.

The production ratios of O_2/CO achieved in the experiment using Ni-YSZ|YSZ|LSM-YSZ cell and Ni-LSM|YSZ|LSM-YSZ cell were fairly close to the stoichiometric ratio of 0.5 (Fig. 4.26). Upon increasing the temperatures to 850 °C and 900 °C and increasing the current density, the production ratios of Ni-YSZ|YSZ|LSM-YSZ cell approached the stoichiometric ratio of 0.5. These results suggested that higher current efficiency for CO and O_2 production was achieved using Ni-YSZ|YSZ|LSM-YSZ cell. Special structure of Ni-YSZ cathode and LSM-

YSZ anode had contributed to improve cell performance by reducing electrodes resistance as well as increasing the length of triple phase boundary.

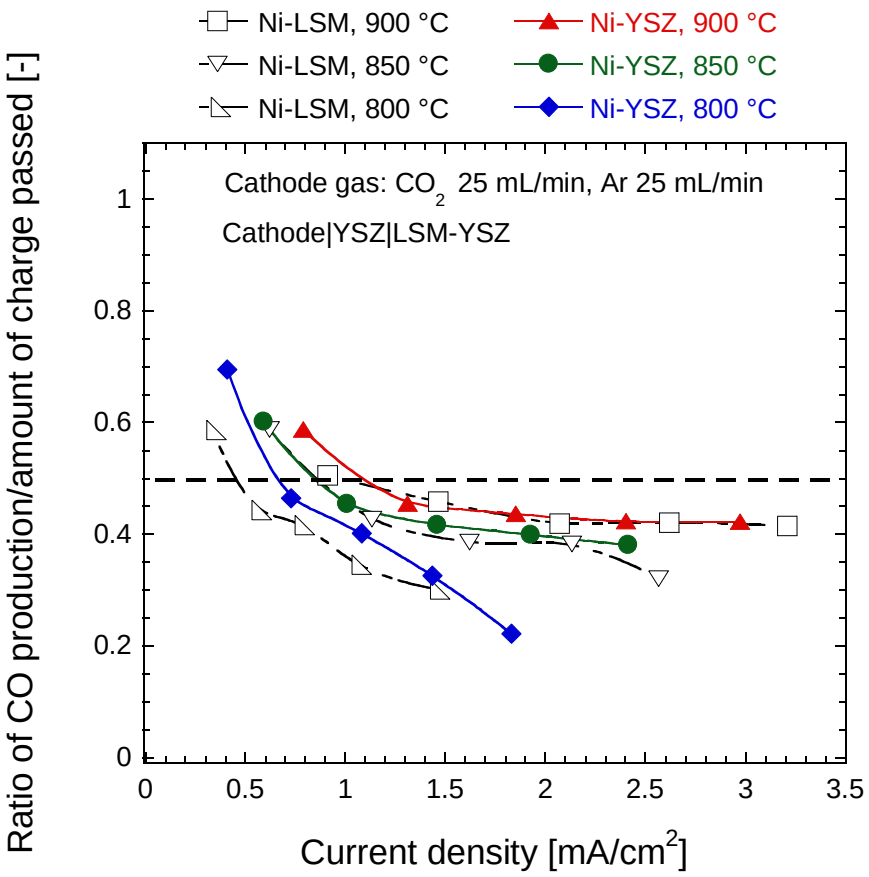

Fig. 4.27 Relationship between the current density and the mole ratio of produced CO and amount of charge passed at 800 °C, 850 °C, and 900 °C with different cathode materials.

The relationship between the current density and the CO/amount of charge passed of Ni-YSZ|YSZ|LSM-YSZ cell and Ni-LSM|YSZ|LSM-YSZ cell is shown in Fig. 4.27. It was observed that at lower current densities, the ratios were somewhat higher than 0.5. When current

densities and temperature increased, the ratios decreased due to decreased CO production rate, resulting in a higher O_2/CO production ratio. This tendency may be a result of deposition of carbon at the cathode at higher current densities. Ni is an excellent catalyst for carbon deposition reactions. The deposited carbon could deactivate the Ni catalyst and could cause rapid cell degradation [16].

4.3.2.3 Effect of CO_2 Concentrations on the Cathode Side at 900 °C

Fig. 4.28 shows the current density at 900 °C under CO_2 concentrations of 20%, 50%, and 80% as a function of applied cell voltage obtained in the experiment using Ni-YSZ|YSZ|LSM-YSZ cell and Ni-LSM|YSZ|LSM-YSZ cell. As for Ni-YSZ|YSZ|LSM-YSZ cell, current densities were slightly affected by CO_2 concentrations at the cathode side. At higher cell voltage, current densities at CO_2 concentration of 20% were slightly higher than those of 50%, and 80%. It was strange to have a sudden increased in current at CO_2 concentration of 20% and decreased in current at CO_2 concentration of 80%. The corresponding CO production rate at CO_2 concentration of 80% in Fig. 4.28 shows increasing in CO production rate while current slightly dropped. It was reasonable to assume high CO_2 electrolysis rate decreased cell current because of CO_2 starvation [17].

Generally speaking, it was observed that current densities achieved in the experiment using Ni-YSZ|YSZ|LSM-YSZ cell at the same CO_2 concentrations were higher than those of Ni-LSM|YSZ|LSM-YSZ cell. Porous structure of Ni-YSZ in cathode side effectively

reduced diffusion resistance and resulted into higher current density. The highest current density of 3.38 mA/cm^2 was measured at CO_2 concentration of 20%.

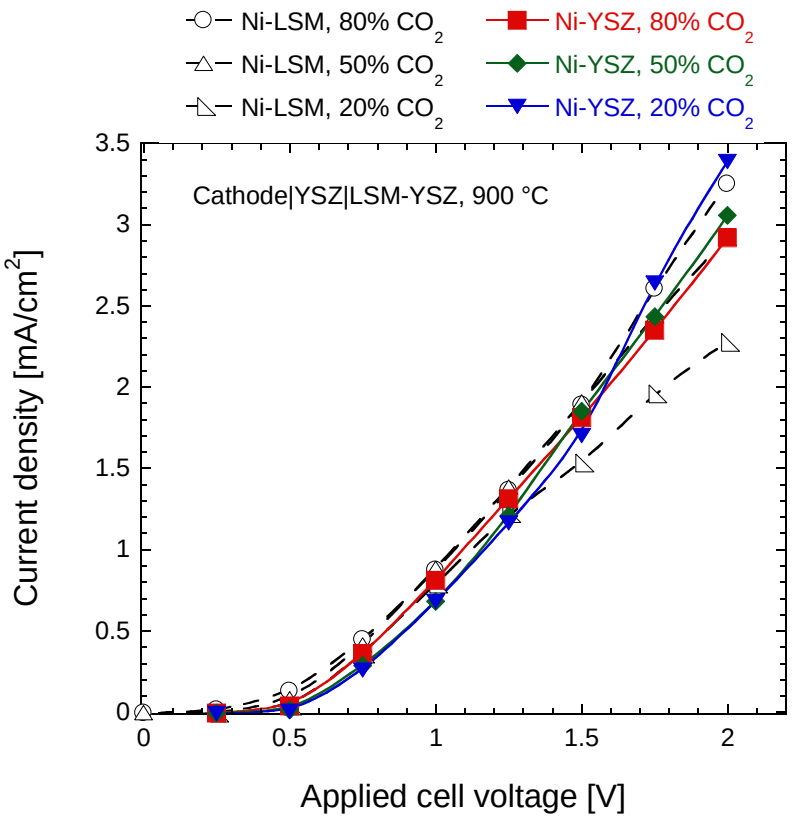

Fig. 4.28 Current density as a function of applied cell voltage at 900 °C under various CO_2 concentrations with different cathode materials.

As shown in Fig. 4.29, CO and O_2 production rates obtained in the experiment using Ni-YSZ|YSZ|LSM-YSZ cell increased with increasing CO_2 concentrations. CO and O_2 production rates obtained in the experiment using Ni-YSZ|YSZ|LSM-YSZ cell were higher than those of Ni-LSM|YSZ|LSM-YSZ cell. At CO_2 concentration of 80%, CO

production rate almost agreed with theoretical value of CO production calculated based on Faraday's law of electrolysis. This result showed that at higher temperatures and higher CO_2 concentrations, Ni-YSZ|YSZ|LSM-YSZ cell was effective for CO_2 electrolysis. The highest CO and O_2 production rates achieved in this study were 0.88 and and 0.38 μmol/(min cm^2) respectively at CO_2 concentration of 80%.

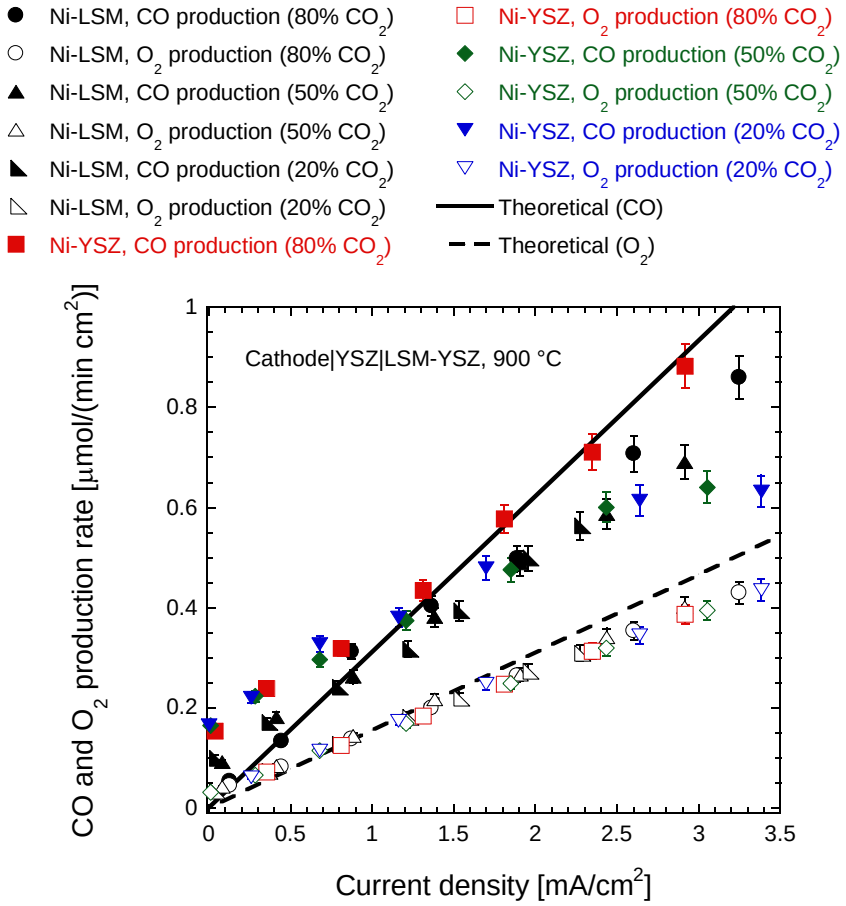

Fig. 4.29 CO and O_2 production rates as a function of current density at 900 °C under various CO_2 concentrations with different cathode materials.

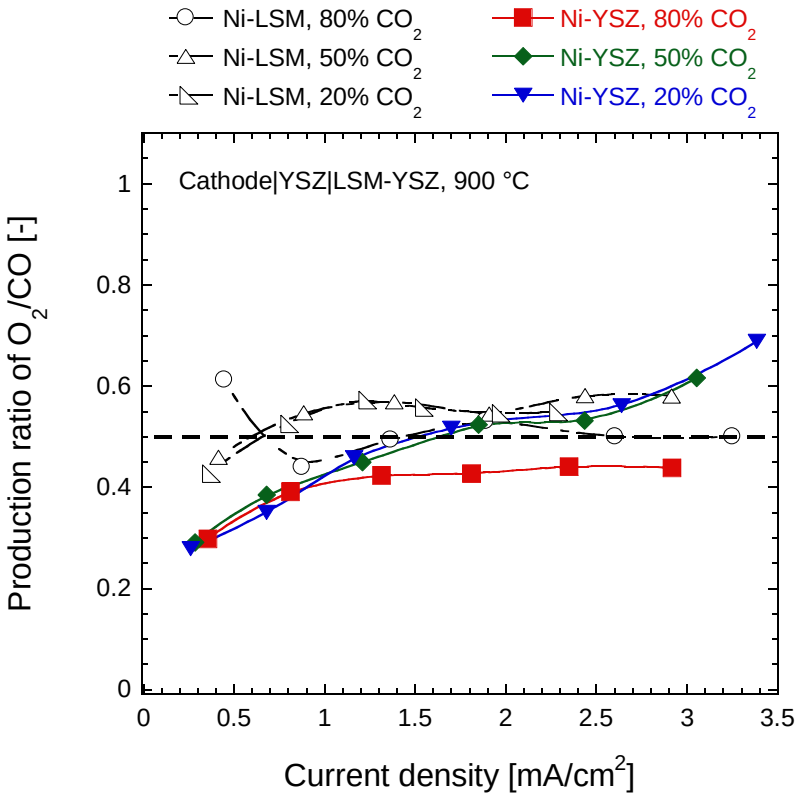

Fig. 4.30 Relationship between the current density and the production ratio of O_2/CO at 900 °C under various CO_2 concentrations with different cathode materials.

During measurement, it was observed that at lower voltage i.e. lower current density, current was mainly consumed for diffusion of CO_2 in the surface of cathode and to overcome the diffusion resistance [6]. Upon increasing cell voltage and increasing CO_2 concentrations, production ratios of O_2/CO obtained from experiment using different cathode materials approached to stoichiometric ratio of 0.5 (Fig. 4.30). The sufficient current was then used for the CO_2 electrolysis. It was also seen that the diffusion resistance decreased while increasing CO_2 concentrations. This resulted into ratio of CO production to amount of

charge passed slightly closer to the stoichiometric ratio of 0.5 (Fig. 4.31).

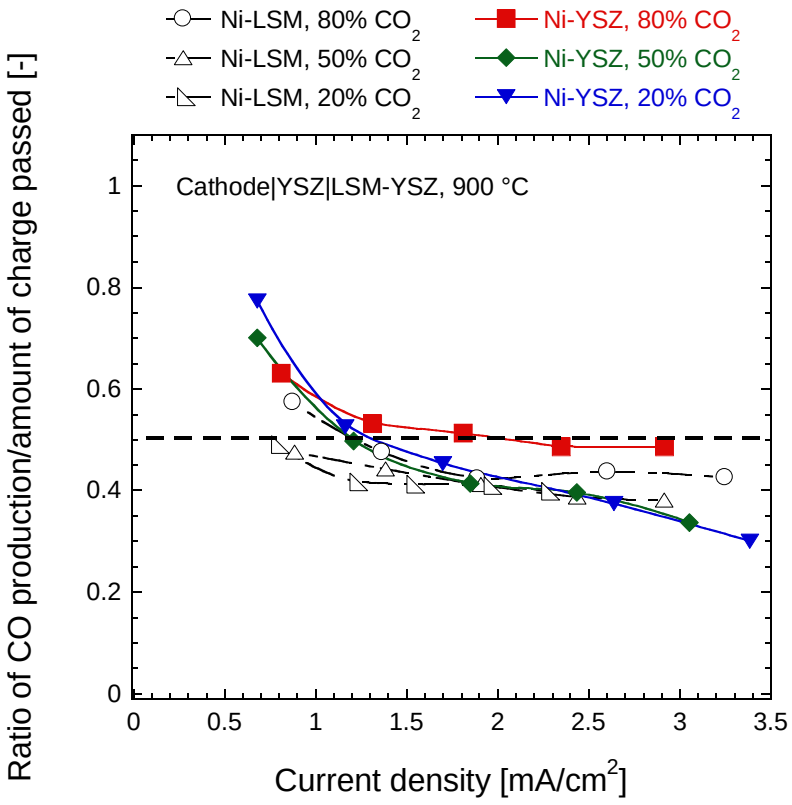

Fig. 4.31 Relationship between current density and ratio of CO production/amount of charge passed at 900 °C under various CO_2 concentrations with different cathode materials.

4.3.2.4 Cell Durability Measurement

Durability measurement of Ni-YSZ|YSZ|LSM-YSZ cell after CO_2 electrolysis for about 77.5 h is shown in Fig. 4. 32. The cell potential was relatively stable over the measurement period of 250 h with the current in the range 0.06-0.08 A. It was observed that current increased with time for 30 h. After that, the current was stable at

0.072 A until 90 h and then slightly decreased until 160 h. Finally, the current increased again to 0.080 A and became stable after 250 h.

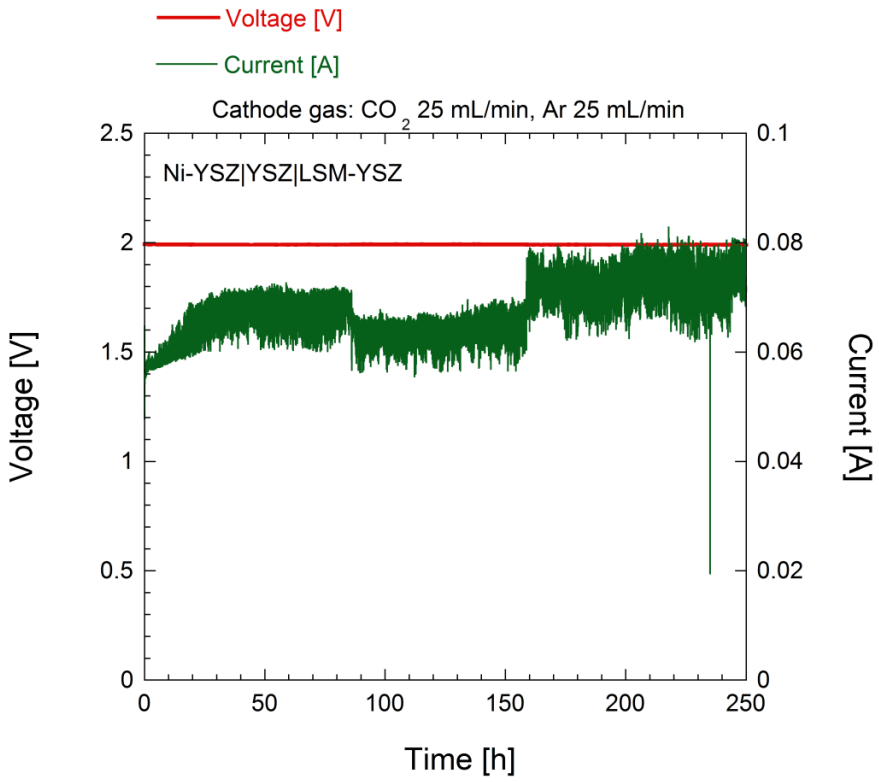

Fig. 4.32 Time history of voltage and current over 250 h at 900 °C.

4.3.2.5 Post Test Material Analysis

After CO_2 electrolysis measurement, cell material characterization was performed using SEM. The Ni-LSM|YSZ|LSM-YSZ cell taken after cell operations is shown in Fig. 4.33 and SEM micrograph of a cross-section of the cell taken after cell operations is shown in Fig. 4.34. It was seen that Ni-YSZ cathode and LSM-YSZ anode were intact and well attached to one another. It was suggested that during high temperature CO_2 electrolysis, the Ni-YSZ and LSM-YSZ particles

remained in good condition. Fig. 4.35 shows SEM micrograph of surface view of Ni-YSZ cathode taken before and after cell operations. After CO_2 electrolysis, Ni-YSZ surface consisted of coarse grains and slightly non-uniform porosity due to long term high temperature process. However, the average particles size of Ni-YSZ cathode before and after CO_2 electrolysis was not significantly changed. It could be due to high dispersion state of YSZ particles in the surface of Ni resulting in the suppression of Ni grain growth during high temperature CO_2 electrolysis.

XRD pattern of cathode-electrolyte sample (Ni-YSZ|YSZ) in Fig. 4.36 shows that NiO peaks appeared after the measurement. It was predicted that some part of cathode electrode was oxidized to NiO at high temperature condition. Due to the absence of H_2 in the cathode side during electrolysis, such an oxidation process might occur.

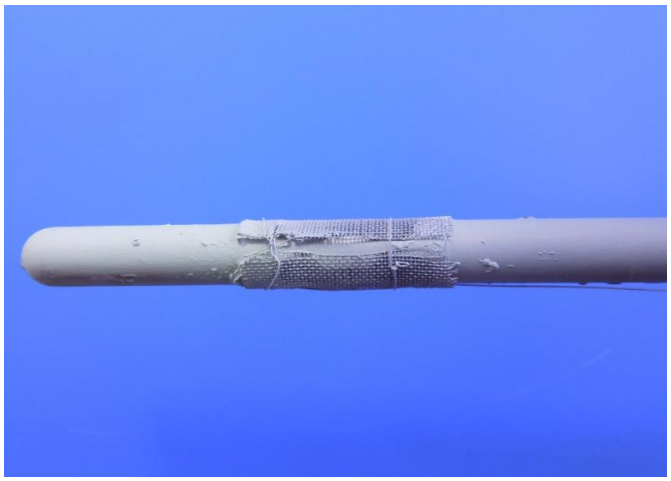

Fig. 4.33 Ni-LSM|YSZ|LSM-YSZ cell taken after cell operation over 300 h.

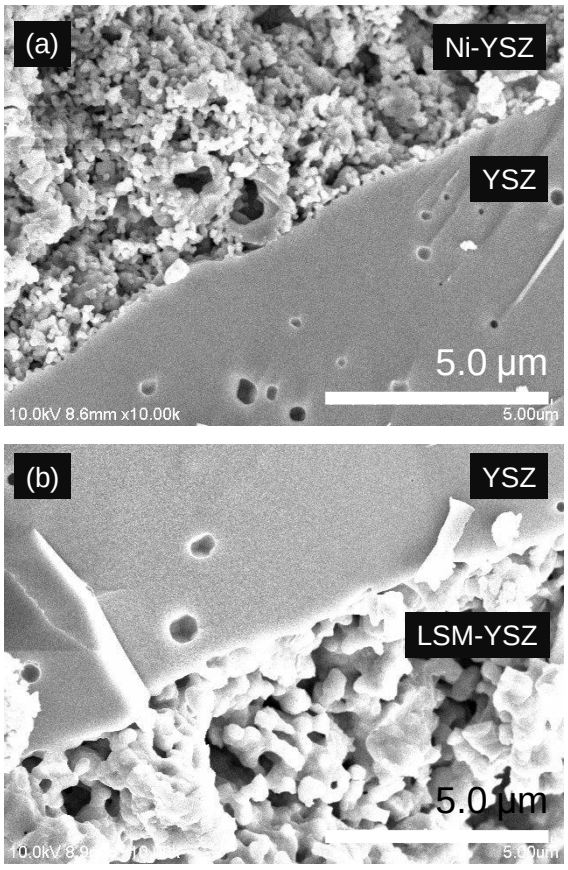

Fig. 4.34 SEM micrograph of a cross-section of the Ni-YSZ|YSZ|LSM-YSZ cell taken after cell operations. (a) Ni-YSZ|YSZ, (b) YSZ|LSM-YSZ.

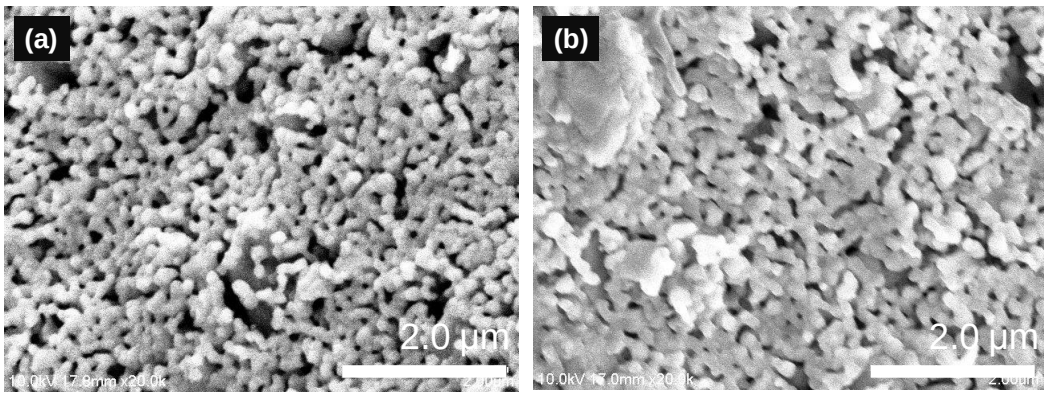

Fig. 4.35 SEM micrograph of surface view of Ni-YSZ cathode. (a) taken before cell operation (after H_2 reduction) and (b) taken after cell operations.

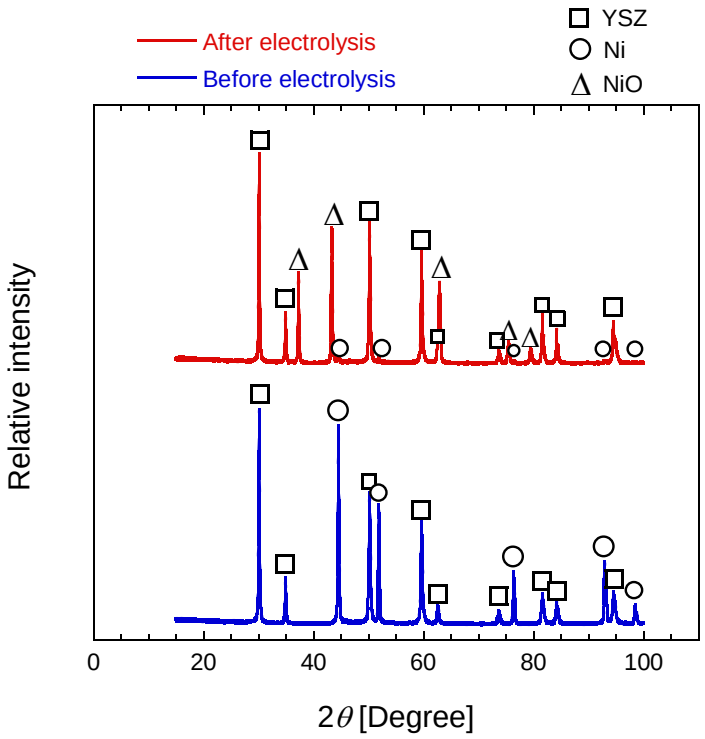

Fig. 4.36 XRD pattern of cathode-electrolyte sample (Ni-YSZ|YSZ) before and after the CO_2 electrolysis measurement.

4.4 Conclusions

Experimental studies based on the ACRES concept of CO regeneration via CO_2 electrolsysi was demonstrated using a Ni-LSM |YSZ|LSM-YSZ cell. Some improvements to the SOEC test reactor were carried out to increase current efficiency of Ni-LSM|YSZ|LSM-YSZ cell. At constant CO_2 flow rate of 25 mL/min in the cathode side, current densities increased with increasing temperature due to increase in the cell resistance. At constant temperature of 900 °C, it was observed that current densities increased with increasing CO_2 concentrations on the cathode side, which was attributed to a decrease in cathode activation and concentration overpotential. On the other

hand, at lower temperature (800 °C) current densities were observed to be independent of CO_2 concentrations in the cathode side due to surface activity became the rate determining step for the electrolysis reaction with decreasing operating temperature.

In addition, microstructure improvement of Ni-YSZ composite cathode through mechanical mixing was also carried out in order to electrochemically enhance the cathode reactivity. It was found that current densities achieved in the experiment with Ni-YSZ|YSZ|LSM-YSZ cell at 800 °C were higher in comparison to current densities achieved in the experiment with Ni-LSM|YSZ|LSM-YSZ cell under same experiment conditions. The special structure of Ni-YSZ cathode and LSM-YSZ anode prepared by ball milling had contributed to increase triple phase boundary length in cathode and anode side resulting into higher CO and O_2 production rates. Post test analysis with SEM showed that the average particles size of Ni-YSZ before and after CO_2 electrolysis was not significantly changed due to high dispersion state of YSZ particles in the surface of Ni resulting in the suppression of Ni grain growth during high temperature CO_2 electrolysis.

References

[1] S.D. Ebbesen, M. Mogensen, Electrolysis of Carbon Dioxide in Solid oxide Electrolysis Cells, *J. Power Sources*, **193**, 349-358, 2009.

[2] Z. Zhan, L. Zhao, Electrochemical Reduction of CO_2 in Solid Oxide Electrolysis Cells, *J. Power Sources*, **195**, 7250-7254, 2010.

[3] C. Yang, A. Coffin, F. Chen, High Temperature Solid Oxide Electrolysis Cell Employing Porous Structured $(La_{0.75}Sr_{0.25})_{0.95}MnO_3$ with Enhanced Oxygen Electrode Performance, *J. Hydrogen Energy*, **35**, 3221-3226, 2010.

[4] P.K. Lohsoontorn, D.J.L. Brett, N. Laosiripojana, Y.M. Kim, J.M. Bae, Performance of Solid Oxide Electrolysis Cells Based on Composite $La_{0.8}Sr_{0.2}MnO_{3-\delta}$–Yttria Stabilized Zirconia and $Ba_{0.5}Sr_{0.5}Co_{0.8}Fe_{0.2}O_{3-\delta}$ Oxygen Electrodes, *J. Hydrogen Energy*, **35**, 3958-3966, 2010.

[5] K. Otake, H. Kinoshita, T. Kikuchi, R.O. Suzuki, CO_2 Decomposition Using Electrochemical Process in Molten Salt, *J. Physics: Conference Series*, **379**, 012038, 2012.

[6] G. Tao, K.R. Sridhar, C.L. Chan, Study of Carbon Dioxide Electrolysis at Electrode/Electrolyte Interface: Part I. Pt/YSZ Interface, *J. Solid State Ionics*, **175**, 615-619, 2004.

[7] P. Plonczak, A.B. Hutter, M. Sogaard, T. Ryll, J. martynczuk, P.V. hendriksen, L.J. Gauckler, Tailoring of $La_xSr_{1-x}Co_yFe_{1-y}O_{3-\delta}$ Nanostructure by Pulsed Laser Deposition, *Advanced Functional Materials*, **21**, 2764-2775.

[8] P. Plonczak, M. Sogaard, A.B. Hutter, P.V. hendriksen, L.J. Gauckler, Electrochemical Characterization of $La_{0.58}Sr_{0.4}Co_{0.2}Fe_{0.8}O_{3-\delta}$ Thin Film Electrodes Prepared by Pulsed Laser Deposition, *J. Electrochem. Soc.*, **159**(5), B471-B482, 2012.

[9] Z. Wang, M. Mori, T. Araki, Steam Electrolysis Performance of Intermediate-temperature Solid Oxide Electrolysis Cell and Efficiency of Hydrogen Production System at 300 Nm^3h^{-1}, *J. Hydrogen Energy*, **35**, 4451-4458, 2010.

[10] T. Ishihara, N. Jirathiwathanakul, H. Zong, Intermediate Temperature Solid Oxide Electrolysis Cell Using $LaGaO_3$ based Perovskite Electrolyte, *J. Royal Soc. Of Chemistry*, **3**, 665-672, 2010.

[11] H. Mitsuyasu, K. Eguchi, H. Arai, Microscopic Analysis of Lanthanum Strontium Managnite/Yttria-stabilized Zirconia Interface, *J. Solid State Ionics*, **100**, 11-15, 1997.

[12] T. Fukui, K. Murata, S. Ohara, H. Abe, M. Naito, K. Nogi, Morphology Control of Ni–YSZ Cermet Anode for Lower Temperature Operation of SOFCs, *J. Power Sources*, **125**, 17-21, 2004.

[13] M. Naito, A. kondo, T. Yokoyama, Applications of Comminution Techniques for the Surface Modification of Powder Materials, *ISIJ Int.*, **33**(9), 915-924, 1993.

[14] J. Chaichanawong, K. Sato, H. Abe, K. Murata, T. Fukui, T. Charinpanitkul, W. Tanthapanichakoon, M. Naito, Influence of Size Distribution of LSM/YSZ Composite Powder on Microstructure and Performance of SOFC Cathode, *Trans. of JWRI*, **34**(1), 2005.

[15] H. Yokokawa, T. Horita, Cathodes, in: S.C. Singhal, K. Kendall (Eds.), High temperature Solid Oxide Fuel Cell-Fundamentals, Design and Application, 119-147, Elsevier, Netherland, 2009.

[16] T. Chen, W.G. Wang, H. Miao. T. Li, C. Xu, Evaluation of Carbon Deposition Behavior on the Nickel/Yttrium-Stabilized Zirconia Anode-Supported Fuel Cell Fueled with Simulated Syngas, *J. Power Sources*, **196**, 2461-2468, 2011.

[17] X. Yang, Cathode Development for Solid Oxide Electrolysis Cells for High Temperature Hydrogen production, PhD Thesis at University of St. Andrews, UK, 2010. Available online at: http://hdl.handle.net/10023/979

Chapter 5

ACRES for Ironmaking Process Driven by HTGR

5.1 Introduction

ACRES with CO_2 electrolysis can be thought to undergo endothermic and need external energy. HTGR is a candidate of a primary energy source for ACRES. High temperature electrolysis of CO_2 for CO regeneration in ACRES driven by the heat output from HTGR is the most applicable combination. This chapter discusses the design analysis of ACRES-HTGR for ironmaking process taking into account Ni-YSZ|YSZ|LSM-YSZ cell experimental results. Japan's original design of HTGR (GTHTR300) with circulating He coolant was used as the HTGR in the design analysis of ACRES for ironmaking process with assumed CO_2 electrolysis temperature of 800 °C.

5.2 Commercial HTGR Design

Application of ACRES to ironmaking process driven by electricity and thermal energy generated from HTGR is presented in Fig. 1.7 in Chapter 1. Regenerated CO is used for the reduction of iron monoxide into pure iron. CO_2 generated from the reduction is regenerated into CO again by the CO_2 electrolysis. O_2 as the by-products of CO can be useful material for other oxidation processes. The use of non-carbon primary energy sources is an essential requirement for practical realization of ACRES. An HTGR is the most suitable energy source for ACRES because of its high temperature output of up to 950 °C with no

carbon emissions and the availability of a sufficient amount of nuclear fuel to meet national demand.

Japan atomic energy research institute (JAERI) later incorporated into Japan atomic energy agency (JAEA) has been designing Japan's original gas turbine high temperature reactor namely gas turbine high temperature reactor 300 (GTHTR300). The greatly simplified design based on salient features of the HTGR with a closed He gas turbine enables the GTHTR300 a highly efficient and economically competitive reactor to be deployed in Japan [1]. The basic design of the Japan's original GTHTR300 for power generation is shown in Fig. 5.1 and its major specification is presented in Table 5.1. It was assumed that this type of GTHTR300 with circulating He coolant was used as the HTGR in the design of ACRES-HTGR for ironmaking process.

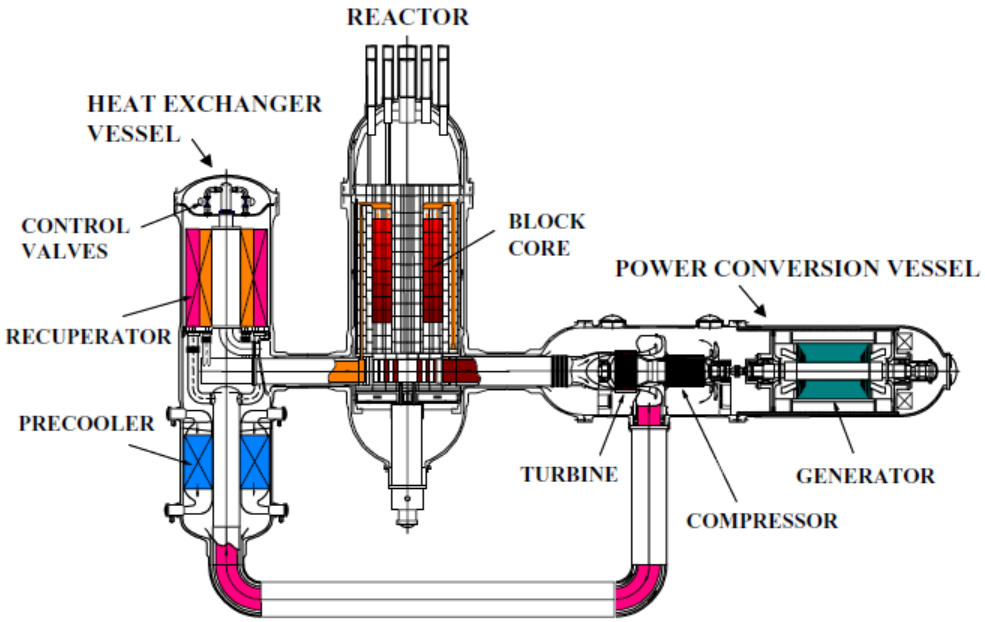

Fig. 5.1 GTHTR300 power generation system [1].

Table 5.1 Major specifications of GTHTR300 [1]

Reactor power [MWt]	600
Reactor inlet/outlet temperature [°C]	587/850
Gas turbine input pressure [MPa]	7
Gas turbine mass flow rate [kg/s]	439
Reactor core height [m]	~8
Inner/outer diameter of core [m]	3.6/5.5
Fuel enrichment [wt%]	14
Average power density [MW/m^3]	5.8
Reactor pressure vessel inner diameter [m]	~7.6
Gas turbine vessel inner diameter [m]	~5.7
Heat exchanger vessel inner diameter [m]	~5.8

5.3 Design of ACRES-HTGR for Ironmaking Process

A combined system with an ACRES CO_2 electrolysis system using heat and power generated by an HTGR within an ironmaking process has been proposed. Such a combined system was evaluated based on the experimental results for the Ni-YSZ|YSZ|LSM-YSZ cell and estimated the scale of the system.

In this evaluation, the SOEC was operated at the thermoneutral voltage (V_{Tn}). At V_{Tn}, the heat consumption from the endothermic electrolysis reaction equals the produced Joule heat within the cell [3-5]. The V_{Tn} is useful for evaluating the heat balance for an SOEC. When the electrolysis voltage is greater than V_{Tn}, the electrical power supplied to the cell is greater than the energy required for electrolysis,

and excess energy is released as thermal heat. On the other hand, an energy supply is required for electrolysis if the voltage is less than V_{Tn} [6]. Therefore, heat control is a critical factor in the design of CO_2 electrolysis system. For CO_2 electrolysis at 800 °C, V_{Tn} is defined as:

$$V_{\mathrm{Tn}} = \frac{\Delta H^{\circ}_{800\ ^{\circ}\mathrm{C}}}{n\mathrm{F}} \tag{5.1}$$

$\Delta H^{\circ}_{800\ ^{\circ}C}$ is the enthalpy change for the reaction (2.3 in Chapter 2) at 0.1 MPa and 800 °C, n = 2 is the number of electrons involved in the partial reactions at the electrodes $CO_2 + 2e^- \rightarrow CO + O^{2-}$ at cathode and $O^{2-} \rightarrow ½O_2 + 2e^-$ at anode. At 800 °C the calculated V_{Tn} was 1.46 V. However, in the calculation, the calculated value of V_{Tn} was rounded up to 1.5 V. Thereafter, a result of 1.5 V was used.

Fig. 5.2 shows CO and O_2 production rates as a function of current density at 800 °C using Ni-YSZ|YSZ|LSM-YSZ cell and Ni-LSM|YSZ|LSM-YSZ cell. At V_{Tn} which assigned to current densities of 1.08 and 0.78 mA/cm^2 respectively, CO and O_2 production rates of Ni-YSZ|YSZ|LSM-YSZ cell were higher than those of Ni-LSM|YSZ|LSM-YSZ cell. In the design analysis of ACRES-HTGR for ironmaking process, CO production rate of 0.27 μmol/(min cm^2) of Ni-YSZ|YSZ|LSM-YSZ cell was therefore used. Summary of results of CO and O_2 production rates of Ni-YSZ|YSZ|LSM-YSZ cell and Ni-LSM|YSZ|LSM-YSZ cell at V_{Tn} is presented in Table 5.2.

Table 5.2 CO and O_2 production rates at V_{Tn} of 1.5 V with different cathode materials measured at 800 °C.

	Ni-YSZ	Ni-LSM
Current density [mA/cm^2]	1.08	0.78
CO production rate [μmol/(min cm^2)]	0.27	0.20
O_2 production [μmol/(min cm^2)]	0.15	0.12

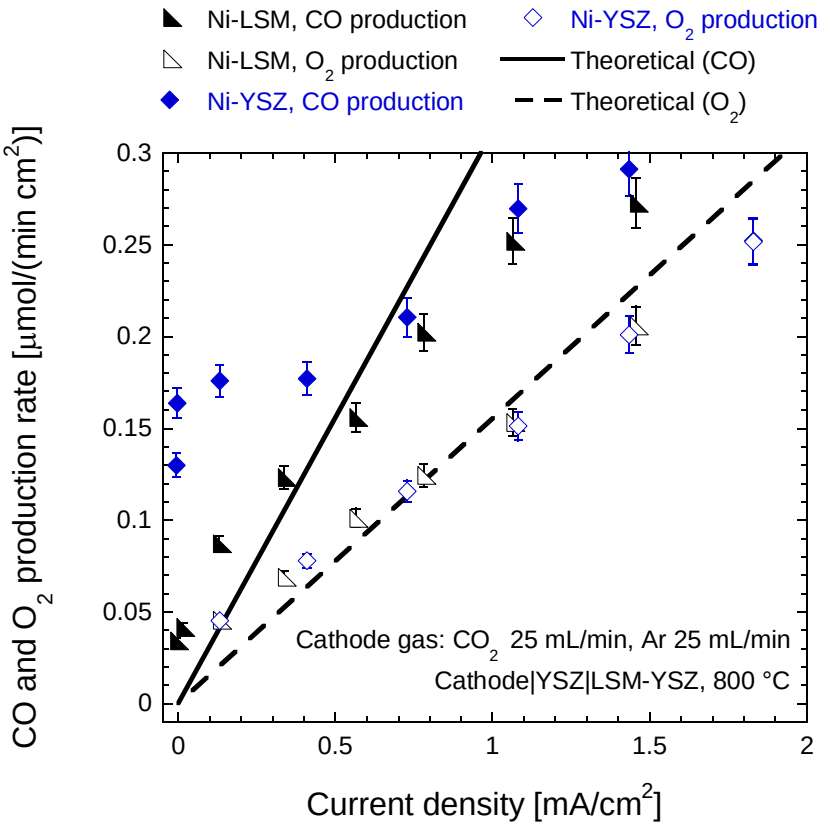

Fig. 5.2 CO and O_2 production rates as a function of current density at 800 °C, with different cathode materials.

In addition, CO production per power consumption at V_{Tn} of Ni-YSZ|YSZ|LSM-YSZ cell was higher than that of Ni-LSM|YSZ|LSM-YSZ

cell (Fig. 5.3). It was concluded that CO_2 electrolysis at 800 °C was effective using Ni-YSZ|YSZ|LSM-YSZ cell.

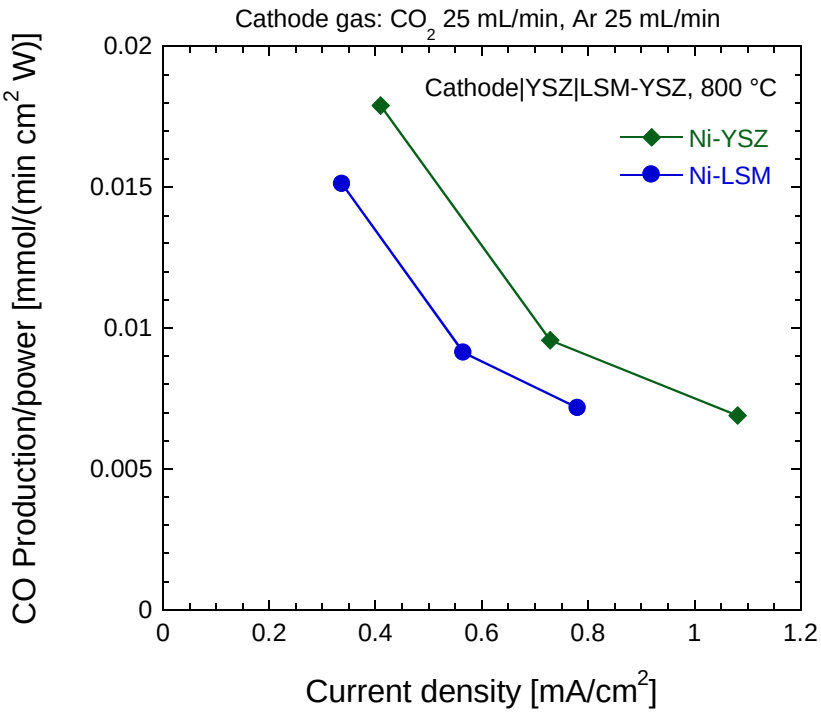

Fig. 5.3 Current density vs. CO production rate per electric power consumption measured at 800 °C with different cathode materials.

5.4 Technical Evaluation of ACRES-HTGR for Ironmaking Process

For the evaluation, it was assumed that CO_2 electrolysis was performed using the high temperature thermal output from the HTGR. Sensible heat output from the HTGR between 850 and 808 °C was initially used to provide heat for the CO_2 electrolysis reaction, and the remaining produced heat (around 808 °C) was used for power production by the gas-turbine power generator [2]. In the calculation, electrolysis reaction was assumed to be 800 °C.

The current density required for efficient electrolysis was 1.08 mA/cm^2 at 800 °C at V_{Tn} of 1.5 V and constant flow rates of CO_2, Ar, and N_2 of 25 mL/min. Based on the experiment results, an SOEC could produce CO at a rate of 4.5×10^{-9} mol/(s cm^2). The results of the energy balance evaluation for the combined system, taking into account the Ni-YSZ|YSZ|LSM-YSZ cell experimental results, are shown in Tables 5.3 and 5.4 and also depicted in Fig. 5.4.

Iron ore was assumed to be pure Fe_2O_3 that was stoichiometrically reduced in the blast furnace (BF) and that the HTGR was operated at full capacity. In the scale estimate, an HTGR providing 600 MW of thermal output was able to produce enough power for high-temperature electrolysis of CO_2 in the ACRES system. When HTGRs were used for the combined system, three HTGR units were required to power the high temperature electrolysis reactions. It was estimated that about 65.6 km^2/BF unit of cell surface area would be required to support CO regeneration by the system. The combined system is expected to contribute to carbon supply security and a low-carbon society by reducing CO_2 emissions by 2954 mol CO_2/(s BF unit) in the ironmaking process and converting it into 1021 mol CO/(s HTGR unit) of useful carbon materials.

Table 5.3 Estimated ACRES-HTGR energy balances for ironmaking process [2].

Parameter	Value
HTGR heat output rate [MWt/HTGR unit]	600
He temperature at outlet of HTGR [°C]	850
He temperature at inlet of CO_2 electrolysis cells [°C]	850
He temperature at inlet of gas turbine [°C]	808
Heat temperature at outlet of gas turbine [°C]	587
Heat input to gas turbine [MWt]	504.5
Heat input into CO_2 electrolysis cells [MWt]	95.5
Power production efficiency of gas turbine [%]	42.7
HTGR electricity output for CO_2 electrolysis [MWe/HTGR unit]	215.5
Electricity demand for CO_2 reduction [kJ/mol CO_2]	210.7
Heat demand for CO_2 electrolysis [kJ/mol CO_2]	93.4
CO_2 emissions from crude iron production per blast furnace [mol CO_2/(s BF unit)]	2954

Table 5.4 Estimated ACRES-HTGR energy balances for ironmaking process, calculated based on the experimental results.

Parameter	Value
CO_2 electrolysis temperature for SOEC [°C]	800
CO regeneration rate from the SOEC experiment [mol CO/(s cm^2)]	4.5×10^{-9}
CO regeneration rate per HTGR [mol CO/(s HTGR unit)]	1021
Iron ore rate for steel production per blast furnace [ton/s]	3.4
Electrode surface area per blast furnace [km^2/BF unit]	65.6
HTGR reactor units per blast furnace [unit]	2.9

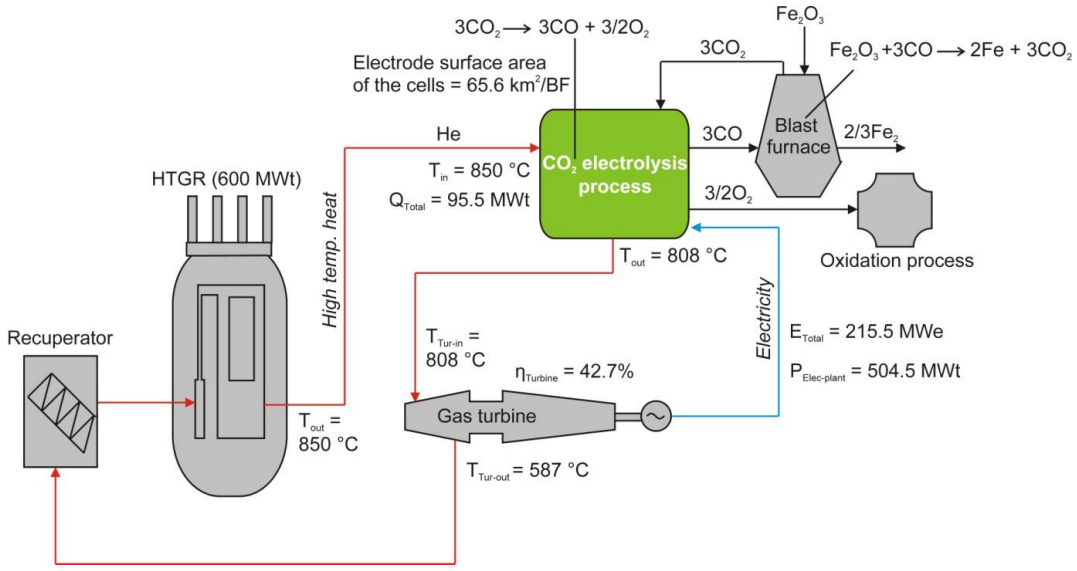

Fig. 5.4 Combination of ACRES-HTGR for ironmaking process.

5.5 Conclusions

The scale of a combined ACRES system with CO regeneration via CO_2 electrolysis driven by HTGR for ironmaking process was estimated based on the experimental results of Ni-YSZ|YSZ|LSM-YSZ cell. In the

evaluation, the SOEC was set at the V_{Tn}, where the heat consumption from the endothermic electrolysis reaction equals the produced Joule heat within the cell. From the evaluation, it was found that the required surface area of the SOECs was estimated to be 65.6 km^2/BF unit for a conventional blast furnace. It is expected that the combined system may contribute to carbon supply security and a low-carbon society.

References

[1] K. Kunitomi, S. Katanishi, S. Takada, X. Yan, N. Tsuji, Reactor Core Design of Gas Turbine High Temperature reactor 300, *Nuclear Eng. Design*, **230**, 349-366, 2004.

[2] Y. Kato, T. Obara, I. Yamanaka, S. Mori, A.L. Dipu, J. Ryu, Y. Ujisawa, M. Suzuki, Performance Analysis of Active Carbon Recycling Energy System, *Prog.* Nucl. *Energy*, **53**, 1017-1021, 2011.

[3] S.H. Jensen, Solid Oxide Electrolyser Cell, PhD Thesis at Technical University of Denmark, Denmark, 2006.

[4] R. Hino, K. Yamada, S. Kasai, Steam Electrolysis, in: X.L. Yan, R. Hino (Eds.), Nuclear Hydrogen Production Handbook, 99-115, CRC Press, USA, 2011.

[5] G.L. Hawkes, J.E. O'Brien, C.M. Stoots, J.S. Herring, M. Shahnam, CFD Model Of A Planar Solid Oxide Electrolysis Cell For Hydrogen Production From Nuclear Energy, The 11th International Topical Meeting on Nuclear Reactor Thermal-Hydraulics (NURETH-11), France, 2005.

[6] Z. Wang, M. Mori, T. Araki, Steam Electrolysis Performance of Intermediate-temperature Solid Oxide Electrolysis Cell and Efficiency of Hydrogen Production System at 300 Nm^3h^{-1}, *J. Hydrogen Energy*, **35**, 4451-4458, 2010.

Chapter 6

Conclusions

The feasibility study of high temperature CO_2 electrolysis using tubular YSZ-based electrolyte was conducted for CO regeneration in ACRES driven by HTGR.

In **Chapter 1** "Introduction to Active Carbon Recycling Energy System" development of new carbon recycling energy system was discussed to reduce emissions of CO_2 to the atmosphere from industrial processes, called ACRES. In this system, carbon in the form of CO is reused cyclically, consuming non-CO_2-emitting primary energy sources, thus reducing emissions of CO_2 to the atmosphere. One promising aspect of CO regeneration using ACRES is that CO_2 electrolysis using SOEC occurs at high temperatures. HTGR is the most suitable energy source for practical application of ACRES to an ironmaking process because of its high temperature output. This doctoral thesis demonstrates the feasibility of CO_2 electrolysis for CO regeneration in ACRES.

In **Chapter 2** "Carbon Dioxide Electrolysis in SOEC", the principle of CO_2 electrolysis using SOEC was presented. CO_2 electrolysis is thought to perform at high temperature since the electrical energy consumption of CO_2 electrolysis becomes lower at a higher temperature like steam electrolysis. Also the kinetics of a SOEC gets increasingly better with increasing temperature and at higher temperature resistance of SOEC decrease. In this study, various

electrode materials were tested for cathode and anode of SOECs to perform CO_2 electrolysis under high temperature operating condition. Given the results of the SOEC experiments, the performance of a combined system with an ACRES-CO_2 electrolysis system using heat and power generated by an HTGR within an iron making system using the most effective SOEC electrode material was evaluated.

In **Chapter 3** "Basic Studies on Carbon Dioxide Electrolysis in YSZ-based Electrolyte" were carried out to study the feasibility of CO_2 electrolysis in SOEC and to investigate the effect of some characteristic indicators to the performance of SOEC. Three CO_2 electrolysis processes were demonstrated using different electrode materials on the YSZ-based electrolyte. Cell-1, with a structure of Pt-LSM|YSZ|Pt-LSM for the cathode|electrolyte|anode, had higher current density levels than those of Cell-2, with a LSM|YSZ|LSM structure, and Cell-3, with a Pt|YSZ|LSM structure due to special structure of Pt-LSM. The CO production rate in Pt-LSM|YSZ|Pt-LSM cell was higher at 900 °C than at 800 °C. A CO production rate of 0.50 μmol/(min cm^2) was measured at an operating temperature of 900 °C with a cell voltage of 2.0 V.

In **Chapter 4** "Improvement of Carbon Dioxide Electrolysis Performance Using Ni-LSM|YSZ|LSM-YSZ Cell and Ni-YSZ|YSZ|LSM-YSZ Cell", some improvements to SOEC test reactor were carried out to increase current efficiency of Ni-LSM|YSZ|LSM-YSZ cell and Ni-YSZ|YSZ|LSM-YSZ cell. In the case of Ni-LSM|YSZ|LSM-YSZ Cell, it was observed that at constant CO_2 flow rate of 25 mL/min in the

cathode side, current densities increased with increasing temperature due to decrease in the cell resistance. At constant temperature of 900 °C, current densities increased with increasing CO_2 concentrations which was attributed to a decrease in cathode activation and concentration overpotential. On the other hand, at lower temperature (800 °C) current densities were observed to be independent of CO_2 concentrations in the cathode side due to surface activity became the rate determining step for the electrolysis reaction with decreasing operating temperature. CO and O_2 production rates of 0.83 and 0.43 μmol/(min cm^2) were achieved at an operating temperature of 900 °C and a current density of 3.21 mA/cm^2 with CO_2 flow rate of 25 mL/min.

In addition, microstructure improvement of Ni-YSZ composite cathode through ball milling was performed in order to electrochemically enhance the cathode and anode reactivity. It was found that current densities achieved in the experiment with Ni-YSZ|YSZ|LSM-YSZ cell at 800 °C were higher compared to those of Ni-LSM|YSZ|LSM-YSZ cell due to special structure of Ni-YSZ and LSM-YSZ through ball milling. CO and O_2 production rates of 0.78 and 0.38 μmol/(min cm^2) respectively were achieved at an operating temperature of 900 °C and a current density of 2.97 mA/cm^2. Durability test and post test material analysis indicated that cell was relatively stable and was in good condition during the CO_2 electrolysis measurement.

In **Chapter 5** "ACRES for Ironmaking Process Driven by HTGR", the scale of a combined ACRES system with CO regeneration via CO_2

electrolysis driven by HTGR for ironmaking process was estimated based on the experimental results of Ni-YSZ|YSZ|LSM-YSZ cell. In the evaluation, the SOEC was set at the thermoneutral voltage where the heat consumption from the endothermic electrolysis reaction equals the produced Joule heat within the cell. From the evaluation, it was found that the required surface area of the SOECs was estimated to be 65.6 km^2/BF unit.

In **Chapter 6**, the study was concluded. CO regeneration in ACRES for the ironmaking process driven by HTGR was feasible using state of the art SOEC technology. It is expected that the combined system may contribute to carbon supply security and a low-carbon society.

Appendix: Gas Chromatograph Calibration

Gas analysis was performed using two gas chromatographs equipped with TCD (GC-8A, Shimadzu). Two columns were used for gas species separator namely PPQ and MS 13X with both using He as carrier gas. The calibration curves for Ar, CO_2 and CO are presented in Fig. A.1, A.2 and A.3 while the calibration curve for N_2 and O_2 are presented in Fig. A.4 and A.5.

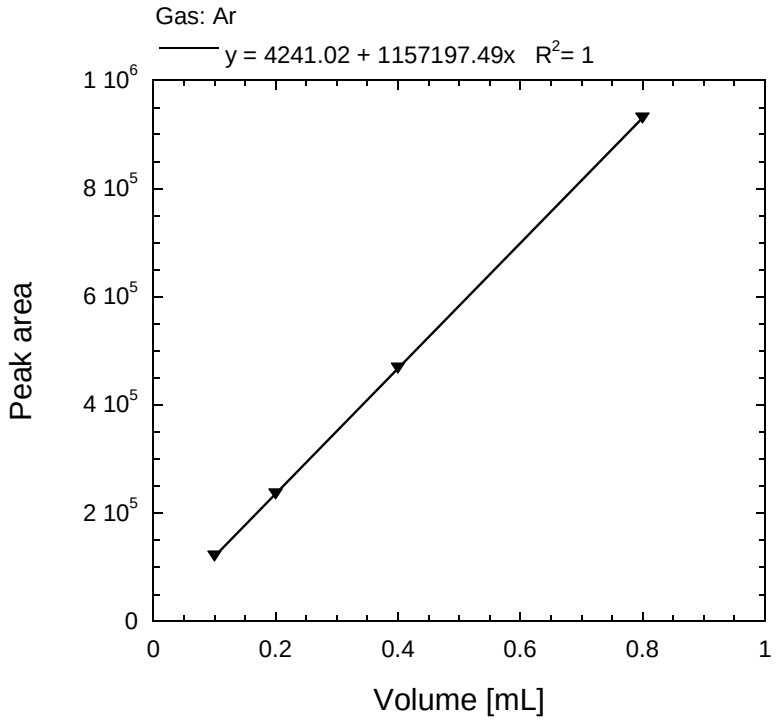

Fig. A.1 Gas calibration curve for Ar with linear regression.

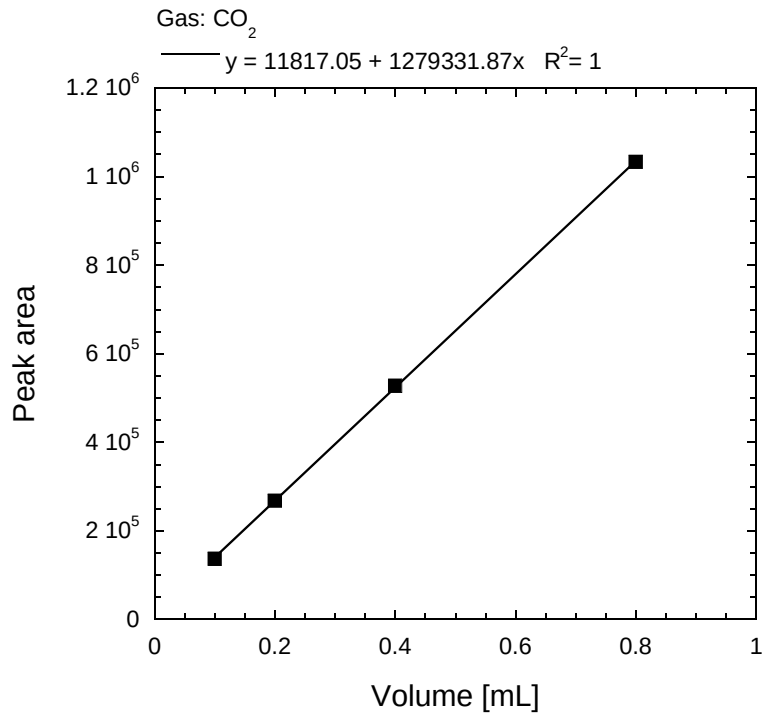

Fig. A.2 Gas calibration curve for CO_2 with linear regression.

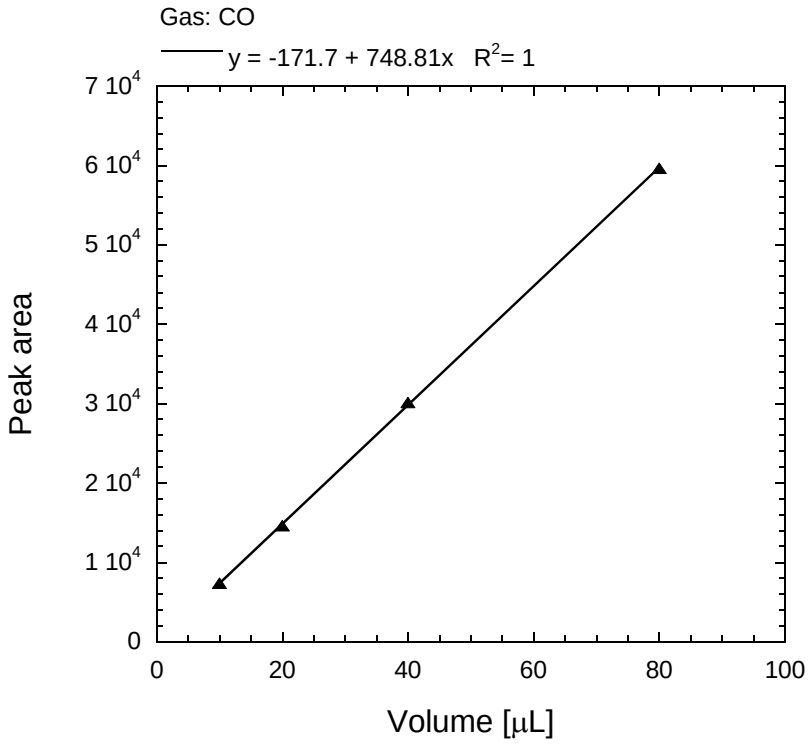

Fig. A.3 Gas calibration curve for CO with linear regression.

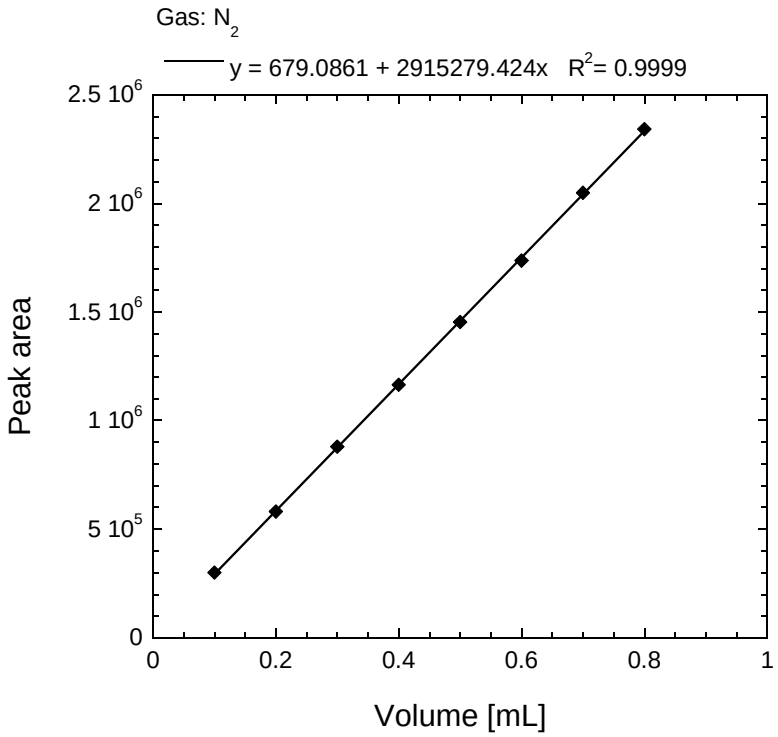

Fig. A.4 Gas calibration curve for N_2 with linear regression.

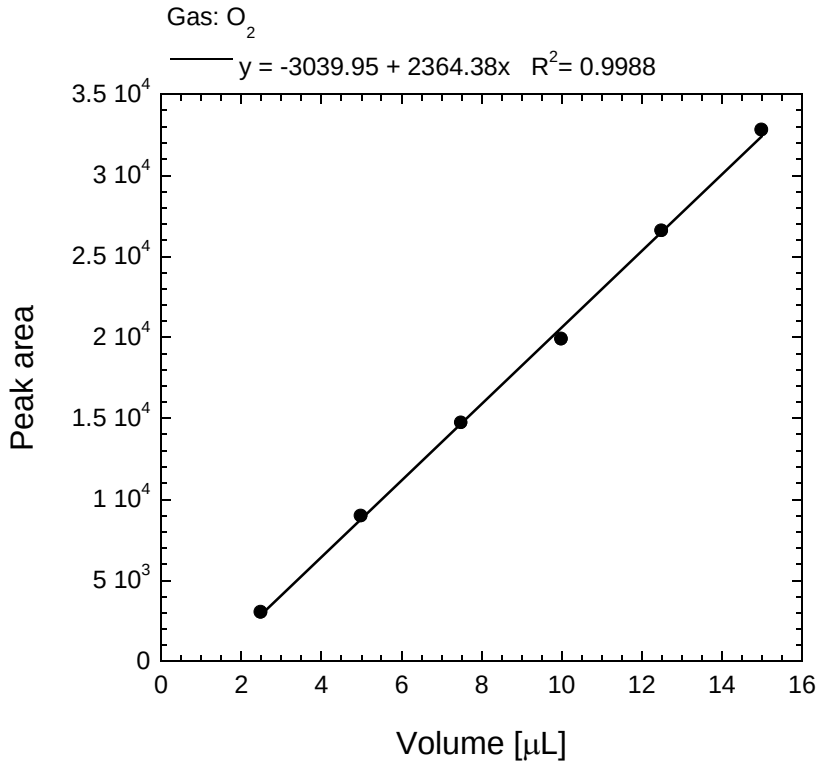

Fig. A.4 Gas calibration curve for O_2 with linear regression.

Achievements

Journal Papers

1. A.L. Dipu, J. Ryu, Y. Kato, Carbon Dioxide Electrolysis for Carbon Recycling Iron-making System, *ISIJ International*, **52**(8), 1427-1432 (2012), Relevant to Chapter 3.
2. A.L. Dipu, Y. Ujisawa, J. Ryu, Y. Kato, Carbon Dioxide Reduction in a Tubular Solid Oxide Electrolysis Cell for Carbon Recycling Energy System, *Nuclear Engineering and Design* (2013), http://dx.doi.org/10.1016/j.nucengdes.2013.11.004, Relevant to Chapter 4.
3. A.L. Dipu, Y. Ujisawa, J. Ryu, Y. Kato, Electrolysis of Carbon Dioxide for Carbon Monoxide Regeneration in Tubular Solid Oxide Electrolysis Cell, *Progress in Nuclear Energy,* Under Review, Relevant to Chapter 4 and Chapter 5.

Conference Contributions

International Conferences (Oral Presentations):

1. A.L. Dipu, G. Fujii, J. Ryu, Y. Kato, *High-temperature Carbon Dioxide Electrolysis by Tubular SOEC for a Carbon Recycling Iron-making Process*, International Conference on Smart Carbon Saving and Recycling for Ironmaking (ICSRI), Kanagawa, Japan, October 2-4, 2013.
2. A.L. Dipu, G. Fujii, J. Ryu, Y. Kato, *High-temperature Electrolysis of Carbon Dioxide in Tubular Solid Oxide Electrolysis Cell*, The 1st International Education Forum on Environment and Energy Science, Hawaii's Big Island, USA, December 14-18, 2012.
3. A.L. Dipu, K. Uruma, J. Ryu, Y. Kato, *Carbon Dioxide Reduction for Carbon Monoxide Production Using Solid Oxide Electrolysis Cell*, The 14th Asia Pacific Confederation on Chemical Engineering (APCChE) Congress, Singapore, February 21-24, 2012.
4. A.L. Dipu, K. Uruma, J. Ryu, Y. Kato, *Study on Electrochemical Decomposition of Carbon Dioxide in a Cell with YSZ Electrolyte*, The 4th International Forum on Multidisciplinary Education and Research for energy Science, Hawaii, USA, December 17-21, 2011.
5. A.L. Dipu, K. Uruma, J. Ryu, Y. Kato, *Investigation of Carbon Dioxide Electrolysis for Carbon Monoxide Production in Solid Oxide Electrolysis Cell*, The 6th Asia-Oceania Top University League on Engineering (AOTULE) Meeting, Beijing, China, October 10-11, 2011.

International Conference (Poster Presentation):

1. A.L. Dipu, J. Ryu, Y. Kato, *Electrolysis of Carbon Dioxide in Tubular Solid Oxide Electrolysis Cell,* UKERC-SPARKS Research Poster Competition 2013, University of Warwick, UK, July 9, 2013.

Domestic Conferences (Oral Presentations):

1. Y. Kato, A.L. Dipu, *Carbon Dioxide Electrolysis in Ni-YSZ|YSZ|LSM-YSZ Cell for a Carbon Recycling Iron-making System*, Japan Society Promotion of Science 54th Committee on Iron-making Meeting,

Tokyo, November 28-29, 2013.
2. A.L. Dipu, Y. Kato, *Investigation of Carbon Dioxide Reduction in Tubular Solid Oxide Electrolysis Cell for a Carbon Recycling Iron-making System*, The 165th The Iron and Steel Institute of Japan Meeting, Tokyo, March 27-29, 2013.
3. A.L. Dipu, G. Fujii, J. Ryu, Y. Kato, *Study on Carbon Dioxide Electrolysis under Various CO_2 Concentrations in Ni-LSM cermet|YSZ|LSM-YSZ Cell*, The 78th Annual Meeting of Society of Chemical Engineers of Japan, Osaka, March 17-19, 2013.
4. A.L. Dipu, K. Uruma, J. Ryu, Y. Kato, *Carbon Monoxide Production Performance by Carbon Dioxide Electrolysis Using YSZ Electrolyte*, The 43th Autumn Meeting of Society Chemical Engineers of Japan, Nagoya, September 14-16 , 2011.
5. A.L. Dipu, K. Uruma, R. Junichi, Y. Kato, *Investigation of Carbon Dioxide Electrolysis for Carbon Monoxide Production in Solid Oxide Electrolysis Cell*, The 3rd Multidisciplinary International Students Workshop, Tokyo, August 4-5, 2011.
6. A.L. Dipu, K. Uruma, J. Ryu, Y. Kato, *Reactivity Measurement of High Temperature Electrolysis of Carbon Dioxide*, The 76th Annual Meeting of Society of Chemical Engineers of Japan, Tokyo, March 22-24, 2011.

Domestic Conference (Poster Presentation):
1. A.L. Dipu, I. Yamanaka, Y. Kato, *Carbon Dioxide Electrolysis in Ni-LSM cermet|YSZ|Ni-LSM cermet Cell*, The 4th Energy-Global Center for Excellence (GCOE) Career Development Program (CDP) Forum-Future Social Standing of Energy Science Doctors, Tokyo, March 5, 2012.

Study Abroad/Internship
1. Visiting student at Massachusetts Institute of Technology (MIT)-H.H. Uhlig Corrosion Laboratory with support from the Tokyo Tech Energy-GCOE, Cambridge, USA, June 17- September 17, 2012.
2. Science Communication for Global Talents-Overseas Internship at Science Museum London and York National Railway Museum with support from the Tokyo Tech-Science and Engineering Communication, London and York, UK, August 17-27, 2011.

Summer/Winter School
1. Imperial College London-UK Energy Research Centre (UKERC) International Energy Summer School with support from UKERC, University of Warwick, UK, July 7-12, 2013.
2. Joint International Centre for Theoretical Physics (ICTP)-International Atomic Energy Agency (IAEA) Winter School in Nuclear Engineering, Trieste, Italy, December 3-7, 2012.

Award

1. Research Encouragement Award from the Japan Society for Promotion of Science (JSPS) 54th Committee on Ironmaking (2013).

Acknowledgements

This work could not have been possible without support from many people. First, and foremost, I would like to thank my academic and doctoral thesis supervisor: Professor Yukitaka Kato for the guidance, advice, encouragement and research opportunities. My special thanks to the following people for the valuable discussion and assistance:

Assistant Professor Dr. Junichi Ryu, Kenichiro Kuroda, Mr. Keirei Uruma, Dr. Hirokazu Ishitobi, Dr. Kim SeonTae, Gentaro Fujii, Ms. Madoka Oizumi, Ms. Kozue Uchiyama, Dr. Hiroyuki Sato, Massimiliano Zamengo, Myagmarjav Odtsetseg, Jun Kariya, Hiroyuki Hatsuda, Yuki Hara, Daiki Takasu, Daiki Tsunoda, Kaoruko Yamamoto, Yoshitomo Sato, Azusa Sakurai, Takafumi Mizuno, Koichi Murata and Mitsuharu Ono.

My sincere gratitude to everyone at H.H. Uhligh Corossion Laboratory who was very helpful and accommodated during my visit to MIT:

Professor Ron Ballinger, Assistant Professor Dr. Mike Short, Mr. Pete Stahle, Ms. Barbara Keesler, Sara, Jennifer, Lindsay, Bradley and Elliot.

To everyone in the Research Laboratory for Nuclear Reactors for good spirit of cooperation. To my friends: Martin, Ari, Batari, Bayu and Annita who have been very understanding and accommodating during my time in Tokyo. To my family for the great support and love. Financial support from MEXT, Energy-GCOE, Sumitomo Metal Corp. and Imperial College-UKERC is gratefully acknowledged.